

**Alma Mater Studiorum - Università di Bologna**

**Dottorato di Ricerca in  
Scienze Farmacologiche, Tossicologiche, dello Sviluppo e del Movimento Umano  
Ciclo XXIX**

**Settore Concorsuale di appartenenza: 03/D1  
Settore Scientifico disciplinare: CHIM/08**

**Design, synthesis and biological evaluation of new  
Transglutaminase 2 inhibitors and zetaCOP1-  
gammaCOP1 interaction disrupters**

**Presentata da  
Chen Huanhuan**

**Coordinatore Dottorato  
Chiar.ma Prof.ssa Patrizia Hrelia**

**Relatore  
Chiar.mo Prof. Vincenzo Tumiatti**

**Esame finale  
Anno 2017**

# Contents

<b>Abstract</b> .....	1
<b>Section I- Transglutaminase 2 inhibitors based multitarget ligands</b> .....	4
1. Introduction.....	5
1.1 Functions of transglutaminase 2.....	5
1.2 Transglutaminase 2- Implications in human diseases.....	7
1.3 Transglutaminase 2 and Alzheimer's disease.....	8
1.4 Transglutaminase 2 inhibitors .....	10
1.4.1 Irreversible TG2 inhibitors.....	10
1.4.2 Reversible TG2 inhibitors.....	12
1.5 Multitarget ligands approach in drug discovery.....	15
1.5.1 Rational design of a multitarget ligand.....	16
1.5.2 Multitarget ligands for the treatment of Alzheimer's disease.....	16
2. Dual inhibitors targeting transglutaminase 2 and histone deacetylase.....	20
2.1 HDAC's role in the pathogenesis of Alzheimer's disease.....	20
2.2 HDAC inhibitors.....	22
2.3 Drug design.....	25
2.4 Methods.....	26
2.4.1 Synthetic methods.....	26
2.4.2 <i>In vitro</i> TG2 inhibition assay.....	28
2.5 Results and discussions.....	29
2.6 Conclusions.....	30
3. Cinnamoyl structure based transglutaminase 2 inhibitors with potential antioxidant activities.....	31
3.1 Oxidative stress in Alzheimer's disease.....	31
3.1.1 Metal ions and A $\beta$ toxicity.....	32
3.1.2 Tau hyperphosphorylation and oxidative stress.....	32
3.2 Cinnamic acid derivatives as antioxidants.....	33
3.2.1 General antioxidant mechanisms of polyphenols.....	33
3.2.2 Classes of polyphenols.....	34
3.2.3 Antioxidant activity of hydroxycinnamic acids.....	36
3.3 Drug design.....	37
3.4 Methods.....	39
3.4.1 Chemical synthesis.....	39
3.4.2 Evaluation of antioxidant activity and <i>in vitro</i> TG2 inhibition assay.....	40
3.4.3 <i>In vitro</i> evaluation of inhibition on A $\beta$ self-induced aggregation and GSK3 $\beta$ activity.....	40
3.5 Results and discussions.....	41
3.6 Conclusions.....	43
4. Fluorescent probe-linked polyamine derivatives for subcellular imaging studies on the role of transglutaminase 2 in Alzheimer's disease.....	44
4.1 Fluorescent process.....	44
4.2 Fluorophores in cell biology.....	46
4.3 Classes of fluorophores.....	47

4.3.1	Coumarins.....	48
4.3.2	Fluoresceins.....	48
4.3.3	BODIPY.....	49
4.3.4	Rhodamines.....	50
4.3.5	Cyanines.....	50
4.3.6	Benzoxadiazoles.....	51
4.4	Drug design.....	52
4.5	Methods.....	54
4.5.1	Chemical synthesis.....	54
4.6	Conclusions.....	56
 <b>Section II- Disrupters of <math>\zeta</math>COP1/<math>\gamma</math>COP1 protein-protein interaction.....</b>		<b>57</b>
1.	Introduction.....	58
1.1	COPI secretory pathway.....	58
1.2	Mechanism of coatomer recruitment to membranes.....	60
1.3	$\zeta$ COP.....	61
1.4	$\zeta$ COP as potential cancer target.....	62
2.	Drug design.....	64
3.	Methods.....	66
3.1	Chemical synthesis.....	67
3.2	Cell viability assay.....	69
3.3	Co-immunoprecipitation assay.....	69
3.4	Docking studies.....	69
3.5	Cell fluorescence imaging.....	69
4.	Results and discussions.....	70
5.	Conclusions.....	73
 <b>Experimental section.....</b>		<b>75</b>
1.	Chemistry.....	75
2.	Biology.....	90
 <b>List of Figures/Tables.....</b>		<b>95</b>
<b>Acknowledgements.....</b>		<b>96</b>
<b>References.....</b>		<b>97</b>

## Abstract

### Section I

Over the last decades, the classic “one disease-one target” drug discovery approach has encountered new challenges by newly established concepts of drug design. Numerous disease systems are generally characterized by dysregulation of multiple biological pathways; this observation fosters the formation of “multifactorial disease” concept. Several efforts were devoted to integrate the complex disease systems to drug discovery process. A new strategy was identified and defined as polypharmacology, which is the treatment of diseases by modulating their multiple targets. In particular, the more recently consolidated “multitarget ligands” (MLs) drug design, designated for the first time by Morphy et al., proposed the development of single chemical entities capable of simultaneously modulating multiple targets to achieve the desired therapeutic effect.

Alzheimer’s disease (AD) is a neurodegeneration disorder, defined as multifactorial disease for the reason of multiple pathogenesis pathways involved in the disease onset and progress; in fact, it is correlated with protein misfolding which leads to hallmarks such as amyloid plaques and neurofibrillary tangles, as well as with events including oxidative stress. The event of oxidative stress in AD promotes amyloid- $\beta$  (A $\beta$ ) toxicity and has been proved to increase tau hyperphosphorylation, through a mechanism involving GSK3 $\beta$  as a key enzyme. In addition, AD has been correlated with dysfunctions at epigenetic level, involving a set of epigenetic factors as causes of its pathogenesis, including the histone deacetylases. Among numerous potential AD targets, transglutaminase 2 (TG2) is one of the most recently identified targets, given its overexpression observed in this neurodegenerative disease. Being responsible of protein cross-linking reactions, TG2 may play an important role in dysfunction of proteins, such as A $\beta$  and protein tau. Moreover, TG2 has been colocalized with AD hallmarks in samples of both animal and human origins. Thus, TG2 inhibitors could represent a promising therapeutic agent for AD’s treatment.

This section illustrates the drug design and development of multitarget ligands targeting simultaneously TG2 and other targets/events implicated in AD’s pathology: a core structure of TG2 inhibitor was taken into consideration and coupled to hydroxamic acid moiety to give potential TG2-HDAC dual inhibitors; by merging the same core structure to the polyphenol moiety of hydroxycinnamic acid derivatives, potential TG2 inhibitors bearing antioxidant activity have been developed. The first series of compounds showed interesting activity profile in *in vitro* assays, with compound **3** being a low micromolar inhibitor of TG2 and good inhibitor for HDACs. The series of antioxidants were additionally evaluated for their potential inhibition toward GSK3 $\beta$  and amyloid

aggregation, and compound **22** turned out to be the most promising derivative with good antioxidant activity and a balanced inhibition profile on both GSK3 $\beta$  and A $\beta$  self-induced aggregation.

At the attempt of achieving a further elucidation of TG2's role in AD, fluorescent probes targeting this enzyme could offer a glimpse into the complexity of this disease. Thus, fluorophores have been conjugated to TG2 inhibitors to construct probes for cell fluorescence imaging studies.

## Section II

Coat protein I (COPI) is a protein complex referred to as coatomer complex. It represents the major component of vesicles that mediate the retrograde transport from endoplasmic reticulum to the Golgi apparatus in eukaryotic cells. In the absence of COPI, cells experience Golgi fragmentation, immature autophagosome accumulation, and ultimately death. A recent function-based genomic screen identified *COPZI*, a gene encoding the coatomer complex subunit  $\zeta$ COP1, as a promising cancer target. In fact, *COPZI* knockdown using siRNA causes tumor-specific growth inhibition without affecting the viability of normal cells. The mechanism of the tumor selectivity of *COPZI* knockdown was explained by remarkably reduced mRNA levels of  $\zeta$ COP2, a functionally redundant isoform of  $\zeta$ COP1. As a result, while normal *COPZ2*-expressing cells survive *COPZI* depletion, *COPZ2*-deficient tumor cells are killed by *COPZI* knockdown. Therefore, a correct function of  $\zeta$ COP1 is crucial for the survival of tumor cells and could be a promising target for the development of anticancer drugs. Compounds capable of interfering with the function of  $\zeta$ COP1, by inhibiting the association of  $\zeta$ COP1 to the coatomer complex, could exert selective antitumor activity. Since the main function of  $\zeta$ COP1 is to form a dimer with  $\gamma$ COP1 within the coatomer complex, disrupters of this  $\zeta$ COP1/ $\gamma$ COP1 protein-protein interaction (PPI) could impair the correct function of  $\zeta$ COP1, thus, being potential anticancer drugs.

Therefore, a cyclic peptide-based compound was designed from *in silico* studies of the interface  $\zeta$ COP1/ $\gamma$ COP1 as potential disrupter of this PPI; moreover, a library of compounds was docked *in silico* to critical areas of the interface and a series of potential small-molecule disrupters of this PPI were identified.



## SECTION I

# **Transglutaminase 2 inhibitors based multitarget ligands**

## 1. Introduction

Transglutaminase 2 (TG2, tissue transglutaminase) is the most well studied and biologically characterized enzymatic isoform within the transglutaminase family. In addition to its role as  $\text{Ca}^{2+}$ -dependent catalyst of post-translational modification of proteins, TG2 plays a role in a number of diseases, such as celiac sprue, Alzheimer's disease, Huntington's disease and certain types of cancer. In particular, numerous evidences from both *in vitro* and *in vivo* studies support the hypothesis that TG2 is involved in the complex pathogenesis of Alzheimer's disease (AD). AD is considered a multifactorial disease and a more appropriate approach for its therapy is based on the design of new multitarget ligands able to interact with the different pathological targets which characterize AD. Hence, potent and selective TG2 inhibitors may provide important indications concerning the chemical features of pharmacophores potentially useful for designing multitarget ligands as new therapeutic agents against AD.

### 1.1 Functions of transglutaminase 2

Transglutaminases were discovered in 1950s as enzymes that catalyze the post-translational modification of proteins by the formation of isopeptide bond. To date, nine members have been characterized within the transglutaminase family, including transglutaminases 1-7, factor XIII A and erythrocyte-band4.2, which prevalently exert functions in blood clotting, wound healing, cell envelope formation, cell matrix stabilization and epidermal differentiation. TG2 is one of these nine members and is one of the most investigated and biologically characterized isoform, being the most frequently occurring member in eukaryotes and present in almost all mammalian cells. As main catalytic activity, TG2 is able to catalyze the  $\text{Ca}^{2+}$ -dependent modification of protein-bound glutamine side chain. In the presence of calcium, the  $\gamma$ -glutamyl side chain of a protein is acylated by active site cysteine (Cys<sup>277</sup>) of TG2 to form a thioester intermediate with the release of ammonia. The intermediate thioester is attacked by a primary amine, being either a small molecule amine or the  $\epsilon$ -amino group of protein-bound lysine residue<sup>1</sup>. This trans-amidation reaction results in the formation of a relatively stable isopeptide bond. TG2 can catalyze also a deamination reaction, where water acts as nucleophile with the consequent conversion of glutamine into glutamate<sup>2</sup>. Given the abundance of glutamine and lysine residues on the proteins in an organism, those residues represent the most important substrate for TG2<sup>3</sup>. Therefore, the enzymatic activity is tightly regulated by different mechanisms to prevent an excessive protein aggregation through crosslinking reaction. Guanosine triphosphate (GTP) and guanosine diphosphate (GDP) can both bind to TG2 and



inhibit the transamidase activity<sup>4</sup>, whereas calcium ionophores capable of transporting free calcium across cell membrane can increase intracellular calcium levels enough to activate intracellular TG2 which is enzymatically latent under physiological conditions<sup>5</sup>. Nitric oxide can abolish the transamidase activity through  $\text{Ca}^{2+}$ -dependent S-nitrosylation of multiple cysteine residues<sup>6</sup>.

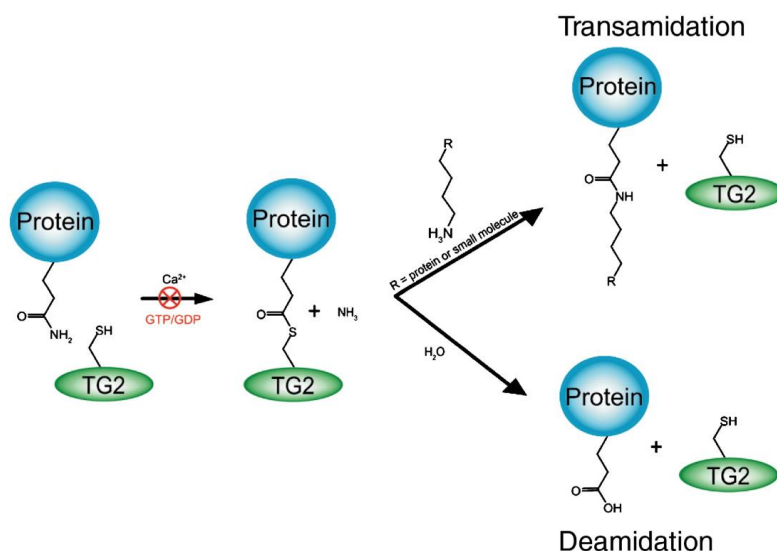


**Figure 1.** TG2 transamidation and deamidation catalytic mechanism<sup>7</sup>.

Under physiological conditions, intracellular TG2 exists in its inactive conformation, due to the low intracellular  $\text{Ca}^{2+}$  concentration. During situations of unbalanced  $\text{Ca}^{2+}$  homeostasis, such as apoptosis or wound healing, TG2 undergoes rapid activation upon binding of  $\text{Ca}^{2+}$  ions. It has been suggested that activated cytosolic TG2 may crosslink intracellular proteins to prevent them from spilling out of a dying cell and causing inflammation<sup>8</sup>. In the extracellular environment, TG2 is mainly transamidase-inactive despite the presence of  $\text{Ca}^{2+}$ . In the extracellular environment, TG2 once associated with cell surface integrin and fibronectin, can transmit signals to intracellular environment affecting cell adhesion, migration and signaling functions, through a mechanism independent of crosslinking activity<sup>9</sup>.

TG2 has been well characterized by X-ray crystallography, in particular in conformations bound with GDP<sup>10</sup> and with a peptidic inhibitor<sup>11</sup>. It consists of four distinct domains: 1) *N*-terminal containing the fibronectin binding site, 2) catalytic core containing the substrate binding pocket and catalytic triad, 3) a  $\beta$ -barrel domain with binding pocket for GTP and interaction site with  $\alpha_1$  adrenergic receptor, 4) C-terminal containing interaction site with phospholipase. This multidomain structure reflects diverse catalytic activities and signaling pathways in which TG2 is involved.

The crystal structures confirm the existence of at least two conformations for TG2: the “closed” ones and the “open” ones. In fact, the binding of GTP or inhibitors to TG2 causes significant

conformational shifts. Although it is clear that multiple TG2 conformations exist, few information is available about the biological relevance of each conformation.

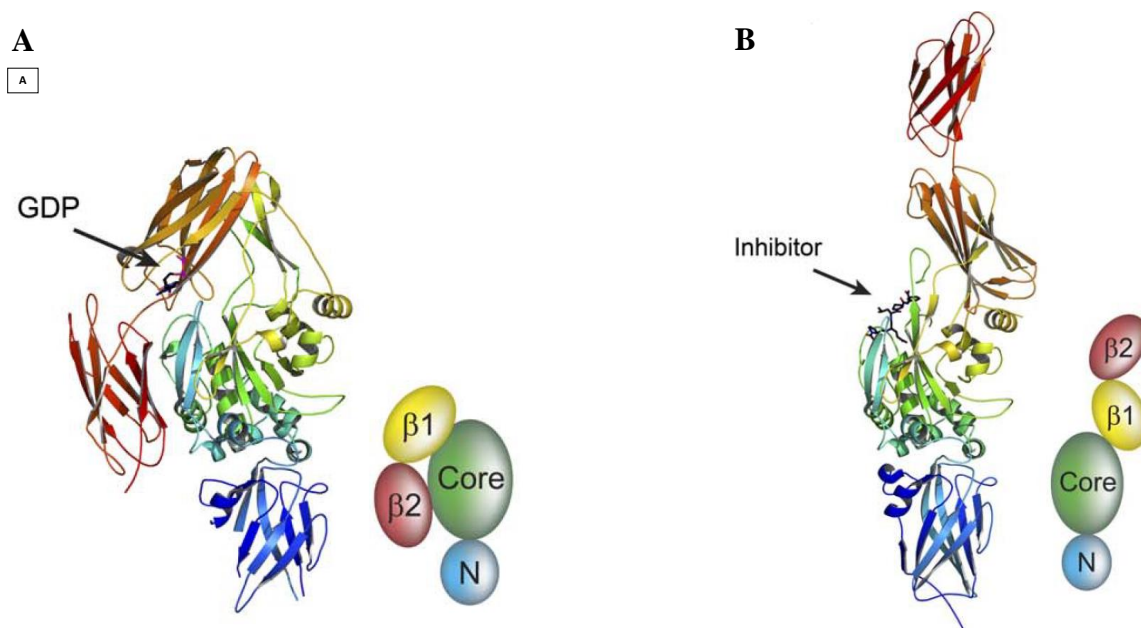


**Figure 2.** X-ray crystal structures of two conformations (open and closed) of human TG2 in complex with GDP in  $\beta 1$ -barrel (A) and with peptidic inhibitor in the active site (B)<sup>11</sup>.

## 1.2 Transglutaminase 2- Implications in human diseases

TG2 is implicated in a number of human diseases, such as celiac sprue, neurodegenerative disorders, diabetes, liver cirrhosis, fibrosis and certain types of cancer. Importantly, the pathology or etiology of most of the aforementioned diseases is likely ascribable to the enzymatic function of TG2.

Celiac sprue is an autoimmune disease characterized by an impairment of the small intestine caused by a class of digestion-resistant proteins called prolamines, characterized by high content of proline and glutamine. TG2 exerts two main functions in the disease pathogenesis: 1) the enzyme deaminates specific glutamine residues in the prolamine proteins leading to an increased binding affinities of these proteins to the human leukocyte antigen (HLA) serotypes, which mediate the T-cell response<sup>12</sup>; 2) The covalent complex TG2-prolamine can finally lead to an autoimmune response by generation of anti-TG 2 antibodies<sup>13</sup>.

There is accumulating evidence that TG2 contributes to the process of cataractogenesis in the eye, through cross-linking of crystallins, the proteins constituting the eye lens, leading to lens opacification and cataract. This seems to correlate with the formation of bis( $\gamma$ -glutamyl)spermidine cross-links between the crystallin proteins<sup>14</sup>.

A number of experimental observations support the hypothesis that TG2 is implicated in tumor progression. Multiple studies showed that TG2 protein is up-regulated in various cancerous tissues including pancreatic carcinoma<sup>15</sup>, breast carcinoma<sup>16</sup> and malignant melanoma<sup>17</sup>. A positive correlation between the drug resistance and metastatic potential of certain cancers with TG2 expression levels has been demonstrated. A unifying molecular mechanism that explains the way how TG2 promotes oncogenesis has not been discovered. At this regard, there are mainly two hypotheses: first, TG2 causes activation of nuclear factor  $\kappa$ B (NF- $\kappa$ B) probably through a crosslinking reaction, thus, consequently promotes expression of anti-apoptotic proteins, such as Bcl-xL; second, TG2 activates the focal adhesion kinase (FAK) with the subsequent activation of anti-apoptotic pathways, such as the P13K/Akt pathway. Furthermore, in a recent study on cancer cell-derived microvesicles, TG2 was shown to play a role in the communication between tumor cells and with normal cells, by inducing transformed characteristic of cancer cells onto normal fibroblasts through the release of microvesicles<sup>18</sup>.

The hallmarks of several neurodegenerative disorders are extensive neuronal loss and progressive formation of insoluble protein aggregates in the affected cerebral regions, such as amyloid plaques and neurofibrillary tangles in Alzheimer's disease, Lewy bodies in Parkinson diseases and huntingtin protein in the homonymous disease. Importantly, all of the disease-related proteins in the aforementioned disorders are good substrates of TG2 *in vitro*<sup>19</sup>. Furthermore, it has been proven that both TG2 and its transamidase activity are increased in the affected cerebral regions of persons suffering from these disorders<sup>20</sup>. These observations suggest that TG2 may be significantly involved in the pathogenesis of neurodegenerative diseases.

### **1.3 Transglutaminase 2 and Alzheimer's disease**

Protein misfolding and the formation of insoluble protein complexes play a central role in the pathogenesis of Alzheimer's disease (AD), characterized by the aggregation of amyloid- $\beta$  (A $\beta$ ) protein in cerebral tissue as senile plaques and the hyperphosphorylation of protein tau as neurofibrillary tangles<sup>21</sup>. However, the underlying mechanisms that trigger the misfolding of self-interacting proteins that eventually results in formation of neurotoxic aggregates remain unclear. Elucidation of the driving forces of protein complex formation in AD has crucial importance for the development of therapies for this disease.

Accumulating evidences support the hypothesis that TG2 may be involved in the abnormal protein aggregation observed in AD. As aforementioned, TG2 is a calcium-dependent enzyme that induces the formation of covalent  $\gamma$ -glutamyl- $\epsilon$ -lysine isopeptide bonds, which results in protein cross-links.

TG2-catalyzed cross-linking induces stable and protease-resistant protein complexes. Inhibition of TG2-catalyzed cross-linking counteracts the formation of protein aggregates, as observed in disease-models of other protein misfolding diseases, in particular, Parkinson's and Huntington's diseases<sup>19b</sup>. With regard to AD, there is compelling evidence from *in vitro* studies, as well as from studies on postmortem human brain tissue of AD patients and animal models that demonstrates a crucial role for TG2 in AD pathology:

- 1) *Aβ and protein tau are good substrates for transglutaminase 2.* In AD, Aβ shifts from soluble monomers to toxic oligomers and eventually forms insoluble mature fibrils. Brain transglutaminases could play a role in the Aβ accumulation. Using a synthetic partial-length of Aβ protein, Ikura et al. demonstrated that this peptide was subject to transamidation catalyzed by transglutaminase resulting in formation of multimeric peptides. The same experiment showed that in the presence of EDTA which chelates calcium ions, multimeric peptides were not produced and the monomer peptide remained unchanged<sup>22</sup>. Protein tau is a microtubule-binding phosphoprotein and functionally regulated by site-specific phosphorylation. In regard to the correlation between TG2 activity and protein tau aggregates, it has been reported that bovine tau protein is an excellent substrate for TG2 through the polyamine incorporation assays, whereas recombinant human tau presents different levels of affinity toward TG2 based on isoform types. This study also demonstrated that TG2-catalyzed cross-links on protein tau is specific only for a small number of glutamine residues, in fact, only few segments on tau are susceptible to the modification induced by the enzyme<sup>23</sup>. Additionally, a study that used co-immunoprecipitation and immunocytochemistry methods confirmed the actual interaction between TG2 and protein tau and their colocalization at intracellular levels<sup>24</sup>.
- 2) *TG2 levels in cerebrospinal fluid are increased in AD.* *In vivo* analysis of cerebrospinal fluid (CSF) in patients affected by AD has revealed that the levels of TG2 are significantly higher in comparison with the control group, whereas CSF tau protein concentration does not change significantly, suggesting that CSF TG2 concentration could be an important biomarker for this neurodegeneration disease<sup>25</sup>.
- 3) *TG2 colocalizes with amyloid deposits in the brains of AD patients.* Several *in vitro* immunochemical studies showed the presence of TG2 in both isolated amyloid plaque cores and cortex tissue sections from patients affected by AD. These results provide evidence that insoluble amyloid deposits may involve TG-mediated cross-linked Aβ-peptide polymer<sup>26</sup>.
- 4) *TG2 activity is increased in AD brain.* In a study conducted by Johnson G.V. et al. that used frozen prefrontal cortex and cerebellum samples from Alzheimer's disease, a total transglutaminase activity significantly higher in the AD prefrontal cortex compared to control was

observed. In addition, the levels of TG2, as determined by quantitative immunoblotting, were elevated approximately 3-fold in AD brain with respect to control. In contrast, in the cerebellum which usually is not impaired in AD, no significant increment in transglutaminase activity or levels has been detected<sup>27</sup>.

5) *Catalytically active TG2 colocalizes with A $\beta$  in AD animal models.* A recent *in vitro* study investigated the role of TG2 in AD pathology using two mouse models that represent early and late stages of pathology development for this purpose. According to the results, the general distribution pattern of TG2 in transgenic mice is similar to the observations in human brains. In fact, there was association of both TG2 and *in situ* active TG2 with A $\beta$  plaques and vascular A $\beta$ , indicating that alike human AD cases, TG2 was associated with A $\beta$  depositions in the animal models. Although spatial overlay of TG2 with A $\beta$  pathology observed in the mouse models was substantially different from observations in human samples, this finding provide evidence for a role of TG2 in A $\beta$  pathology<sup>28</sup>.

In summary, given these evidences on the role of TG2 in the initiation and development of protein aggregates in AD, its distribution overlay with the disease hallmarks and its increased activity in the same pathology, it is highly suggested the possibility to use inhibitors of the cross-linking activity of TG2 as a new therapeutic approach for AD.

## 1.4 Transglutaminase 2 inhibitors

The range of pathologies in which TG2 is implicated demonstrated the need for potent TG2-specific inhibitors. To date, TG2 inhibitors have been generally divided into two classes based on the inactivating mechanism of the enzyme: reversible (competitive and non-competitive) and irreversible inhibitors.

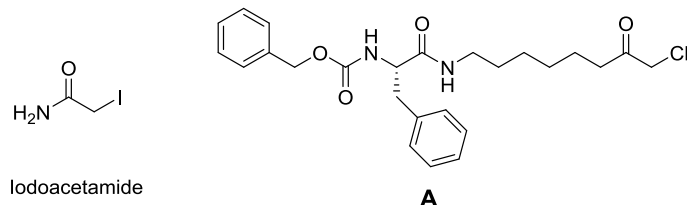
### 1.4.1 Irreversible TG2 inhibitors

Most irreversible TG2 inhibitors are designed to target the active site cysteine (Cys<sup>277</sup>) using electrophilic functional groups. These inhibitors prevent enzyme activity by covalently modifying the enzyme, thereby preventing substrate binding.

- Halomethyl carbonyl inhibitors

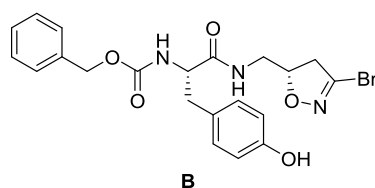
This class of inhibitors has been developed based on the structure of iodoacetamide, which was one of the first irreversible inhibitors and was able to inactivate guinea pig liver TG2<sup>29</sup>. More recently, the Keillor group made a series of chloromethyl ketones and combined them with a Cbz-Phe

scaffold, where Cbz functional group was previously assessed to be essential for active site recognition<sup>30</sup>. The best inhibitor (compound **A**) showed a  $K_i = 6\mu\text{M}$  and a good specificity profile with very low reactivity toward glutathione, the most abundant physiological thiol present in living cells<sup>31</sup>.



- 3-Halo-4,5-dihydroisoxazole inhibitors

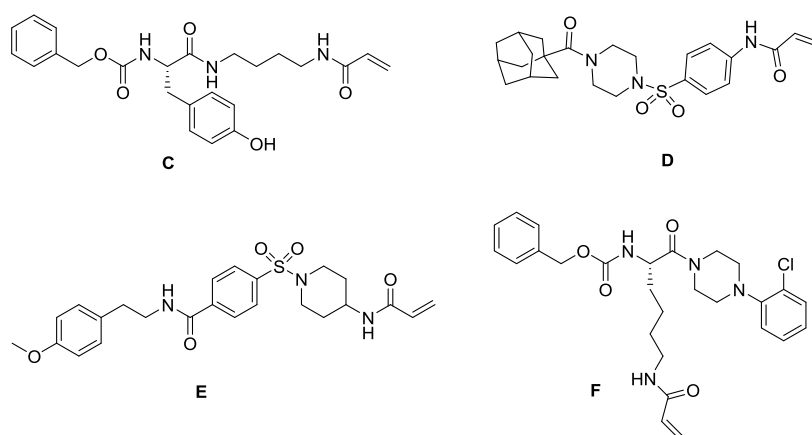
Acivicin is a natural product that is known to inhibit several cysteine-dependent enzymes. The scaffold 3-halo-4,5-dihydroisoxazole showed to be able to alkylate the active site cysteine of two bacterial glutamine amidotransferases<sup>32</sup>. A number of TG2 inhibitors structurally containing the 3-halo-4,5-dihydroisoxazole warhead have been developed. In particular, Khosla group synthesized a large series of 3-bromo analogs where the electrophilic warhead is linked to a Cbz moiety through a peptidic spacer. The dihydroisoxazole compounds were assayed against recombinant human TG2 using an enzyme-coupled assay, where glutamate dehydrogenase was used to couple ammonium ion, a product of the TG2-catalyzed reaction. The most potent derivative was compound **B**, which showed high specificity for human TG2 but essentially no reactivity toward physiological thiols, and exhibited good oral bioavailability in mice<sup>33</sup>. Importantly, compound **B** showed excellent synergism with antitumor drug carmustine, against refractory glioblastoma in mice, through a mechanism that involves disruption of fibronectin assembly in extracellular environment<sup>34</sup>.



- $\alpha,\beta$ -unsaturated amide

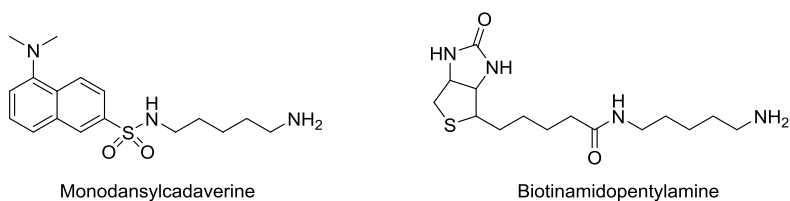
$\alpha,\beta$ -unsaturated amide, termed “Michael acceptors”, have been used to inhibit many cysteine proteases showing good outcome<sup>35</sup>. Keillor and coworkers synthesized novel TG2 irreversible inhibitors by attaching an  $\alpha,\beta$ -unsaturated amide to the typical Cbz-Phe scaffold and varying the chain length of the spacer. It was noted that a spacer length of four methylene units (compound **C**) provided a potent inhibitor with inhibitory efficiency of 42-fold more efficient than the same Cbz-Phe scaffold bearing a halo-dihydroisoxazole group<sup>31</sup>.

Compound **D** is identified as a potent TG2 inhibitor during an extensive drug-screening against the enzyme conducted by a biomedical foundation for Huntington's disease. This compound exhibited an  $IC_{50}$  of 10nM against recombinant human TG2 and showed an enormously higher selectivity against other TG isoforms, such as FXIIIa, TG6, TG1 and TG3<sup>36</sup>. Low plasma stability of compound **D** led to the development of two newer compounds (**E** and **F**) which demonstrated superior plasma stability and resistance to glutathione conjugation<sup>36</sup>.

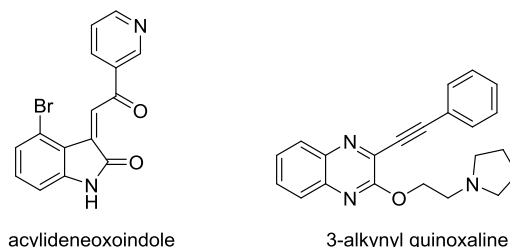


#### 1.4.2 Reversible inhibitors

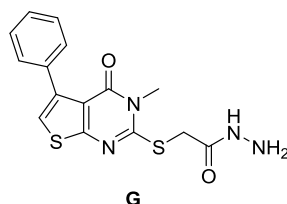
The first reversible inhibitors used in TG2 related research were amine-bearing molecules, typically characterized by a medium to long saturated aliphatic chain with a terminal amine group. Some of the most commonly used competitive amine inhibitors include putrescine, monodansylcadaverine, 5-biotinamidopentylamine and fluorescein cadaverine<sup>37</sup>. These inhibitors exert their activity by competing with the natural amine substrate in the cross-linking reaction. Thus, TG2 is still enzymatically active in the presence of competitive amine inhibitors. One compound of this class is represented by cystamine, which is a diamine capable of competitive amine inhibition through its reduced form, cysteamine<sup>38</sup>. However, lack of selectivity has been observed for cystamine, since it inhibits also the thiol-dependent protease caspase 3 and causes increased production of glutathione inside of cells<sup>39</sup>. The amine competitive inhibitors were extensively used in the early research studies on transglutaminases, although useful for *in vitro* studies, they have limited applications since the resulting aminated protein could elicit autoimmune response *in vivo*<sup>40</sup>.



Recently developed TG2 reversible inhibitors with competitive inhibition mechanisms include: 1) acylideneoxindoles derivatives, based on the structure of isatin whose analogs are widely used as reversible inhibitors of Cys-dependent proteases<sup>41</sup>; 2) 3-alkynyl quinoxaline derivatives identified through screening of 1000 small molecules as TG2 inhibitors using a cancer cell proliferation inhibition assay<sup>42</sup>.



TG2 is allosterically deactivated upon binding of guanine nucleotides, as aforementioned, thus, there has been an effort to develop reversible TG2 inhibitors targeting the GDP/GTP pocket on the enzyme. Non-hydrolysable GTP analogs, such as GTP $\gamma$ S and GMP-PCP, have been used as reversible inhibitors<sup>4</sup>. A new class of allosteric TG2 inhibitors, discovered during high throughput screening, is structurally characterized by the thieno[2,3-*d*]pyrimidin-4-one acylhydrazides backbones<sup>43</sup>. In particular, the compound **G** showed to be a slow-binding inhibitor that likely does not bind at the enzyme's active site but rather at the enzyme's GTD binding site and that was non-competitive with the standard acyl-donor and acyl-acceptor substrates<sup>44</sup>.



- *Trans*-cinnamoyl inhibitors of TG2

One of the most promising TG2 reversible inhibitors recently discovered is represented by the *trans*-cinnamoyl derivatives inhibitors. As aforementioned, starting from a comparative study between Cbz-Gln-Gly versus Boc-Gln-Gly-binding modes via molecular modeling, the group of Keillor discovered the importance of Cbz protecting group to confer active site recognition and improve affinity. Further investigation of the rigidity of the Cbz group led to the identification of *trans*-cinnamoyl derivatives as competitive and reversible inhibitors with IC<sub>50</sub> value for guinea pig liver transglutaminase as low as 18 $\mu$ M<sup>45</sup>. The enzyme inhibition assay was performed using the kinetic analysis by Michaelis-Menten equation, based on UV-visible detection of a chromogenic TG2 substrate. According to the structure-activity relationship (SAR) study, the most potent inhibitors are



divided into two subclasses, depending on the nature of the heteroaromatic substituent (HET) moiety: cinnamoyl benzotriazolyl amide and 3-substituted cinnamoyl pyridines, referred to more commonly as azachalcones. Initial SAR investigations on the aromatic scaffold of cinnamoyl moiety showed that substituents in *para* position improved the affinity with enzyme. In particular, substituents with a  $sp^2$ -hybridized oxygen, such as  $NO_2$ , BOCNH, FmocNH and  $MeO_2C$ , conferred the best inhibitory activity. While the HET moiety seemed involved in hydrogen bond connection inside the enzyme, thus, aromatic moiety possessing hydrogen bond acceptor like benzotriazolyl and pyridinyl group is mandatory for a good affinity for this series of compounds. Finally, evaluation on the importance of the length and flexibility of the linker between the two aromatic moieties showed that introduction of a supplementary conjugated alkene was detrimental to the affinity for TG2, in comparison with the cinnamic double bond. Moreover, the reduction of the alkene or replacement with methylene/ether led to a loss of activity. For the selectivity studies of this new family of TG2 inhibitors, several representative compounds were tested as inhibitors on Factor XIIIa, a transglutaminase isoform, and Caspase 3, a cysteine protease with acyl transfer mechanism similar to that of TG2. As results, most of these compounds showed a good selectivity profile, since no inhibitory effect was detected on these enzymes even at concentration approaching the limits of their solubility.

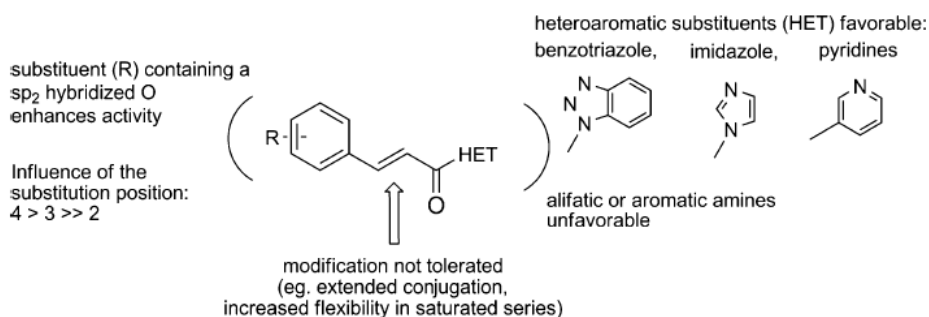
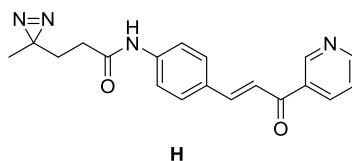


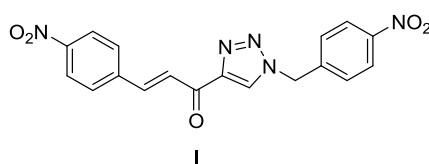
**Figure 3.** General structure of cinnamoyl derivatives and their SAR tendencies.

Subsequent labeling experiments with an azachalcone derivative (compound **H**) were performed to determine the binding mode of the cinnamoyl inhibitors<sup>46</sup>. This inhibitor with  $IC_{50} = 28\mu M$  was designed to incorporate the photolabile diazirine moiety. Photoactivation of diazirine generates diazo and carbene derivatives that react rapidly to covalently label residues in their proximity. The following LC-MS analysis indicated that Cys230 located inside the hydrophobic groove was primarily labeled. Modeling simulations suggest that Cys230 is more exposed in the “closed” conformation of TG2 rather than the “open” conformation, in agreement with the result of docking

studies. These findings suggest the hypothesis that *trans*-cinnamoyl inhibitors favorably interact with the “closed” conformation of TG2.



A more recently developed class of 4-nitrocinnamoyl triazoles by Keillor group<sup>47</sup> highlighted an inhibitor (compound I) which exhibited IC<sub>50</sub> value of 2.1 μM, representing the most potent inhibitor of this class and provided a promising scaffold for building novel TG2 inhibitors.



### 1.5 Multitarget ligands approach in drug discovery

Over the last decades, most drug discovery efforts were aimed at single-target compounds. However, not all diseases succumb to this “one disease-one target” approach. Disease systems are generally characterized by the dysregulation of multiple biological pathways and efforts of integrating the complex disease systems to drug discovery process led to a new concept, termed polypharmacology: the treatment of diseases by modulating multiple targets. Besides the approaches of drug cocktail and multicomponent drugs, the more recently consolidated strategy of polypharmacology is the development of multitarget ligands (MLs). Multitarget ligands, designated firstly by Morphy et al.<sup>48</sup>, are single chemical entities capable of modulating simultaneously multiple targets involved in a certain disease. MLs are gaining increasing attention from the drug discovery community and a plethora of multitarget ligands have been developed for the treatments of various diseases, by offering a number of potential advantages over the drug cocktail or multicomponent drugs: 1) less costly and complicate in clinical development because predicting the pharmacokinetics of a single compound is much easier than a drug cocktail; 2) improved efficacy due to the synergistic effect of simultaneously inhibiting multiple targets; 3) improved safety with reduced risk of drug-drug interactions; 4) simplified therapeutic regime and improved compliance.

### 1.5.1 Rational design of a multitarget ligand

A general drug design for MLs starts with identification of two pharmacologically relevant targets, A and B, located on complementary pathological pathways, followed by verifying the potential synergistic effect from hitting the two targets simultaneously. Afterwards, the pharmacophores responsible for binding to target A and B must be identified, and finally, the pharmacophores can be linked together in one single entity to obtain hybrid, fused or chimeric dual-target ligands.

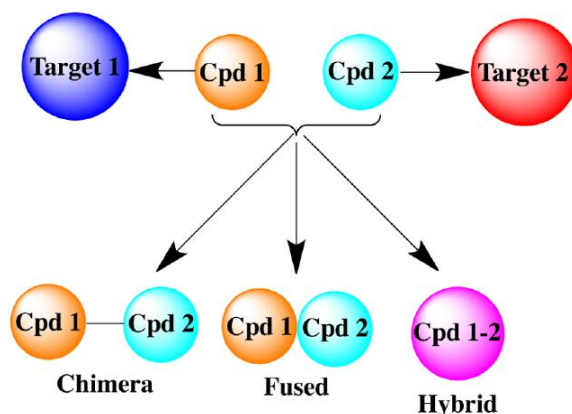


**Figure 4.** Dual-target ligand design strategy<sup>49</sup>.

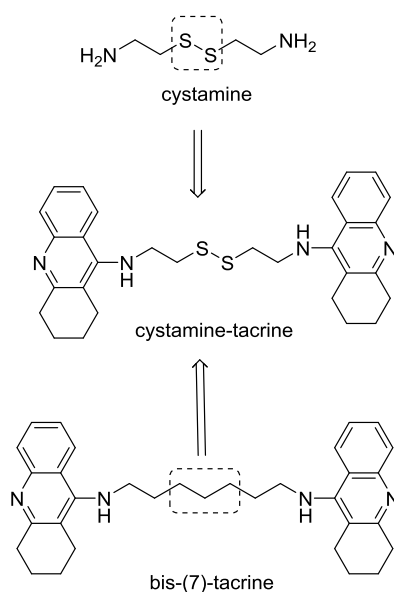
However, there are two main challenges correlated to the development of MLs. First, suboptimal physicochemical properties are frequently encountered with the MLs. In fact, MLs currently developed tend to be larger and more lipophilic than marketed drugs and are also less efficient than a broad set of preclinical compounds in terms of their binding energy per unit of molecular weight or lipophilicity, with detrimental consequences for oral bioavailability<sup>50</sup>. A recent paper from Hopkins et al. showed that there is a reverse correlation between the mean molecular weight of compounds and the total number of targets that those compounds were found to show a minimal activity. This finding suggests that smaller molecules are more likely to establish interactions with multiple biological targets<sup>51</sup>. Secondly, the lead-to-drug optimization is much more complex for multitarget compounds: the binding affinity profiles must be balanced with multiple biological targets. Therefore, the ratio of activities at the different target must be adjusted to achieve a good pharmacological profile for the MLs.

### 1.5.2. Multitarget ligands for the treatment of Alzheimer's disease

As aforementioned, AD pathogenesis involves a complex interplay of genetic and biochemical factors and is phenotypically characterized by hallmarks like A $\beta$  peptide accumulation and increased phosphorylation of the microtubule-associated tau protein. Multitarget ligands represent a promising

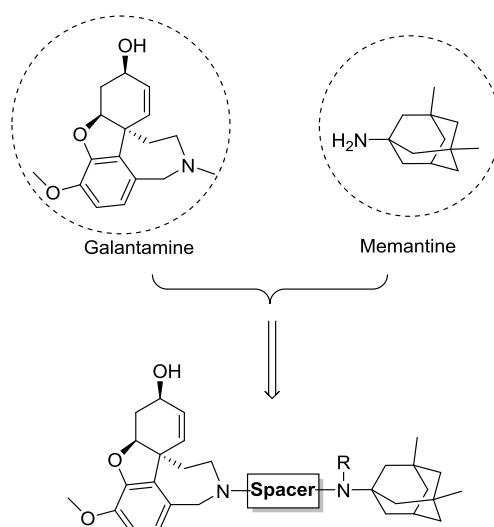
approach for the treatment of this multifactorial disease. To date, a number of MLs toward different AD's pathological targets were developed and showed interesting biological profiles. Some potential MLs for AD treatment are reported below.

The dimer bis-(7)-tacrine was one of the first homodimers reported in the literature with increased acetylcholinesterase (AChE) affinity, exhibiting a 1000-fold higher inhibitory potency compared to tacrine. The inhibitory profile is due to a simultaneous interaction with both active site and peripheral site of AChE, furthermore, the compound is capable to inhibit the AChE-induced A $\beta$  aggregation with an IC<sub>50</sub>=41.7 $\mu$ M<sup>52</sup>. Minarini and coworkers proposed modifications on the structure of bis-(7)-tacrine by replacing the aliphatic linker with cystamine, which has shown important neuroprotective properties<sup>53</sup>. The resulting dimer cystamine-tacrine was able to inhibit AChE (IC<sub>50</sub>=5.04 nM), BuChE (IC<sub>50</sub>=4.23 nM), self-A $\beta$  aggregation (IC<sub>50</sub>=24.2 $\mu$ M) and AChE-induced A $\beta$  aggregation (52.6%), exhibiting additional neuroprotective effect on SH-SY5S cell line against H<sub>2</sub>O<sub>2</sub>-induced oxidative injury<sup>54</sup>.

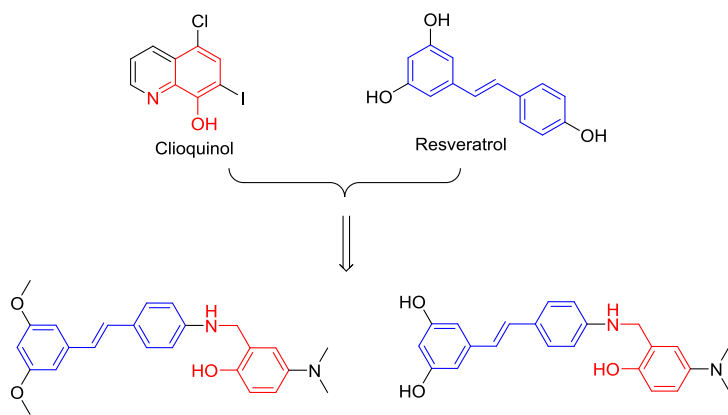


The current standard of care for AD is a combination of an AChE inhibitor with the non-competitive *N*-methyl-D-aspartate receptor (NMDAR) antagonist, memantine<sup>55</sup>. The reason for this combination therapy is that the NMDAR antagonist would stop or delay neurodegeneration, while the AChE inhibitor would improve memory and cognition by stimulating the surviving neurons. Simoni et al. combined in single new chemical entities the pharmacophoric moieties of memantine and galantamine, two marketed drugs for the treatment of AD, with the latter one being an AChE inhibitor<sup>56</sup>. The new chimera compounds were initially investigated by docking simulations based on the crystallographic structure of AChE complexed with an inhibitor. The derivatives with various

spacer lengths were then tested against AChE and NMDAR. The most potent derivative, endowed with a spacer of eight methylene units, showed an  $IC_{50}$  value of 0.52nM against AChE, albeit it turned out to be a weak binder toward NMDAR with  $IC_{50}$  in micromolar range. This series of compounds has highlighted the inherent difficulty of balancing the affinity profiles against different targets, when discovering and developing MLs. Interestingly, these molecules showed to be active also toward NMDAR containing the NR2B subunit, a receptor subunit particularly implicated in pathological process linked to overexcitation of glutamatergic pathways. Finally, several derivatives of this series exhibited a remarkable neuroprotective profile by inhibiting the NMDA-induced neurotoxicity.



Lu and coworkers<sup>57</sup> have reported some multitarget directed ligands by combining the stilbene moiety of resveratrol with clioquinol. Resveratrol, a natural product with a stilbene structure, has been shown to function as an anti-AD agent through the inhibition of A $\beta$  aggregation by scavenging oxidants and exerting anti-inflammatory activities<sup>58</sup>, while clioquinol is a well-known metal chelator which significantly decreased the rate of cognitive decline in moderately severe AD patients in a phase II clinical trial<sup>59</sup>. Two derivatives of these fused MLs exhibited significant inhibition of A $\beta$  aggregation, metal-chelating ability, disaggregation of A $\beta$  fibrils generated by self- and Cu(II)-induced A $\beta$  aggregation, antioxidant activity, acceptable MAO-A and MAO-B inhibition, moderate AChE inhibition and low neurotoxicity. One derivative of the series was able to cross the blood-brain barrier *in vitro* and did not exhibit acute toxicity in mice at doses up to 2000 mg/kg.



## 2. Dual inhibitors targeting Transglutaminase 2 and Histone Deacetylase

This chapter focuses on the development of inhibitors designed to hit simultaneously two important targets implicated in the pathogenesis of Alzheimer's disease (AD): Transglutaminase 2 (TG2) and histone deacetylase (HDAC). The role that TG2 plays in AD pathology has been elucidated in the first chapter, while HDAC, a class of enzymes importantly involved in epigenetic modification of gene expression by influencing the status of histone acetylation, has been proved to play a key role in various diseases of central nervous system (CNS), including the AD. The inhibitors were designed following the frame-combination method to achieve a multitarget activity, in particular by combination of the *trans*-cinnamoyl moiety of a potent TG2 inhibitor and the hydroxamic acid functionality, an excellent zinc chelating agent demonstrated to be responsible of HDAC's inhibition. The synthesized multitarget ligands have been evaluated for *in vitro* inhibition activity on hTG2 and all compounds of the series showed good inhibition activities towards this AD target, while the results on HDACs inhibition will be ready shortly.

### 2.1 Histone acetylation's role in the pathogenesis of Alzheimer's disease

Epigenetic processes include histone modifications (acetylation, phosphorylation, methylation, ubiquitination and ADP ribosylation), DNA methylation and gene silencing by non-coding RNAs. Histone acetylation and deacetylation regulate gene transcription by altering the chromatin structure and the accessibility to transcription factors. Levels of histone acetylation depend on the activities of histone acetylases (HATs) and histone deacetylases (HDACs), which add or remove acetyl groups from histone proteins, respectively. Although transcriptional regulation is highly complex and dynamic, in general an increase in histone acetylation causes remodeling of chromatin from a tightly packed configuration to a loosely packed one, which subsequently leads to transcriptional activation; conversely, a decrease in histone acetylation generally results in transcriptional silencing. Therefore, an upregulation of transcription can be achieved by either stimulating HATs or inhibiting HDACs.

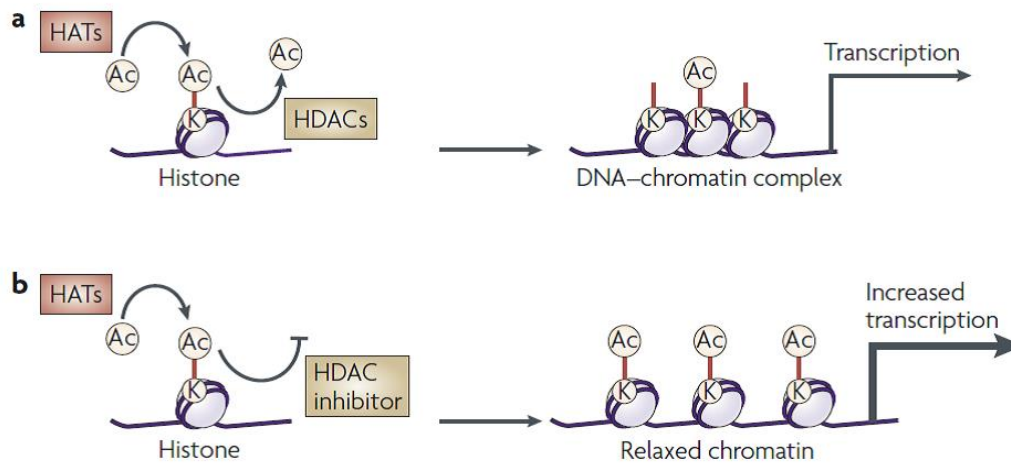


**Figure 5.** Effect of HDAC inhibitors on chromatin remodelling and transcription<sup>60</sup>.

HDACs repress transcription by removing an acetyl group from lysine residues on histone tails and thus compacting chromatin. In addition, a number of non-histone cellular proteins are substrates for HDACs, which mediate diverse biological functions via transcriptional-dependent as well as independent mechanisms.

Mammalian HDAC enzymes are classified into four major classes: (1) Class I HDACs contain ubiquitously expressed HDACs 1, 2 and 3, and the muscle-specific HDAC8; (2) Class II HDACs further separated into two subclasses: class IIa including HDACs 4, 5, 7 and 9 which show distinct tissue-specific patterns of expression, predominantly in muscle and heart; class IIb includes the unusual HDAC6, which deacetylates  $\alpha$ -tubulins and alters microtubule stability, and HDAC10 not yet well characterized; (3) Class III HDACs are named sirtuins and includes SirT1-7, sharing their homology sequence to the yeast Sir2; (4) The class IV enzyme HDAC11 is structurally different from the class deacetylases I and II, and its function is poorly known. Class I, II, and IV HDACs are  $Zn^{2+}$ -dependent enzymes, while Class III HDACs enzymes are dependent on nicotinamide adenine dinucleotide ( $NAD^+$ ) to carry out their catalytic functions.

The superfamily of HDACs has been recognized as an important therapeutic target for a broad range of human diseases, particularly for cancer treatment. More recently, increasing studies point out another important application of HDAC-based therapeutics: as potential treatment for human CNS disorders. Genetic evidences suggest crucial roles for HDACs and HATs in the maintenance of CNS homeostasis and a possible correlation between mutations in gene encoding histone-binding proteins and neurological disorders. In fact, HDAC inhibitors showed interesting results in several *in vitro* studies for the investigation of their potential therapeutic effects in CNS diseases, such as psychiatric disorders, Rubinstein-Taybi syndrome, motor-neuron disease and Huntington's disease<sup>60</sup>. In



particular, HDACs have been correlated directly to AD in several studies. The isoform HDAC2 is widely expressed in CNS and negatively regulates memory and synaptic plasticity, it is overexpressed in the post-mortem brain samples of AD patients and its knockdown by shRNA restores the synaptic plasticity and decreases memory impairments in AD model mice<sup>61</sup>. These findings highlight the important role of HDAC2-regulated chromatin modification in regulating the synaptic plasticity and memory formation in the cognitive impairment context of AD. Furthermore, an increased HDAC6 protein level is observed in the cortices and hippocampus of AD postmortem brain samples<sup>62</sup> and reducing endogenous HDAC6 results in the restore of learning and memory deficits in AD mouse model<sup>63</sup>. The mechanism is likely correlated with the involvement of HDAC6 in tau metabolism, in fact, the selective inhibitor of HDAC6, tubacin, represses tau phosphorylation<sup>62</sup>. This enzymatic isoform has been observed to act as regulatory protein of the ubiquitin-proteasome system as well, thus, is intimately linked to the aggregation of misfolded mutant proteins which represents a hallmark of many neurological disorders<sup>64</sup>.

HDAC inhibitors exhibited neuroprotective, neurotrophic and anti-inflammatory properties, and improve neurological performance -learning and memory- in neurodegenerative disease models. Particularly, studies demonstrated that treatment with HDAC inhibitors could affect the AD pathology: 1) Sung et al. demonstrated that a mercaptoacetamide-based class II HDAC inhibitor and a hydroxamide-based class I and II inhibitor can reduce A $\beta$  levels<sup>65</sup>; 2) In an AD mice, daily injections of 4-phenylbutyrate reversed spatial memory deficits by normalizing tau hyperphosphorylation in the hippocampus without affecting A $\beta$  levels<sup>66</sup>; 3) As aforementioned, HDAC6 inhibition by tubacin reduces the protein tau phosphorylation.

## 2.2 HDAC inhibitors

Trichostatin A (TSA) is the first natural hydroxamate discovered to inhibit HDACs. The crystal structure of this inhibitor complexed with a bacterial HDAC-like protein (HDLP) illustrated the chemical structural features of the HDAC catalytic core, as well as the configuration of interaction inhibitor-enzyme. According to the revealed structure, the active site of HDAC consists of a tubular pocket, a zinc-binding site and two Asp-His charge-relay system. TSA binds the enzyme by inserting its long aliphatic chain into the HDLP pocket making multiple contacts to the tube-like hydrophobic portion of the pocket. The hydroxamic acid group coordinates the zinc in a bidentate fashion resulting in a penta-coordinated Zn<sup>2+</sup>, while the aromatic dimethylamino-phenyl group of the TSA chain makes contacts at the pocket entrance capping the pocket<sup>67</sup>. The human HDACs crystal

structures has been revealed later and its structural analysis showed the common active site features in agreement with the ones observed in bacterial HDLP.

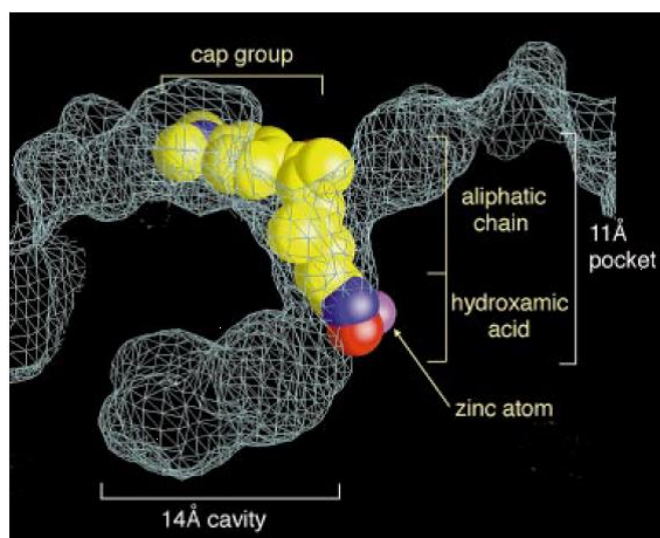


**Figure 6.** Representation of TSA in the active-site of HDLP<sup>67</sup>.

Generally, the pharmacophore of HDAC inhibitors is composed of three regions: a ‘cap’ region or ‘surface recognition domain’, which occludes the entrance of the active site pocket; a ‘zinc-binding group’ which chelates the zinc ion in the active site and is required for catalytic function; and a ‘linker’ region, which connects the two moieties.

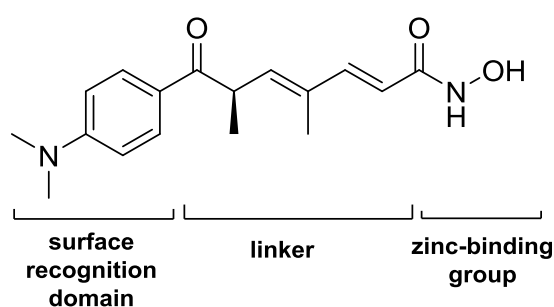


**Figure 7.** TSA and general structural illustration of HDAC inhibitors.

HDAC inhibitors can be divided into several classes based on the chemical structures: hydroxamates, benzamides, aliphatic acids and cyclic peptides.

- *Hydroxamates*. The most important compounds of this class are represented by TSA and SAHA, structurally characterized by the presence of a hydroxamic acid function, which is an optimal chelating agent for  $Zn^{2+}$  present in the catalytic active site of HDACs. SAHA, or vorinostat, is a pan-inhibitor of class I, II and IV HDACs and demonstrated activity in low nanomolar range<sup>68</sup>.

It is the first HDAC inhibitor to be approved for anticancer treatment by FDA. Following SAHA, many structural analogs have been synthesized, such as Belinostat and Panobinostat.

- *Benzamides*. This class includes two derivatives, Mocetinostat and Etinostat (MS275), both achieved in clinical trials. The former one is a class I and IV HDACs inhibitor, while the latter is a selective inhibitor for class I.
- *Aliphatic acids*. Valproic acid and phenylbutyrate belong to this class and are relatively weak inhibitors of the HDACs with activity in millimolar range.
- *Cyclic peptides*. The only member of this class is represented by Romidepsin, a natural product which showed to be active at nanomolar concentrations, and was approved as anticancer agent.

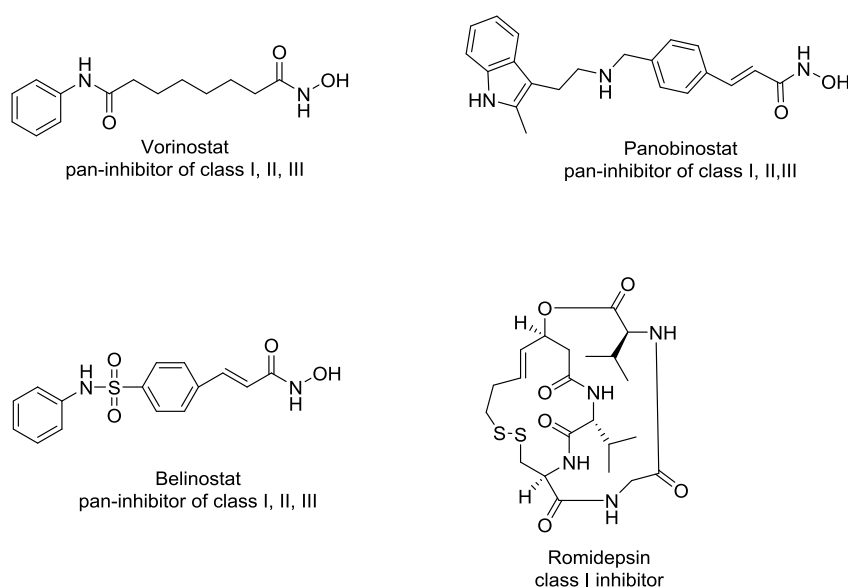


**Figure 8.** FDA approved HDACs inhibitors.

An important drawback of most HDAC inhibitors is the lack of isoform-selectivity, which makes it difficult to determine whether the biological outcome is due to inhibition of a specific HDAC or by inhibition on multiprotein complexes, besides the undesirable clinical effects due to off-target activity. Hence, new trend in the field of HDAC inhibitor drug discovery is the development of isoform-specific HDAC inhibitors, and to date, a handful of these selective inhibitors has emerged.

**Table 1.** Isoform-specific HDAC inhibitors.

HDAC inhibitor	Specificity	Stage	Diseases
Compound 60	HDAC1,HDAC2	Preclinical	Neurology
MRLB-223	HDAC1,HDAC2	Preclinical	Cancer
RG2833; 109	HDAC3	Phase I trial	Friedreich's ataxia
RGFP966	HDAC3	Preclinical	Cancer, neurology
BG45	HDAC3	Preclinical	Cancer
Rocilinostat (ACY-1215)	HDAC6	Phase IIa trial	Cancer
ACY-738, ACY-775	HDAC6	Preclinical	Neurology
Tubacin	HDAC6	Preclinical	Cancer
Tubastatin A (tubastatin)	HDAC6	Preclinical	Inflammation, neurodegeneration
C1A	HDAC6	Preclinical	Cancer
HPOB	HDAC6	Preclinical	Cancer
Quinazolin-4-one derivatives	HDAC6	Preclinical	Alzheimer's disease
PCI-34051	HDAC8	Preclinical	Cancer
C149	HDAC8	Preclinical	Cancer
Jδ	HDAC8	Preclinical	NA
BRD73954	HDAC6,HDAC8	Preclinical	NA

### 2.3 Drug design

AD pathogenesis involves a complex interplay of genetic and biochemical factors and a therapy aimed at hitting diverse pathological pathways is strongly recommended. Given the evidences that both transglutaminase 2 and HDACs play important role in the pathology of AD and both overexpressed in this neurodegenerative disease, inhibition of these two enzymes could produce additive or synergic amelioration of the pathology. This hypothesis is supported by a study (unpublished results) which demonstrated that treatment with Vorinostat and cystamine on neuronal cells results in a synergic neuroprotective effect against excitotoxicity induced by glutamate; additionally, according to a study on Huntington's disease (HD), combinatorial treatment of SAHA, cystamine and Congo red improved survival of *Drosophila* HD model<sup>69</sup>. Therefore, the aim is to apply the 'multitarget ligands' approach to develop an inhibitor active on both two biological targets, through combination of pharmacologically important fragments for each target to give a single chemical entity.

To the purpose of designing a TG2-HDAC dual inhibitor, we selected a potent TG2 inhibitor bearing the *trans*-cinnamoyl structure, the compound **1**, which was found to be a reversible competitive inhibitor with  $IC_{50}=28\mu M$ . According to the structure-activity relationship studies, the large substituents on the cinnamoyl aromatic ring in the *para* position gave the best results<sup>46</sup>. Thus, by replacing this substituent on compound **1** with an aliphatic chain bearing hydroxamic acid, the zinc

chelating group responsible of HDACs inhibition exhibited by Vorinostat, we designed a series of new compounds **2-4** where the two fragments are connected through a linker.

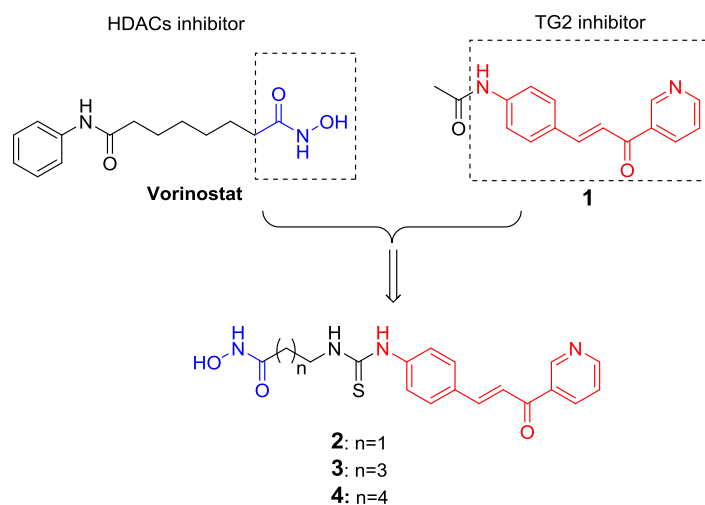


**Figure 9.** Drug design of compounds **2-4**.

The conjugates **2-4** are structural analogs with difference in the linker length, which is composed of 2, 4 and 5 methylene units, respectively, along with a thiourea bond, chosen for the reason of synthetic accessibility. The derivative characterized by three methylene units as linker was designed as well, but the chemical synthesis could not be accomplished despite numerous synthetic attempts. We postulated that these new chemical conjugates would maintain inhibition activity on HDACs and TG2 by the reason of the presence of both pharmacophores; additionally, we assume that the bulky *trans*-cinnamoyl moiety would serve as ‘surface recognition group’ for HDACs, allowing favorable orientation of hydroxamic acid inside the active site pocket.

## 2.4 Methods

Compounds **2-4** were synthesized and studied in *in vitro* inhibition assays on TG2, while the inhibition activities on HDACs are still under investigation. According to the preliminary data, the compounds showed good inhibition activities on TG2 in an assay conducted on human recombinant transglutaminase 2 using a chromogenic donor substrate.

### 2.4.1 Synthetic methods

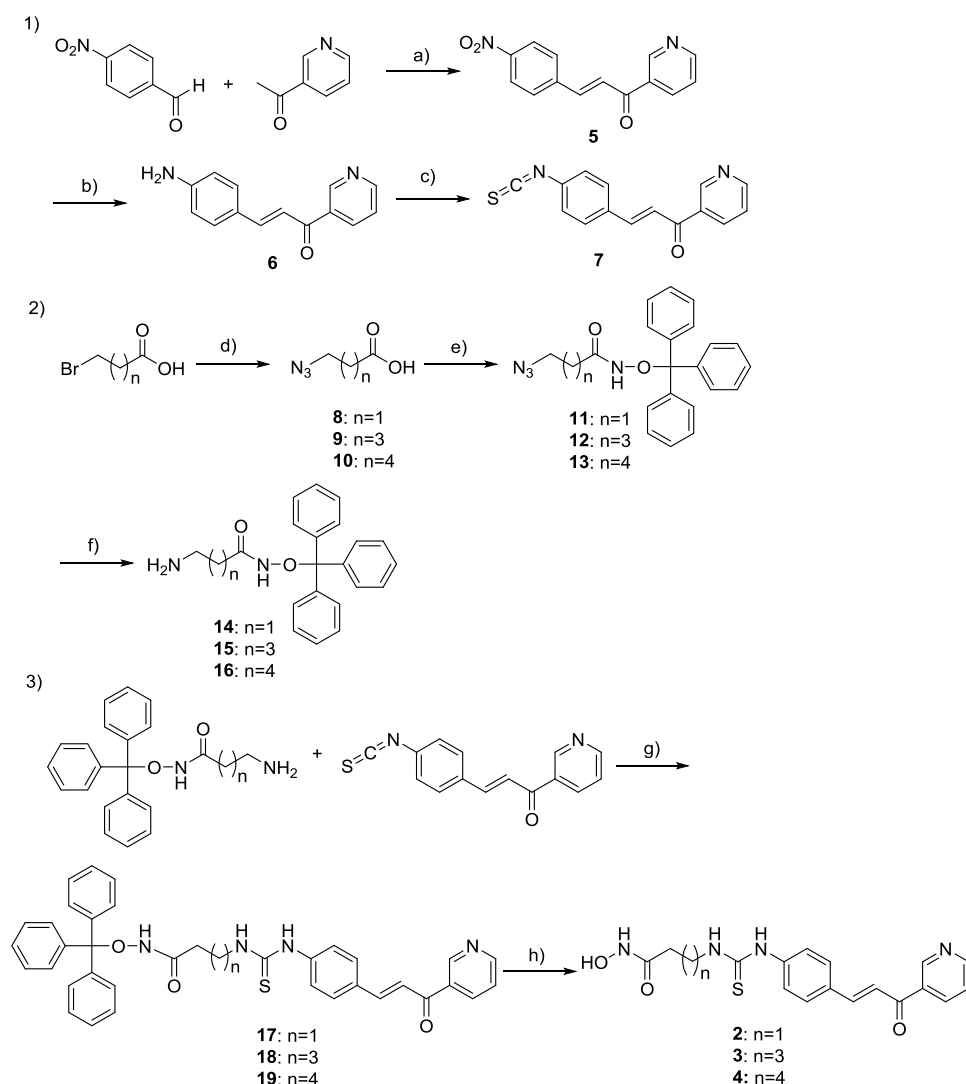
The compounds **2-4** were synthesized following the scheme 1: The *trans*-cinnamoyl moiety was synthesized starting from an aldol condensation reaction between 3-acetylpyridine and *para*-nitro substituted benzaldehyde in basic conditions to give compound **5**, followed by reduction of nitro

group into the correspondent amine using Tin(II) chloride to afford compound **6**. The amine group was then transformed into isothiocyanate (compound **7**) by reacting with 1,1'-Thiocarbonyldi-2(*1H*)-pyridone.

For the synthesis of the aliphatic chain bearing hydroxamic acid, commercially available bromo-alkyl carboxylic acids were subjected to nucleophilic substitution to replace the halogen with azide group by reacting with sodium azide to give compounds **8-10**. Afterwards, the carboxylic acid was reacted with O-Tritylhydroxylamine in a coupling reaction to give the correspondent protected hydroxamic acids **11-13**. The azide group was then converted to amine through Staudinger reaction using triphenylphosphine.

The two moieties were finally linked together in a coupling reaction where the electrophilic carbon of isothiocyanate reacts with the nucleophilic amine to form a thiourea bridge connecting the two fragments.

Finally, the trityl group of hydroxamic acid was cleaved in acidic conditions in the presence of triethylsilane as scavenger to afford the final products **2-4**. The derivative characterized by a linker of three methylene units was not obtained despite numerous synthetic attempts.



**Scheme 1.** a) KOH, MeOH/H<sub>2</sub>O, 30min, r.t.; b) SnCl<sub>2</sub>, EtOH, 30min, 70°C; c) 1,1'-Thiocarbonyldi-2(1H)-pyridone, DCM, overnight, r.t.; d) NaN<sub>3</sub>, DMF, 5h, reflux; e) O-Triptylhydroxylamine, IBCF, NMM, THF, 2h, r.t.; f) PPh<sub>3</sub>, DCM, overnight, r.t.; g) DCM, overnight, r.t.; h) TFA, Et<sub>3</sub>SiH, r.t., 30 min.

#### 2.4.2 *In vitro* TG2 inhibition assay

According to a study conducted by Keillor group, TG2 reacts with *N*-Cbz-Glu( $\gamma$ -p-nitrophenylester)Gly, a TG2 acyl-donor substrate analog, to undergo rapid acylation that can be followed spectrophotometrically at 400nm. The inhibition activity of the synthesized compounds **2-4** was evaluated using this method on human recombinant TG2. The IC<sub>50</sub> values were determined based on the inhibition of the enzymatic reaction of 2.2mM of *N*-Cbz-L-Glu( $\gamma$ -p-nitrophenylester)Gly with 0.5mU of human recombinant TG2.

Briefly, kinetic runs were recorded at 25°C on a UV-visible spectrophotometer at 405nm, in a buffer composed of 3-(*N*-morpholino)propanesulfonic acid (MOPS, pH = 7.0), CaCl<sub>2</sub> and EDTA. Each kinetic assay was performed using 180 $\mu$ L buffer, 5 $\mu$ L of a DMSO stock solution of substrate *N*-Cbz-

Glu( $\gamma$ -p-nitrophenylester)Gly, 10 $\mu$ L of a solution of hTG2 and 0 to 5 $\mu$ L of a DMSO stock solution of inhibitor. IC<sub>50</sub> values were obtained as the negative x-intercept of a Dixon plot.

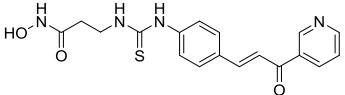
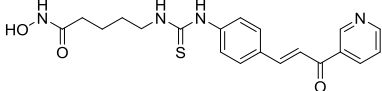
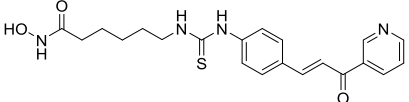
## 2.5 Results and discussions

The test compounds were subject to preliminary studies for *in vitro* evaluation of the inhibition activity on hTG2 enzymatic function and the IC<sub>50</sub> values are reported in Table 2.

From an analysis of the results, the compound **3** exhibited the best activity with IC<sub>50</sub>=13 $\mu$ M. Among the class of *trans*-cinnamoyl inhibitors, endowed with a competitive reversible mechanism of inhibition, the IC<sub>50</sub> for the most potent inhibitor was determined to be 2.1 $\mu$ M. This inhibitor belongs to the subclass of cinnamoyl-triazoles (see chapter 1); while the best inhibitor of the subclass of cinnamoyl-pyridine showed an IC<sub>50</sub> value of 21 $\mu$ M, as reported in literature. All three synthesized derivatives **2-4** of the series are characterized by cinnamoyl-pyridine structure, and showed a good TG2 inhibition activity. In particular, the compound **3** could be considered the most potent cinnamoyl-pyridine inhibitor reported so far in literature.

The structural difference within this series of compounds resides in the chain length of the linker. An observation on inhibition potency of these compounds could drive to the conclusion that the presence of a bulky moiety in *para* position on the aromatic ring is not harmful in terms of inhibition activity, in agreement with observations reported in literature. Furthermore, the results show that the chain length can affect the inhibitor's activity and the derivative with four methylene units probably fits better than other analogs in the active site of the TG2 enzyme.

**Table 2.** IC<sub>50</sub> values of the TG2 inhibitors **2-4**.

Compound	Structure	IC <sub>50</sub> ( $\mu$ M)
<b>2</b>		24.3 $\pm$ 1.2
<b>3</b>		13.3 $\pm$ 1.5
<b>4</b>		22.1 $\pm$ 2.0



## 2.6 Conclusions

The series of derivatives **2-4** were designed to be dual inhibitors targeting simultaneously HDACs and TG2, by incorporating the *trans*-cinnamoyl fragment for TG2 inhibition and hydroxamic acid moiety for the inhibition of HDACs.

At the time of edition for the present manuscript, we cannot elaborate final conclusions. However, preliminary *in vitro* data showed that the compounds of this series are good TG2 inhibitors. The best inhibitor was compound **3**, which exhibited an IC<sub>50</sub> value of 13μM and could be the most potent inhibitor within the subclass of *trans*-cinnamoyl pyridines currently developed and reported. The mode of inhibition of these compounds is currently under investigation; while studies on the inhibition activity on HDACs are in progress.

### **3. *Trans*-cinnamoyl structure based transglutaminase 2 inhibitors with potential antioxidant activities**

Oxidative stress is one of the key factors in the AD's pathology, and among various cell damage mechanisms, it promotes A $\beta$  toxicity and increases tau hyperphosphorylation where the enzyme GSK3 $\beta$  could be involved in the pathological mechanisms. Natural antioxidants like hydroxycinnamic acids, including caffeic acid, ferulic acid etc., exert neuroprotective activities against neuronal cell damage induced by oxidative stress. Based on the *trans*-cinnamoyl structure which is essential for TG2 inhibition, addition of hydroxyl groups on the aromatic ring allowed the obtainment of a series of compounds designed as 'fused' multitarget ligands, which could be TG2 inhibitors and at the same time antioxidant agents. *In vitro* antioxidant evaluation outlined one compound of the series as a good antioxidant and endowed with interesting biological activity toward A $\beta$  self-aggregation process and GSK3 $\beta$  enzyme activity. Against expectation, the slight structural modifications determined an almost complete loss of inhibition toward TG2.

#### **3.1 Oxidative stress in Alzheimer's disease**

Oxidative stress is a mechanism of cell damage characterized by excessive production of highly reactive free radicals. It is the result of an imbalance in pro-oxidant/antioxidant homeostasis, which leads to the generation of toxic reactive oxygen species (ROS). The instability of free radicals is due to the presence of an unpaired electron on the outer orbital. This is responsible for the high reactivity of these species. ROS can potentially react with many cellular components including lipids, proteins and DNA, resulting in impaired cellular functions and formation of toxic species, such as peroxides, aldehydes and cholesterol oxide.

Unsaturated lipids are particularly susceptible to oxidative modification and lipid peroxidation is a sensitive marker of oxidative stress. Lipid peroxidation, which is the result of the attack by radicals on the double bond of unsaturated fatty acids, generates lipid peroxy radicals which initiates a chain reaction and breakdown products such as 4-hydroxy-2,3-nonenal (HNE), acrolein and malondialdehyde, molecules highly toxic for cells and all increased in neurodegenerative models<sup>70</sup>. The excessive production of ROS leads to dysregulation of intracellular calcium signaling and such dysregulation has been widely observed in neurodegenerative diseases<sup>71</sup>. One of the downstream events that occurs in response to an ROS-induced calcium influx is an excitotoxic response<sup>72</sup>, that is activation of glutamate receptors that triggers a cascade of events leading to cell death. Excitotoxic

response has been implicated in several neurological conditions as well as neurodegenerative diseases such as AD, Parkinson Disease (PD) and Huntington's disease<sup>73</sup>.

The neurons are particularly susceptible to oxidative stress for several reasons. The first one is that the membrane of neuron cells contains elevated amount of unsaturated fatty acids, which are excellent substrate for the lipid peroxidation chain reactions; the second one, is that neuronal functions require a large amount of energy generated through oxidative phosphorylation reactions; the third one, is that the brain is an organ that concentrates metal ions, such as copper and iron. Therefore, the vulnerability of neuron cells to the oxidative stress is strongly related to the pathogenesis of neurodegenerative diseases.

### *3.1.1 Metal ions and A $\beta$ toxicity*

The hypothesis that oxidative stress could be an important factor to AD's pathogenesis and progression is widely accepted. A support to this hypothesis is the correlation found to exist between metal ions and amyloid- $\beta$  peptide (A $\beta$ ).

As a general principle, the chemical origin of the majority of ROS is the reaction of molecular oxygen with the redox-active metals, copper and iron. The ability of these metal ions of initiating redox cycling and activating molecular oxygen is the basis of function for most of enzymes.

A $\beta$  is the major component of amyloid plaques and studies showed that there were remarkably high concentrations of Cu, Zn and Fe in the amyloid deposit in AD-affected brains<sup>74</sup>. The cause of the neuronal cell loss in AD might be related to oxidative stress from excessive free-radical generation and the major source of oxidative stress in the brain of AD is likely the transition metals Cu and Fe when bound to A $\beta$ <sup>75</sup>. According to a study by Opazo et al., when Cu<sup>2+</sup> or Fe<sup>3+</sup> coordinate A $\beta$ , extensive redox chemical reactions take place that reduce the oxidation state of both metals and produce H<sub>2</sub>O<sub>2</sub> from O<sub>2</sub> in a catalytic manner<sup>76</sup>. The formal reduction potential of Cu<sup>2+</sup> to Cu<sup>+</sup> by A $\beta$ <sub>42</sub> is highly positive and typical of strongly reducing cupro-proteins. The toxicity of A $\beta$  against neuronal cells is enhanced by the presence of Cu, which is usually present in culture media. A $\beta$  possesses histidine residues at positions 6, 13 and 14 forming a structural element that enable A $\beta$  to coordinate transition metal ions<sup>77</sup>; in fact, studies confirmed that histidine is the principal site of metal coordination.

### *3.1.2 Tau hyperphosphorylation and oxidative stress*

Tau hyperphosphorylation appears to be a critical event leading to abnormal aggregation and disrupted function of tau in affected AD neurons. As a prominent early event during AD

pathogenesis, oxidative stress is believed to have important connections with tau phosphorylation and the formation of neurofibrillary lesions.

Several studies performed on cellular or animal models of tau pathology have established that overexpression of mutant forms of human tau increases both expression of oxidative markers and the sensitivity of neurons to oxidative molecules. In fact, following overexpression of wild-type tau in a neuroblastoma cell line, an increased susceptibility to H<sub>2</sub>O<sub>2</sub> was observed<sup>78</sup>. Furthermore, using transgenic mice carrying human tau<sup>P301L</sup> protein, biochemical analysis showed an increased ROS production and lipid peroxidation in the brain, elevated activities of antioxidant enzymes and evidence of mitochondrial dysfunction<sup>79</sup>. In another mice model expressing human tau<sup>P301S</sup> protein, tau hyperphosphorylation and tangle formation were detected and associated with GSK3β activation. In these mice, also elevated protein carbonyl levels, an indicator of protein oxidation, were detected in the brain<sup>80</sup>. These studies establish that expression of tau mutants in animal models induces oxidative stress in neurons.

From the other hand, there are evidences suggesting that accumulation of ROS can directly stimulate tau hyperphosphorylation and aggregation. 4-hydroxy-2-nonenal (HNE), a product of lipid peroxidation, facilitates aggregation of phosphorylated tau *in vitro*<sup>81</sup> and induces tau hyperphosphorylation<sup>82</sup>. Also oxidized fatty acids have been shown to stimulate tau polymerization *in vitro*<sup>83</sup>. However, the mechanism by which oxidative stress affects tau phosphorylation remains in discussion. GSK3β, a serine/threonine kinase, is involved in tau hyperphosphorylation. Lovell et al. reported that the treatment of primary rat cortical neuron cultures with a combination of cuprizone, a copper chelator, Fe<sup>2+</sup> and H<sub>2</sub>O<sub>2</sub> significantly increased GSK3β activity and pathologic tau hyperphosphorylation. Treatment of the same cultures with LiCl, an inhibitor of GSK3β, remarkably decreased abnormal tau phosphorylation, suggesting that GSK3β could be the enzyme involved in tau hyperphosphorylation in oxidative conditions<sup>84</sup>. Moreover, treatment of neuronal cells exposed to H<sub>2</sub>O<sub>2</sub> with GSK3β inhibitors protected the cells against oxidative stress. By contrast, higher concentrations of the same inhibitors induce opposite effects<sup>85</sup>.

These studies suggest that GSK3β plays important roles in tau pathologies and mild inhibition of its activity may prevent tau phosphorylation induced by oxidative stress.

### **3.2 Cinnamic acid derivatives as antioxidants**

Polyphenols are naturally occurring compounds found largely in the fruits, vegetables, cereals and beverages. They are secondary metabolites of plants and are generally involved in defense against ultraviolet radiation or aggression by pathogens. They consist of a large variety of molecules, but most of these compounds arise from a common structural origin: the amino acids phenylalanine or

tyrosine. Biosynthesis through the phenylpropanoid pathway produces the large variety of the plant polyphenols, including cinnamic acids, benzoic acids, flavonoids, proanthocyanidins, coumarins, stilbenes and lignans.

Dietary polyphenols are thought to be beneficial for human health by exerting various biological effects, such as free-radical scavenging, metal chelating, modulation of enzymatic activity and alteration of signal transduction pathways<sup>86</sup>. Epidemiological studies have shown some relationships between consumption of polyphenol-rich foods and prevention of diseases, such as cancer, coronary heart disease, diabetes and neurodegenerative diseases<sup>87</sup>.

### 3.2.1 General antioxidant mechanisms of polyphenols

In the last decade, polyphenols are subject of increasing scientific interest because of their beneficial effects on human health. Their antioxidant properties are the most widely investigated therapeutic activity<sup>88,87</sup>.

The chemical structure of polyphenols confers them the ability to act as free radical scavengers. In fact, phenolic hydroxyl groups are good hydrogen donors, thus, can react with reactive oxygen and reactive nitrogen species<sup>89</sup> in a termination reaction, which breaks the cycle of generation of new radicals. Following interaction with the initial reactive species, a radical form of the antioxidant-phenoxyl radical is produced, having a much greater chemical stability than the initial radical. The interaction of the hydroxyl groups of phenolics with the  $\pi$ -electrons of the benzene ring allows the free radical to be stabilized by delocalization.

The antioxidant capacity of phenolic compounds is also attributed to their ability to chelate metal ions<sup>90</sup>, such as iron, a redox-active metal that catalyzes free radicals formation. Other authors refer to the inhibition of oxidases, such as lipoxygenase (LO), cyclooxygenase (CO), myeloperoxidase (MPO), NADPH oxidase and xanthine oxidase (XO)<sup>91</sup>, as important mechanisms for avoiding the generation of higher amounts of ROS *in vivo*, as well as organic hydroperoxides.

On the other hand, to date, a number of polyphenols, such as quercetin, myricetin, kaempferol and caffeic, chlorogenic and ferulic acids, have been reported to possess also pro-oxidant activity<sup>92</sup>. However, it is recognized that the pro-oxidant activity of natural polyphenols has a more specific preference against certain cellular targets and appears to play a role in the prevention of certain types of cancer<sup>93</sup>.

### 3.2.2 Classes of polyphenols

Polyphenols can be sub-classified into four main groups: flavonoids, phenolic acids, stilbenes and lignans.

Flavonoids comprise the most studied group of polyphenols. This group has a common basic structure consisting of two aromatic rings (ring A and ring B) bound together through a three carbon chain that form a closed pyran ring (ring C). More than 4000 varieties of flavonoids have been identified, many of which are responsible for the attractive colors of the flowers, fruits and leaves and constitute a protection from UV radiation. Based on the variation in the type of heterocycle involved, flavonoids may be divided into six subclasses: flavonols, flavones, flavonones, flavanols, anthocyanins and isoflavones. Flavonoids became the subject of medical research and have been reported to possess many beneficial properties, including antioxidant, anti-inflammatory, antimicrobial, antiviral, antiallergic, anticancer activity<sup>94</sup>.

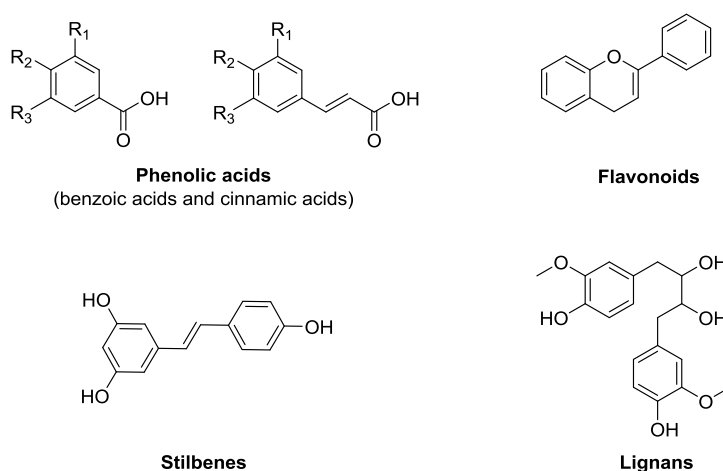


**Figure10.** Chemical structures of different classes of polyphenols.

Stilbenes contain two phenol moieties connected by an ethene bridge. Occurrence of stilbenes in the human diet is quite low. Most stilbenes in plants act as antifungal response to infection or injury. One of the best studied naturally occurring polyphenol stilbene is resveratrol, found largely in grapes and extensively studied for its antioxidant activity<sup>95</sup>. While lignans are diphenolic compounds that contain a 2,3-dibenzylbutane structure that is formed by the dimerization of two cinnamic acid residues, and linseed represent the richest dietary source. Several lignans are considered to be phytoestrogens.

The class of phenolic acids are found abundantly in foods, and divided into two subclasses: benzoic acid derivatives and cinnamic acid derivatives. The hydroxybenzoic acids have generally low concentration in plants with exception of certain red fruits, black radish and onions<sup>96</sup>. The cinnamic acid derivatives are presently more abundantly in plants and generally are more efficient as antioxidant in comparison with their benzoic counterparts. They are biosynthesized from L-phenylalanine via deamination by phenylalanine ammonia-lyase (PAL). Among the most well-

known hydroxycinnamic acids, there are caffeic acid, ferulic acid, chlorogenic acid and *p*-coumaric acid, as well as some esterified forms such as caffeic acid phenethyl ester and ferulic acid phenethyl ester.

### 3.2.3 Antioxidant activity of hydroxycinnamic acids

Over the past decades, the antioxidant property of hydroxycinnamic acids was extensively investigated and some structure-activity relationships were already published.

Caffeic acid is the most predominant phenolic acid in sunflower seeds and it demonstrated high inhibition efficiency on lipid oxidation in studies that investigated the antioxidant and free radical scavenging properties of six natural hydroxycinnamic acid compounds using three different evaluation models: Rancimat method, 1,1-diphenyl-2-picrylhydrazyl (DPPH) scavenging model and oil-in-water emulsion system<sup>97</sup>. Some researchers reported that the thermal decomposition products of caffeic acid showed antioxidative activity stronger than caffeic acid itself<sup>98</sup>.

Chlorogenic acid is an ester formed between caffeic acid and quinic acid. It is widespread in plants and the level in coffee beans is elevated constituting up to 10% of the weight. Although chlorogenic acid is considered as an antioxidant, it demonstrated less activity than its metabolite, caffeic acid<sup>97</sup>. The uptake of chlorogenic acid by mucosal cells is much less than that of caffeic acid and the protective effect by the two compounds is almost the same. This finding suggests that the antioxidant activity of chlorogenic acid derives from the fraction of caffeic acid hydrolyzed in intestine as reported in a study on protective effect of chlorogenic acid and caffeic acid against ischemia/reperfusion injury carried out in the rat small intestine<sup>99</sup>.

Ferulic acid occurs widely in grain foods and vegetables. Phenethyl esters of caffeic acid and ferulic acid are the major components in honeybee propolis, a folk medicine used as anti-inflammatory agent for centuries. Ferulic acid showed a lower antioxidant activity in comparison with other hydroxycinnamic acids, like caffeic and sinapic acid. Additionally, alkyl ferulates showed the same activity against DPPH radical but their activity was lower in comparison with ferulic acid. Whereas in other methods using ethanol-buffer system and liposome system, esters of ferulic acid resulted more active than ferulic acid<sup>100</sup>.

*p*-Coumaric acid is another hydroxycinnamic derivative which demonstrated to be capable of scavenging OH radicals and reducing low-density lipoprotein (LDL) peroxidation, according to a study on the antioxidant mechanisms of this compound<sup>101</sup>. This study investigated whether *p*-coumaric acid (CA) could act as a direct scavenger of reactive oxygen species and whether it could minimize the oxidation of LDL. *In vitro* electron spin studies were conducted to determine the ability for CA of scavenging ROS and altering LDL oxidation. CA effectively scavenged OH in a dose-

dependent manner with IC<sub>50</sub> for ·OH scavenging of 4.72 mM. CA was administered to rats and levels of 8-epiprostaglandin F<sub>2a</sub> were monitored as a LDL oxidation marker. The results showed that oral administration for 30 days significantly inhibited LDL oxidation.

According to SAR studies, with regard to the aromatic substitution, the order of effectiveness of antioxidant activity within the class of hydroxycinnamic acids was: *p*-hydroxydimethoxy > dihydroxy > *p*-hydroxy methoxy > *p*-hydroxy. The increase of methoxy groups or the catechol structure substantially increased the antioxidant activity of the compounds by further stabilizing the phenoxyl radical. The antioxidant capacity of phenols is ascribed to the formation of resonance-stabilized phenoxyl radicals after reacting with oxidants<sup>102</sup>. This activity is strengthened by the presence of a second hydroxyl group, as in caffeic acid, by virtue of the formation of an intramolecular hydrogen bond. Moreover, in the case of Cu(II)-catalyzed oxidation, only the presence of two hydroxyl groups in *ortho* position can allow the formation of Cu(II)-phenolic acid complex, resulting in a chelating effect towards the metal<sup>103</sup>.

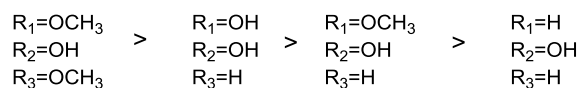
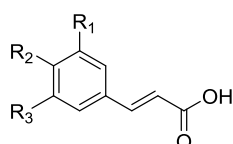


**Figure 11.** General structure-activity relationships for hydroxycinnamic acids.

Most of the hydroxycinnamic acids exhibit neuroprotection activities. Ferulic acid provided neuroprotection against oxidative stress-related apoptosis following cerebral ischemia/reperfusion injury in rats<sup>104</sup>; also, it showed to regulate positively the expression level of  $\gamma$ -enolase, a neuron-specific enolase with neuroprotective effect, in brain injury and glutamate exposure-induced neuronal cell death<sup>105</sup>. Caffeic acid was demonstrated to exert protective effect against hydrogen peroxide-induced oxidative damage on brain tissue<sup>106</sup>.

### 3.3 Drug design

Oxidative stress is a one of the key factors in the AD's onset and progression and as explained in this chapter, it is correlated to A $\beta$  and protein tau pathways, since it promotes A $\beta$  toxicity and *vice versa*, and increases tau hyperphosphorylation, probably through a mechanism of enhancing GSK3 $\beta$



activity. Hydroxycinnamic acids are a class of phenolic acids with assessed antioxidant activity exerting neuroprotective activities against neuronal cell damage induced by oxidative stress. On the other hand, *trans*-cinnamoyl derivatives showed important inhibition activity towards transglutaminase 2, an enzyme significantly involved in AD pathogenesis, and whose expression is significantly increased in brain areas affected by AD, as described in the chapter 1. Therefore, the aim of constructing a multitarget ligand in this context can be realized by designing a chemical entity that could be a good TG2 inhibitor and at the same time endowed with antioxidant activity. Comparison between hydroxycinnamic acids and *trans*-cinnamoyl derivatives highlights a clear structural similarity- the cinnamoyl backbone; this means that it would be convenient to build a ‘fused’ multitarget ligand, where the identical fragment from two molecules is overlapped into a single molecule.

Based on the SAR studies, for TG2 inhibition, the pyridine moiety and cinnamoyl backbone are essential for the biological activity, with pyridine replaceable by a heterocyclic ring capable of hydrogen bond formation. While substituents on the benzene ring should contain a sp<sup>2</sup>-hybridized oxygen, such as NO<sub>2</sub>, BOCNH, FmocNH and MeO<sub>2</sub>C, with *para* position conferring the best activity. Concerning the hydroxycinnamic acids, the level of the antioxidant activity depends on the presence of OH groups in *ortho* position and methoxy groups, whereas esterification of the acid group confers, in some cases, a more potent antioxidant activity, suggesting that structural modification in this portion is feasible and not harmful in term of activity. Therefore, by overlapping the cinnamoyl backbone, we designed a series of derivatives **20-24** as potential *trans*-cinnamoyl TG2 inhibitors bearing antioxidant activity.

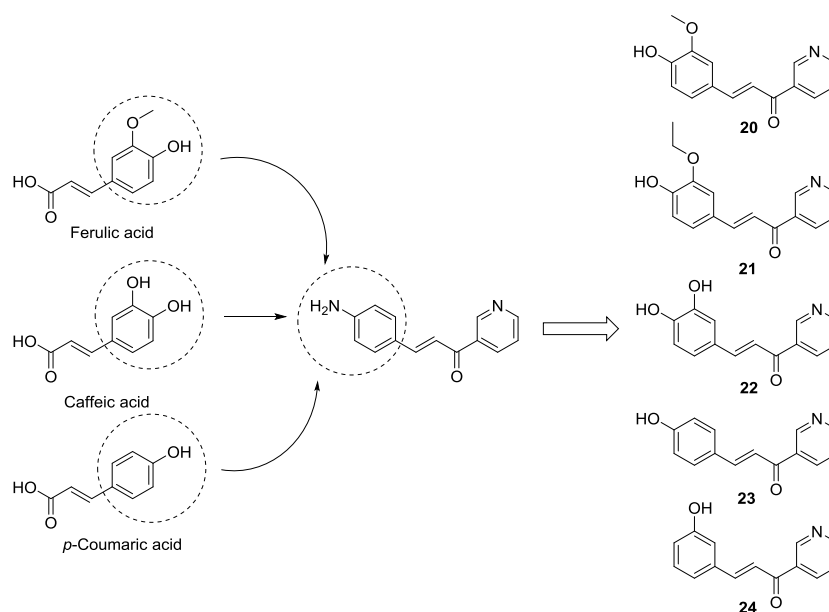


**Figure12.** Drug design of compounds **20-24**.

In particular, compounds **20** and **21** are analogs to ferulic acid where **21** presents an ethoxy group instead of methoxy. By replacing the aromatic ring with catechol moiety of caffeic acid, compound **22** was designed. Compound **23** derives from *p*-coumaric acid, whereas compound **24** is an analog with hydroxyl group in *meta* position on the benzene ring.

By designing this series of compounds, we postulate that since the *trans*-cinnamoyl structure and pyridine are unmodified, the inhibition activity on TG2 would be preserved, while inserting hydroxyl groups on benzene ring we would obtain a phenol/catechol fragment, which would additionally confer an antioxidant property to these molecules, as observed for the hydroxycinnamic acids.

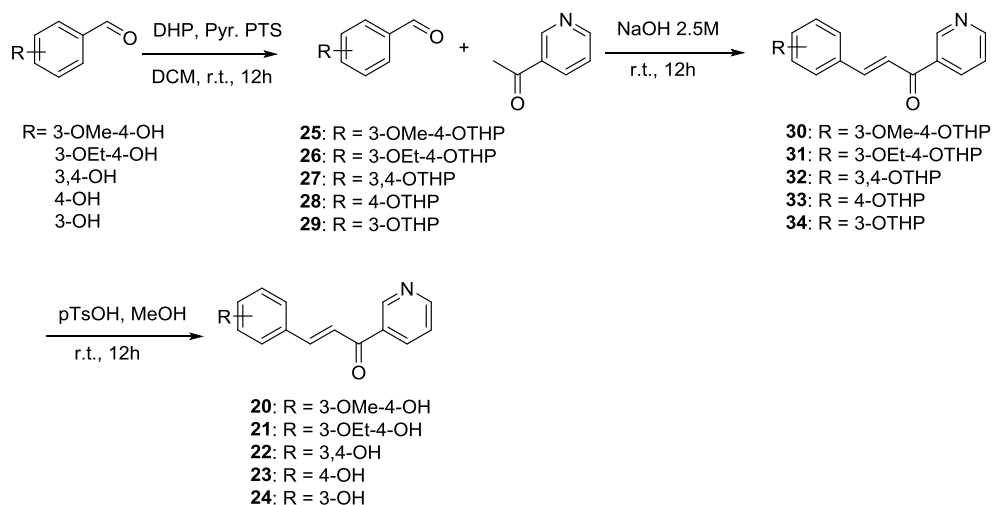
### 3.4 Methods

The series of compounds **20-24** have been synthesized and were primarily subject to evaluation for their antioxidant activity using a method based on autoxidation measurement. The inhibition activity on TG2 was determined using chromogenic substrate, as reported in chapter 2. Additionally, the compounds were investigated for their potential inhibition effects on A $\beta$  self-aggregation process and on GSK3 $\beta$  enzyme activity. These two targets are strictly related to the formation of senile plaque and neurofibrillary tangles, respectively, which represents two main hallmarks in AD pathology.

#### 3.4.1 Chemical synthesis

The compounds **20-24** were synthesized following the procedure reported in Scheme 2. Briefly, the phenolic groups of the appropriate aldehyde were protected as tetrahydropyranyl ethers by reacting with 3,4-dihydro-2*H*-pyran in the presence of pyridinium-*p*-toluenesulfonate as catalyst. This last reagent was synthesized by reacting *p*-toluenesulfonic acid with pyridine. The resulting derivatives **25-29** were subject to aldol condensation reaction with 3-acetylpyridine in basic conditions to give the derivatives **30-34**. Tetrahydropyranyl protecting groups were cleaved using *p*-toluenesulfonic acid in methanol affording the final products **20-24** as phenolic analogs.

Scheme 2



### 3.4.2 Evaluation of antioxidant activity and *in vitro* TG2 inhibition assay

The compounds were firstly tested to assess the antioxidant property *in vitro*. To this aim, the method of measurement is based on the comparison between the extent of the autoxidation of the substrate both in the presence and in the absence of antioxidants. In particular, the autoxidation level was measured through determination of oxygen consumption in a closed system. In a typical experiment, cumene is used as oxidizable substrate and 2,2'-azobis-isobutyronitrile (AIBN) as oxidation initiator: a solution of cumene in chlorobenzene (PhCl) containing AIBN was equilibrated at 30°C with an identical reference solution. After equilibration and when a constant O<sub>2</sub> consumption was reached, a concentrated solution of the antioxidant was injected in the sample flask. The oxygen consumption in the sample was measured after calibration of the apparatus. The inhibition rate constants  $K_{inh}$  were determined by using the kinetic equations.

The *in vitro* inhibition assay on TG2 was performed following the method reported in chapter 2.

### 3.4.3 *In vitro* evaluation of inhibition on A $\beta$ self-induced aggregation and GSK3 $\beta$ activity

The inhibitory potency of compounds **20-24** on amyloid fibrils formation was determined using Thioflavin T (ThT) fluorescence assay. ThT is a fluorescent dye widely used for the identification and quantification of amyloid fibrils because of its strong interaction with these proteins. Inhibition studies were performed by incubating previously prepared A $\beta_{42}$  samples with and without tested inhibitors. Specifically, inhibitors were screened in a 0.2:1 ratio with A $\beta_{42}$ . After incubation, samples were diluted to a final volume containing 1.5 $\mu$ M ThT. The fluorescence intensity was determined

( $\lambda_{\text{ex}} = 446\text{nm}$ ;  $\lambda_{\text{em}} = 490\text{nm}$ ). Blanks containing inhibitor and ThT were also prepared and measured as references for the fluorescence-quenching effects.

GSK3 $\beta$  is an isoform of glycogen synthase kinase-3 and plays an important role in tau hyperphosphorylation, as previously discussed. Since it is a kinase enzyme, ATP is an essential factor to the enzymatic function and ADP represents one important reaction product. The inhibition activity on GSK3 $\beta$  using a UHPLC-UV method is determined by measuring the ADP signal on a chromatographic run. In particular, to a 40 $\mu\text{l}$  of assay solution composed of GSK3 $\beta$  (2.5ng/ $\mu\text{l}$ ), ATP cofactor (250 $\mu\text{M}$ ) and GSM substrate (250 $\mu\text{M}$ ), test inhibitors were added and the reaction was incubated at 30 $^{\circ}\text{C}$  for 30 min before being analyzed via UHPLC/UV method. The samples were injected to an equilibrated reversed phase column C8, and subjected to chromatographic separation of ATP and ADP under optimized conditions. Parallel analysis of a blank sample was performed as control of ATP spontaneous hydrolysis.

### 3.5 Results and discussions

As reported in Table 3, all test compounds displayed an increased antioxidant activity compared to the reference compound, ethyl ferulate, an ester form of ferulic acid. In particular, compound **22**, containing 3,4-dihydroxy substitution on the aromatic ring, displayed the highest activity as antioxidant against the autoxidation process induced by AIBN in presence of cumene as oxidative substrate. Furthermore, its antioxidant effect was double-confirmed in an additional experiment using 2,2-azobis(2-amidinopropane) dihydrochloride (AAPH) as oxidative initiator. Compound **24** showed to be a good antioxidant as well with  $K_{\text{inib}}$  comparable to that of compound **22**, whereas other analogs showed an antioxidant activity just slightly higher than the reference compound. In addition to  $K_{\text{inib}}$  values, the number of peroxy radical trapped by a single antioxidant molecule, indicated as “N” in Table 3, was also evaluated. Compound **22** showed the highest “N” value of the entire series demonstrating to be the most interesting antioxidant of the series.

Analysis of the results related to TG2 inhibition highlights the finding that all compounds of the series are endowed with a poor inhibition activity towards this enzyme. These results are unexpected, since the *trans*-cinnamoyl moiety was chosen for the design of these antioxidants/TG2 inhibitors considering that derivatives characterized by this scaffold showed inhibition activity towards TG2 in low micromolar range, as reported in literature (see chapter 1). However, despite of the chemical features of the compounds **20-24** which closely resemble the structure of well-known TG2 inhibitors, their inhibition activity resulted in a millimolar range or even higher in the case of compound **23**. As showed by the results, the activity toward TG2 depends on the nature of the substituent on the aromatic ring, underlining the importance role of aromatic substitution pattern for TG2 inhibition.

However, these results might contribute to optimize SAR studies on *trans*-cinnamoyl derivatives as TG2 inhibitors. In fact, investigations on *trans*-cinnamoyl inhibitors of TG2 carried out by Keillor and coworkers, which included cinnamoyl-pyridinyl derivatives with substituents in *para* and *meta* positions, drove the conclusion that a sp<sup>2</sup>-hybridized oxygen is crucial for biological activity. In the compounds series **20-24**, the oxygen of OH group has a sp<sup>3</sup> hybridization, which should accordingly possess less activity on the target.

Considering the similarity of these derivatives with some natural compounds such as caffeic acid and polyphenols such as resveratrol, two natural compounds characterized by a large spectrum of interesting beneficial effects against AD<sup>106</sup>, this series of compounds was further evaluated for their inhibition on specific oxidative stress-related event/target involved in AD. In particular, compounds **20-24** were investigated for their ability to inhibit GSK3 $\beta$ , a key enzyme in AD correlated with tau hyperphosphorylation, as well as against the aggregation of A $\beta$  protein, responsible of the neuronal toxicity in AD, as previously discussed. As shown in the Table 3, concerning inhibition activity on GSK3 $\beta$ , although introduction of a pyridinyl group improved the inhibition activity compared to ethyl ferulate, all compounds, except **22**, showed poor performance even at concentration of 50 $\mu$ M. Surprisingly, compound **22**, structurally similar to caffeic acid with 3,4-dihydroxy substitution on benzene ring, turned out to be a good GSK3 $\beta$  inhibitor with an IC<sub>50</sub>=24.36  $\pm$  0.01  $\mu$ M. Low inhibition exhibited by other compounds shows that the increase of lipophilicity by introducing a methoxy or ethoxy group as in **20** and **21** or the presence of a single hydroxy group on the benzene ring as in **23** and **24**, determines a decrease of inhibition potency on GSK3 $\beta$ . With regard to A $\beta$  anti-aggregation activity, the *in vitro* assay showed similar results, in fact, all the compounds, with the exception of **22**, exhibited poor inhibition on A $\beta$ <sub>42</sub> self-aggregation with percentage of inhibition ranging between 5.8 and 21.5 at 50 $\mu$ M. Compound **22** is, again, the most active of the series with 91.5% of inhibition at the same drug concentration and an IC<sub>50</sub> value of 9.0  $\pm$  1.4 $\mu$ M.

Therefore, the substitution pattern on the aromatic ring of *trans*-cinnamoyl structure is essential to the antioxidant activity and even more important for the inhibition activity on A $\beta$  self-aggregation and GSK3 $\beta$ .

**Table 3.** Results of antioxidant activity, inhibition activity on TG2, A $\beta$  self-aggregation and GSK3 $\beta$  for compounds **20-24** and Ethyl ferulate as reference compound.

Compound	Antioxidant activity in PhCl <sup>a</sup> (T=30°C)		TG2 IC <sub>50</sub> ( $\mu$ M)	GSK3 $\beta$		A $\beta$ <sub>42</sub> self-induced aggregation	
	K <sub>inh</sub> /M <sup>-1</sup> s <sup>-1</sup>	N		% inhibition (50 $\mu$ M)	IC <sub>50</sub> ( $\mu$ M)	% inhibition (50 $\mu$ M)	IC <sub>50</sub> ( $\mu$ M)
<b>20</b>	6.5 $\pm$ 0.2 $\cdot$ 10 <sup>3</sup>	2.1 $\pm$ 0.1	688 $\pm$ 67	37.18 $\pm$ 0.14	n.d	17.5 $\pm$ 1.7	n.d
<b>21</b>	5.5 $\pm$ 0.3 $\cdot$ 10 <sup>3</sup>	2.1 $\pm$ 0.1	484 $\pm$ 64	39.55 $\pm$ 0.85	n.d	18.8 $\pm$ 0.5	n.d
<b>22</b>	6.2 $\pm$ 0.5 $\cdot$ 10 <sup>5</sup> 2.9 $\pm$ 0.5 $\cdot$ 10 <sup>5b</sup>	2.6 $\pm$ 0.3 4.5 $\pm$ 0.2	1001 $\pm$ 53	n.d.	24.36 $\pm$ 0.01	91.5 $\pm$ 0.5	9.0 $\pm$ 1.4
<b>23</b>	5.2 $\pm$ 0.3 $\cdot$ 10 <sup>3</sup>	2.0 $\pm$ 0.2	> 2000	25.18 $\pm$ 0.01	n.d	21.5 $\pm$ 5.8	n.d
<b>24</b>	1.3 $\pm$ 0.2 $\cdot$ 10 <sup>5</sup>	1.9 $\pm$ 0.2	266 $\pm$ 13	43.55 $\pm$ 0.01	n.d	5.8 $\pm$ 5.3	n.d
Ethyl Ferulate	4.2 $\pm$ 0.2 $\cdot$ 10 <sup>3</sup>	2		9.04 $\pm$	n.d		

<sup>a</sup> Autoxidation experiments using 2,2'-azobis-isobutyronitrile (AIBN) as oxidation initiator and cumene as substrate in solution of chlorobenzene (PhCl) at 30°C

<sup>b</sup> Autoxidation Experiment performed in Phosphate buffer 0.1M, pH 7.4, THF 3.1M, AAPH 25mM, T=30°C

### 3.6 Conclusions

Among the series of compounds **20-24**, designed as TG2 inhibitors bearing antioxidant activity, compound **22** emerged as the most important derivative characterized by interesting biological profiles. Unexpectedly, all the compounds showed weak inhibitory activities towards TG2, despite their chemical structures are very similar to the scaffold of well-known TG2 inhibitors. However, these findings might contribute for a further insight of how the substituents on aromatic rings could significantly affect the TG2 inhibition activity. Nevertheless, the goal related to the design of new multitarget ligands against AD was fulfilled by additional analysis on specific oxidative stress-related AD targets, including GSK3 $\beta$  enzyme activity and A $\beta$  self-induced aggregation process. In this context, compounds **20-24** showed to be mild inhibitors against amyloid aggregation and GSK3 $\beta$  enzyme activity, with exception of compound **22** which showed a much higher inhibition potency against the targets. Importantly, compound **22** exhibited a well-balanced micromolar inhibition towards both two targets (IC<sub>50</sub> of 24 $\mu$ M and 9 $\mu$ M for GSK3 $\beta$  and A $\beta$ <sub>42</sub> self-aggregation, respectively), overcoming one of the challenges in multitarget ligands drug design, which is to achieve a drug with balanced affinity/activity toward the biological targets taken into consideration.

## **4. Fluorescent probe-linked polyamine derivatives for cell imaging studies on the role of transglutaminase 2 in Alzheimer's disease**

Small-molecule fluorescent probes are indispensable tools for biology/biomedicine, being used as biomolecule labels, enzyme substrates, environmental indicators and cellular stains. Accumulating evidence demonstrated that the enzyme TG2, responsible of protein cross-linking catalysis, is an important target for AD, as illustrated in chapter 1. TG2 is also able to catalyze substrates including A $\beta$  and protein tau, two proteins functioning abnormally in AD. However, elucidation concerning the mechanism by which TG2 is involved in AD is desired. Therefore, this chapter focuses on the development of fluorescent probes derived from a combination of fluorophores with TG2 inhibitors, designed for the purpose of cell imaging studies. These probes could be used as a biological tool for the investigation of the biochemical mechanisms by which TG2 exerts its role in AD.

### **4.1 Fluorescence process**

Fluorescence occurs when the excited state of a molecule by absorption of light relaxes to the ground state through emission of a photon. In fact, absorption of light by a molecule converts the singlet electronic ground state ( $S_0$ ) to the excited state ( $S_1$ ,  $S_2$ ). The decay of the excited state can occur with photon emission (fluorescence) or in a nonradiative fashion. This nonradioactive quenching of the excited state can occur through one of a variety of processes, including bond rotation or vibration, molecular collision, and photoinduced electron transfer (PeT). The excited state can also undergo intersystem crossing to the triplet excited state ( $T_1$ ) and subsequent relaxation by either photon emission (phosphorescence) or nonradiative decay. Another important pathway for decay of the singlet excited state involves 'Forster resonance energy transfer' (FRET) to an acceptor molecule: this process is distance-dependent and can be used to assess the proximity of labeled entities.

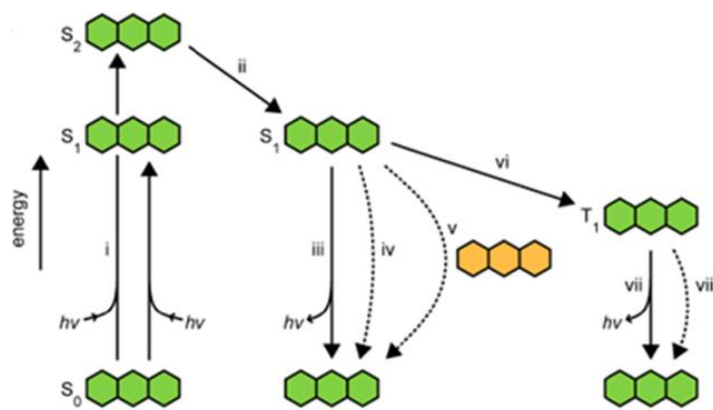


**Figure 13.** Jablonski diagram showing (i) absorption of a photon leading ground state  $S_0$  to an excited state, (ii) internal conversion to  $S_1$ , (iii) fluorescence, (iv) nonradiative decay, (v) Forster resonance energy transfer (FRET), (vi) intersystem crossing to  $T_1$ , (vii) phosphorescence, and (viii) nonradiative decay.

The key parameters of the phenomenon of fluorescence are:

- Maximal absorption ( $\lambda_{\max}$ ): energy between the ground state and the higher energy level.
- Extinction coefficient ( $\epsilon$ ): the absorptivity of a molecule at  $\lambda_{\max}$ , defined by Lamber-Beer law.
- Maximal emission wavelength ( $\lambda_{\text{em}}$ ): it's longer than  $\lambda_{\max}$ , because of energy losses by solvent reorganization or other process.
- Stokes shift: the difference in  $\lambda_{\max}$  and  $\lambda_{\text{em}}$ .
- Quantum yield ( $\Phi$ ): the ration of photons emitted and photons absorbed; the higher is quantum yield, more efficient is the fluorescence process.

The utility of a particular fluorophore is dictated by its specific chemical properties, such as reactivity, lipophilicity, pKa and stability, and photophysical properties including  $\lambda_{\max}$  and  $\lambda_{\text{em}}$ . A parameter for meaningful comparisons between two fluorescent molecules is the product of the extinction coefficient and quantum yield ( $\epsilon \times \Phi$ ): this value allows comparison of the photon yield of different classes of fluorophores under the same light intensity.



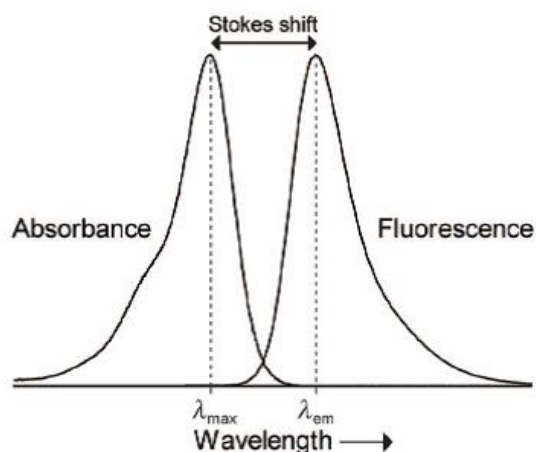


**Figure14.** Generic absorption and emission spectra.

## 4.2 Fluorophores in cell biology

Fluorescence has been long used to visualize cell biology at many levels, from molecules to complete organisms. Originally, fluorescence was mainly observed from small organic dyes attached by means of antibodies to the protein of interest in fixed and permeabilized cells. Later, these dyes were improved to be able to recognize directly the biomolecular target. More recently discovered fluorescent proteins have enabled noninvasive imaging in living cells. Meanwhile, semiconductor nanocrystals have been developed with higher brightness and photostability than previous fluorophores, but their targeting currently remains challenging.

- *Small organic fluorophores.* The use of small-molecule fluorophores began to emerge during the 19<sup>th</sup> century with the development of synthetic dyes in modern chemical industry, when the synthetic methodology was focused on organic colorants and their derivatives. As the industry evolved, the effort was shifted from dyes to drugs, leading synthetic chemist to focus on pharmacological agents. Today, however, there is a growing need of small-molecule fluorophores as tools used in biology and biomedicine. Small-molecule dyes have undergone optimization of wavelength range, brightness photostability and reduction in self-quenching, through chemical strategies such as extension of conjugation, rigidification through extra rings, and decoration with electron-withdrawing substituents, such as fluorines.
- *Fluorescent proteins.* The first fluorescent proteins to become useful in cell biology were phycobiliproteins, pigments extracted from cyanobacteria. However, their applications were limited to antibody conjugates for cell surface labeling, due to their excessive size (200kD) that limit diffusion through membrane. Discovery of green fluorescent protein (GFP) represents a

revolutionary achievement in cell imaging. GFP alone or expressed in genetic fusions with other proteins enabled visualization of target proteins in a totally noninvasive way, since the fluorescence is generated by spontaneous cyclization and oxidation of three amino acids buried at the heart of the beta barrel. Following GFP, a variety of homologous fluorescent proteins with different colors have been discovered or developed.

- *Quantum dots.* Quantum dots (QDs) are inorganic nanocrystals that fluoresce at sharp and discrete wavelengths depending on their size, have high extinction coefficients (10 to 100 times those of small fluorophores and FPs), and have good quantum yields. Crucial for biological applications was the development of coatings that make QDs water soluble and allow conjugation to antibodies. However, the large size of QDs conjugated to biomolecules prevents efficient traversal of intact membranes, limiting their use to permeabilized cells or extracellular proteins.

Fluorophores find wide applications in cell biology studies including investigation of proteins, nucleic acids, enzyme activities, cell stains etc. In the context of proteins, fluorophores could be used in studies of protein expression, protein localization, protein diffusion and trafficking, conformational changes and protein turnover. Moreover, the protein activity can be manipulated using chromophore-activated light inactivation, generally by means of the ROS generated by the protein itself. With regard to enzyme activity studies, fluorogenic substrates for endogenous enzymes have been used to detect whether the enzyme is in active versus latent or inhibited states. The latter distinction is particularly important for proteases, because for many proteases, only a small fraction of the total pool is active. Because of the great importance of proteases in infectious diseases, apoptosis, inflammation, tumor development, and metastasis, several approaches have recently been developed for imaging protease activity in intact animals<sup>107</sup>. Another noteworthy example of using fluorophore probes to study enzymatic activity is reported by Rianes et al.<sup>108</sup>, where a fluorogenic esterase substrate was chemically coupled to RNase A. The endocytosis process followed by fluorescence microscopy allowed the visualization of the entire process with temporal and spatial resolution.

### **4.3 Classes of small-molecule fluorophores**

Fluorescent compounds based on synthetic small molecules are powerful tools to visualize biological events in living cells and organisms. Small-molecule fluorophores are generally used in antibody conjugates for protein visualization in the cell environment or coupled to an enzymatic substrate to generate a fluorogenic substrate that allows the studies of enzyme activity. Over the years, small-

molecule fluorophores have been subject to wide chemical modifications to generate a large variety of derivatives with the aim of improving their chemico-physical properties. Nevertheless, several “core” fluorophores with excellent spectral characteristics and high chemical stabilities can be identified.

The six major classes of small-molecule fluorophores include: coumarins, fluoresceins, boron dipyrromethene (BODIPY) dyes, rhodamines, cyanines and benzoxadiazoles.

#### 4.3.1 Coumarins

The coumarin scaffold is a privileged structure in organic chemistry, occurring in numerous natural products and pharmacological agents. Substitution at the 7-position with electron-donating groups yields highly fluorescent molecules. The prototypical coumarin fluorophore is 4-methyl-7-hydroxycoumarin (4-MU), which absorbs UV light ( $\lambda_{\text{max}} = 360 \text{ nm}$ ) and emits blue light ( $\lambda_{\text{em}} = 450 \text{ nm}$ ). This and related compounds are the basis for many fluorescent labels, fluorescent sensors, and fluorogenic enzyme substrates. The  $\text{pK}_{\text{a}}$  of 4-MU is 7.8, making the molecule sensitive to changes in pH under physiological conditions. The related 7-amino-4-methylcoumarin (AMC) displays similar spectral properties, which are constant above pH 5. Different reactive groups are compatible with this fluorophore and are typically attached at the position 3 or 4 to yield biomolecule labels.

Peptidyl derivatives of AMC are widely used to measure protease activity<sup>109</sup>. AMC has also been elaborated to prepare substrates for other enzymes including histone deacetylases<sup>110</sup> and esterases<sup>111</sup>.

#### 4.3.2 Fluoresceins

The prototype of this class is fluorescein, synthesized in 1871; it remains one of the most widely used fluorophores in modern biochemical, biological and medicinal research. This dye can exist in seven prototropic forms, with the most biologically relevant molecular forms being the monoanion and the dianion that interchange with a  $\text{pK}_{\text{a}}$  of 6.4<sup>112</sup>. The dianion is the most fluorescent form with a  $\lambda_{\text{max}}$  of 490 nm and  $\lambda_{\text{em}}$  of 514 nm, and a quantum yield of 0.95. As in the case of the hydroxycoumarins, substitution with fluoro or chloro groups causes a decrease in  $\text{pK}_{\text{a}}$ , generating dyes with less pH sensitivity and more photostability. A key property of fluorescein is equilibrium between an “open” fluorescent quinoid form and a “closed” nonfluorescent lactone. Attaching blocking groups on the phenolic oxygens through ester or ether bonds can modulate this equilibrium; this strategy has been used to prepare fluorogenic substrates for many enzymes.

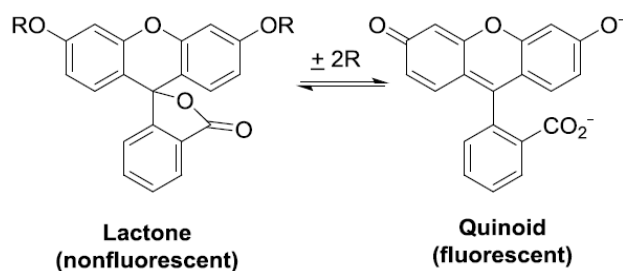


**Figure 15.** Equilibrium between the open and closed forms of fluorescein.

The fluorescein scaffold continues to be used to build a variety of sophisticated probes for different applications. Fluorescein is an extremely versatile core dye, since various modifications such as addition of fluoro and chloro groups can yield fluorophores with different  $pK_a$  and chromatic properties<sup>113</sup>. Fluorescein can be decorated with reactive groups to yield important biomolecule labels<sup>114</sup> and can also serve as a scaffold for preparing indicator molecules. In particular, the pH sensitivity of fluorescein has been exploited to prepare small-molecule pH sensors<sup>115</sup>. Changes in the  $pK_a$  of fluorescein can be used as an index to report on the status of fluorescein-labeled biomolecules<sup>112</sup>. By addition of chelating moieties to the core structure, fluorescein is used also as ions sensor: the fluorescent complex allows the measurement of calcium ions fluxes in living cells, as well as detection of other ions including sodium, zinc, mercury, palladium and fluoride<sup>116</sup>. By replacing the carboxylic group on fluorescein with other substituents, the group of Urano and coll. discovered a series of finely tunable fluorescein-based probes with high sensitivity and has been applied as probe for the enzyme activity of  $\beta$ -galactosidase<sup>117</sup> and further modifications allowed the construction of a probe used in *in vivo* animal model for tumor imaging<sup>118</sup>.

#### 4.3.3 BODIPY

The boron difluoro dipyrromethene (BODIPY) dyes have several characteristic properties including neutral charge, small Stokes shift and insensitivity of fluorescence to environmental changes. The prototypical BODIPY dye is the tetramethyl compound, which exhibits  $\lambda_{max}/\lambda_{em} = 505 \text{ nm}/516 \text{ nm}$  and  $\Phi = 0.80$ . Derivatives characterized by this scaffold are more photostable than fluorescein and are especially useful where neutral charge and environmental insensitivity are advantageous. Another important property of this class of dyes is the tunability of wavelength through appropriate substitution. BODIPY dyes can thus serve as surrogates for traditional dyes such as fluorescein, rhodamine and many others.

The probes built on the BODIPY scaffold is centered largely on fluorescent labels, and less frequently used as ions indicator. The nonpolar character of BODIPY allows incorporation into

lipophilic probes<sup>119</sup>. Moreover, the small Stokes shift of BODIPY dyes causes efficient self-quenching of over-labeled biomolecules. This phenomenon can be utilized to create useful protease substrates, because proteolysis of densely labeled proteins leads to an increase in fluorescence intensity. One example is BODIPY-FL labeled casein used in an autoquenching assay for proteolytic activity of calpain, a cysteine protease<sup>120</sup>.

#### 4.3.4 Rhodamines

Rhodamines are amino counterpart of fluorescein with certain advantages over it, including lower pH-sensitivity, higher photostability, and tunable spectral properties. The prototypical rhodamine is the tetraalkylated variant sulforhodamine B. This fluorophore absorbs in the green and emits in the yellow ( $\lambda_{\text{max}}/\lambda_{\text{em}} = 565 \text{ nm}/586 \text{ nm}$ ). A more common rhodamine label is tetramethylrhodamine, which bears a carboxyl group on its phenyl ring that enables easier conjugation to biomolecules or attachment of ion-recognition motifs. In addition to modifications on the phenyl ring, changing the substituent patterns on the aniline nitrogens can modulate its spectral properties. Similar to fluoresceins, replacement of the xanthene oxygen with another atom, such as C or Si can modify spectral properties.

The tunability of the rhodamine structure makes this dye class a useful scaffold for fluorescent probes. Accordingly, rhodamines remain the most useful basis for fluorescent labels. Rhodamine labels are often paired with fluorescein derivatives for FRET-based experiments because of efficient energy transfer between these xanthene compounds, where fluorescein is used as donor and rhodamine serves as FRET acceptor<sup>121</sup>. As in the case of fluoresceins, rhodamines that contain an *ortho*-carboxyl group on the phenyl ring exist as an equilibrated mixture of the open fluorescent quinoid form and a closed nonfluorescent lactone form, and acylation of the nitrogens locks the molecule into the lactone form. This property can be exploited to prepare fluorogenic molecules for enzymatic studies. In fact, N-acyl rhodamine 110 has been used to build useful caspase substrates to assay apoptosis<sup>122</sup>, also used as substrates for phosphatases<sup>123</sup>, esterases<sup>108</sup>, and metal-ion catalysis in a cellular context<sup>124</sup>.

#### 4.3.5 Cyanines

General properties of the cyanine dyes include large extinction coefficient values, highly tunable structures and excellent photostability. Prior to 1993, the utility of cyanines in biological research was primarily as a stain for cellular membranes or DNA. The development of indocarbocyanine dyes bearing sulfonate groups and functional groups for bioconjugation brought this dye class into the realm of fluorescent labels for proteins and nucleic acids.

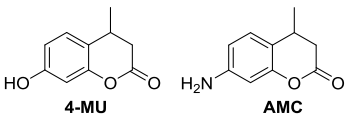
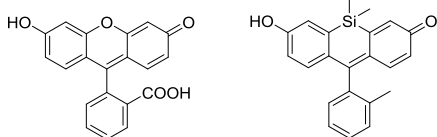
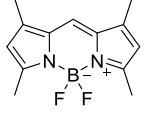
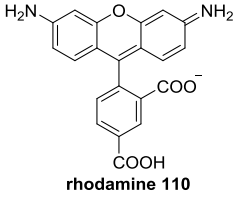
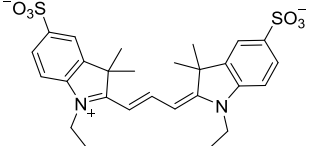
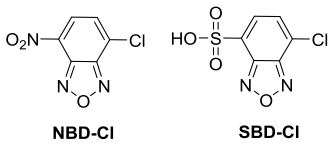
The most well-known cyanine dyes in modern bioresearch are the CyDye fluorophores, characterized by a sulfoindocyanine structure. The CyDyes are useful biomolecular labels and are now the standard fluorophores for microarrays and many other analyses<sup>125</sup>. CyDye pairs are also often used for FRET experiments<sup>126</sup> and can be utilized as photoswitchable probes for ultra-high-resolution imaging<sup>127</sup>.

#### 4.3.6 Benzoxadiazoles

The prototypical dye core of benzoxadiazoles is 4-nitrobenz-2-oxa-1,3-diazole (NBD). Addition of substituent in position 7 yields several derivatives including NBD-Cl<sup>128</sup>, and replacement of nitro group by sulfonate gives SBD-Cl. In particular, amine adducts of NBD-Cl emit in the green region of spectrum with  $\lambda_{\text{max}}=465\text{nm}$  and  $\lambda_{\text{em}}=535\text{nm}$ . This low-weight fluorophore allows conjugates with small molecules, such as sugars, retaining the biological activity<sup>129</sup>.

The environmentally sensitive fluorescence of NBD derivatives can be exploited in a variety of ways, including the preparation of lipid probes<sup>129</sup> and novel kinase substrates. In a work by Dai et al., a ‘caged’ form of NBD has been utilized as a sensor for protein kinase activity. In particular, enzyme activity of protein kinase C is critical in mitosis phase around the time point of nuclear envelope breakdown (NEB). In order to establish whether protein kinase C activity is present prior to, during, or after NEB event, a NBD-labeled peptide substrate was used since it fluoresces upon phosphorylation by the enzyme. In this way, the fluorescent sensor contributed to assess intracellular protein kinase activity at precise time intervals in reference to NEB event.

**Table 4.** Six classes of small-molecule fluorephores.

<b>A. Coumarins</b>	<b>B. Fluoresceins</b>
 <p>4-MU      AMC</p>	
<b>C. BODIPY dyes</b>	<b>D. Rhodamines</b>
 <p>tetramethyl BODIPY</p>	 <p>rhodamine 110</p>
<b>E. Cyanines</b>	<b>F. Benzoxadiazoles</b>
	 <p>NBD-Cl      SBD-Cl</p>

#### 4.4 Drug design

As illustrated in the chapter 1, accumulating evidences support the hypothesis that TG2 may be involved in the abnormal protein aggregation observed in AD, and there is compelling evidence from *in vitro* studies, as well as from studies on postmortem human brain tissue of AD patients and animal models that demonstrates a crucial role for TG2 in AD pathology. In fact, TG2 has been demonstrated to be colocalized in different biological samples with AD's hallmarks – senile plaques and neurofibrillary tangles; moreover, A $\beta$  and protein tau have been shown to be good substrates to TG2.

Despite numerous evidences of correlations between TG2 and AD's pathology have been reported, further clarification concerning how TG2 is involved in this neurodegenerative disease is desired, and studies to this aim are underway.

In the attempt of investigating the mechanism by which TG2 could be involved in AD's pathogenesis, we proposed the design of a series of fluorophore-linked polyamine structure based TG2 inhibitors and their potential utilization as probes for cell imaging studies. Fluorescence cell imaging has been widely used as an important tool toward understanding of cellular dynamic

processes in living cells and visualization of compartments or macromolecules/drugs localization inside fixed or living cells. The aim of constructing fluorophore-labeled TG2 inhibitors is, therefore, to visualize the cellular compartment in which enzymatically active TG2 is mainly present, and possibly to have a glimpse into the dynamic processes in which TG2 is involved.

Polyamine chains, such as cadaverin, spermine, putrescine etc. are well-known TG2 reversible inhibitors with a competitive mechanism against the transamidase activity (see chapter 1). In literature, TG2 inhibitors based on fluorescent polyamine structure have been reported, including monodansylcadaverine and fluorescein-cadaverine. Therefore, polyamine with amine groups linked through alkyl chains of various lengths (5, 3-4-3, 3-3-3, 3-2-3 and 3-3) have been designed as ligands to TG2 enzyme.

Concerning the small-molecule fluorophores, each class of derivatives is characterized by a specific spectral features and chemico-physical properties, such as absorption, emission, lipophilicity and  $pK_a$ . Thus, three types of fluorophores have been selected for the labeling of polyamine chains, in order to have a range of choices for the identification of the most appropriate fluorescent probe, that shows good performance in cellular environment and allows high resolution imaging.

On these bases, we designed and synthesized the series of fluorescent TG2 inhibitors **35-49**, through the combination of the three fluorophores with five polyamine chains, as shown in Table 5. This series of compounds are supposedly to be TG2 reversible inhibitors, for the reason of the presence of primary amine groups, which represent good ligands to TG2 in competition with the natural substrate. The fluorophore moieties are coupled to the polyamine chains through formation of amide bond, thiourea bond or directly by nucleophilic substitution.

The compounds will undergo *in vitro* assay for the assessment of inhibitory activity toward the target enzyme TG2; afterwards, the derivatives with positive results will be subject to further investigations, including activity evaluation on neuronal cells and cell imaging studies.



Table 5. Drug design of compounds 35-49.

Compound	Fluorophore	Polyamine chains
35		R1=
36		R2=
37		R3=
38		R4=
39		R5=
40		R1=
41		R2=
42		R3=
43		R4=
44		R5=
45		R1=
46		R2=
47		R3=
48		R4=
49		R5=

## 4.5 Methods

The series of compounds 35-49 have been synthesized; and the biological evaluation studies are still in progress.

### 4.5.1 Chemical synthesis

The compounds 35-49 have been synthesized following the Schemes 3 and 4.

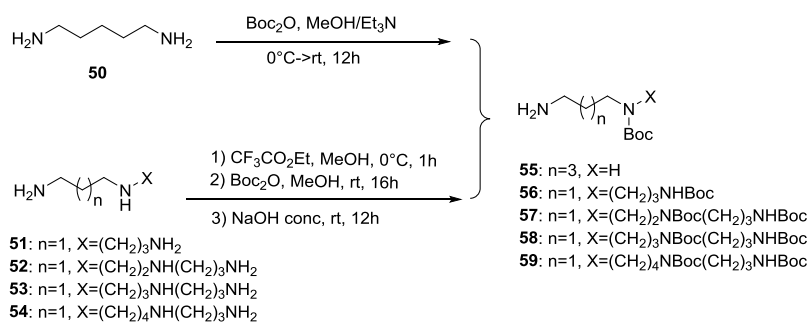
The unprotected polyamine chains commercially available were subject to reactions shown in Scheme 3 to obtain an appropriate protection on amine groups. In particular, the diamine derivative 50 was monoprotected at the amine group by reaction with *tert*-butyl dicarbonate (Boc<sub>2</sub>O) in controlled conditions; while tri-amine 51 and tetra-amines 52-54 were firstly monoprotected at the

primary amine using ethyl trifluoroacetate by keeping under control the reaction conditions; afterwards, the remaining amine groups were protected using Boc<sub>2</sub>O. Trifluoroacetyl group was cleaved in basic conditions to give the desired products **55-59**: mono-Boc diamine **55**, di-Boc tri-amine **56** and tri-Boc tetra-amines **57-59**.

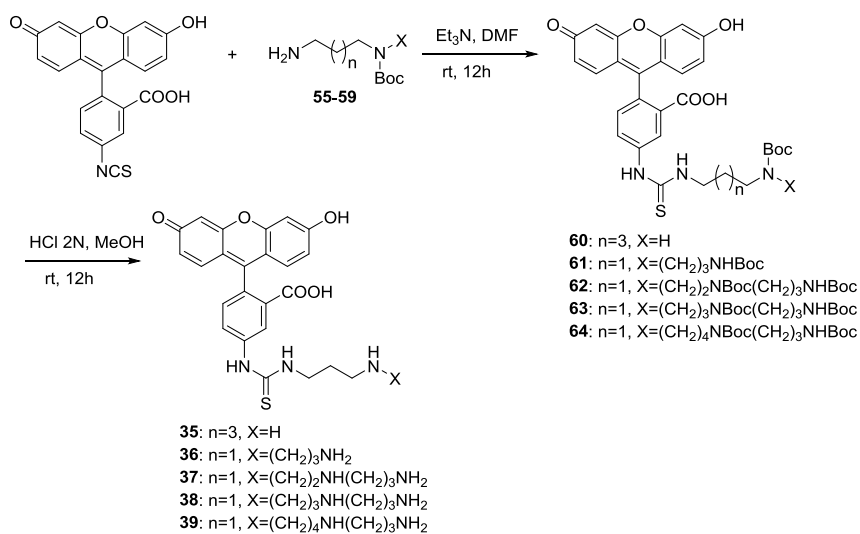
The resulting protected polyamines were coupled to the respective fluorophore as described in **Scheme 4**. In particular, the polyamines were reacted with fluorescein isothiocyanate, where amine made nucleophilic attack to the electrophilic carbon of NCS to form a thiourea bond and gave the intermediates **60-64**, which were subject to Boc deprotection to yield the final products **35-39**.

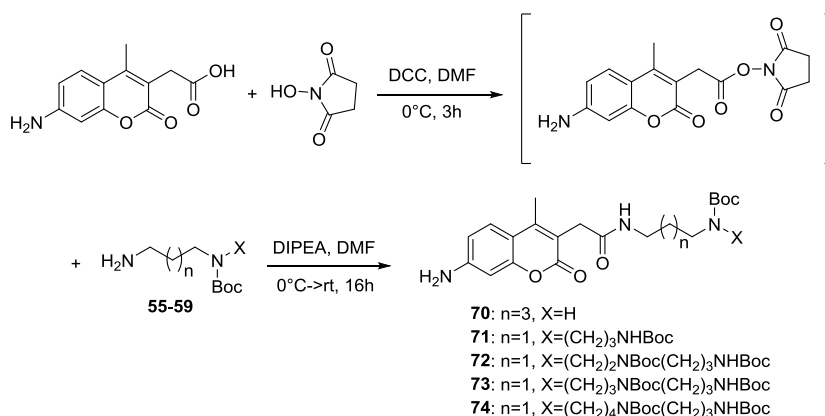
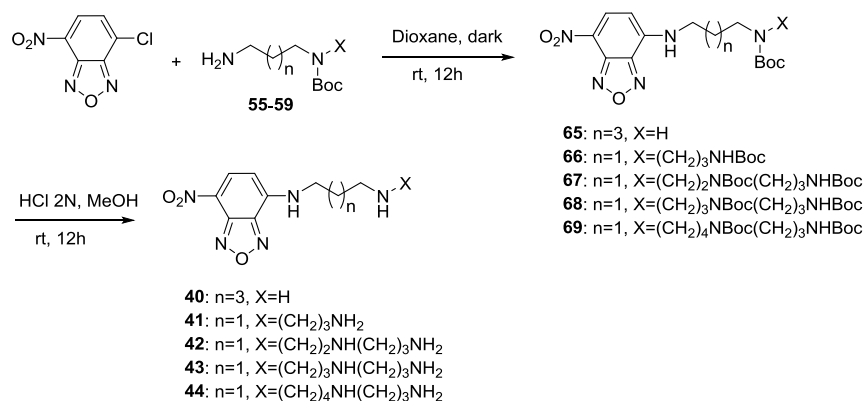
Similarly, nucleophilic substitution between polyamine and 4-chloro-7-nitrobenzofurazan gave the conjugates **65-69**; the subsequent cleavage of Boc protection in acidic conditions gave the final products **40-44**. Finally, synthesis of the third class of conjugates was started with the activation of the carboxylic acid on coumarin derivative using N-hydroxysuccinimide, followed by reaction with the respective polyamine to yield the intermediates **70-74**. Boc deprotection gave the final products **45-49** as chlorohydrate salts.

**SCHEME 3**



**SCHEME 4**





## 4.6 Conclusions

The synthesized series of compounds **35-49** will be evaluated firstly for their potential inhibition effect on TG2 in both cell-free and cell-based *in vitro* studies; secondly, they will be subject to cell imaging studies at the aim of an elucidation concerning the role of TG2 in AD's pathological mechanisms.

## SECTION II

# Disrupters of $\zeta$ COP1/ $\gamma$ COP1 protein-protein interaction

## 1. Introduction

Coat protein I (COPI) is a protein complex referred to as coatamer complex. It represents the major component of vesicles that mediate the retrograde transport from endoplasmic reticulum to Golgi apparatus in eukaryotic cells. In the absence of COPI, cells experience Golgi fragmentation, immature autophagosome accumulation, and ultimately death. A recent function-based genomic screen identified *COPZ1*, a gene encoding the coatamer complex subunit  $\zeta$ COP1, as a promising cancer target. In fact, *COPZ1* knockdown using siRNA causes tumor-specific growth inhibition without affecting the viability of normal cells. The mechanism of this tumor selectivity of *COPZ1* knockdown was revealed by the finding that the mRNA level of  $\zeta$ COP2 is drastically reduced in tumor cells as consequence of gene silencing of *COPZ2*. Thus, while normal cells express two isoforms,  $\zeta$ COP1 and  $\zeta$ COP2, tumor cells have only  $\zeta$ COP1. As a consequence, normal cells are not killed by *COPZ1* knockdown, because the isoform  $\zeta$ COP2 can functionally replace  $\zeta$ COP1; while tumor cells cannot survive the same depletion, because of the absence of  $\zeta$ COP2. Therefore,  $\zeta$ COP1, the protein encoded by the *COPZ1* gene, is crucial for the survival of tumor cells and could be a promising target for the development of anticancer drugs.

This chapter focuses on the development of potential anticancer drugs capable of disrupting the main function of  $\zeta$ COP1, which is the interaction with  $\gamma$ COP1 inside the coatamer complex. To this aim, a peptide-based inhibitor for this protein-protein interaction (PPI) has been designed and synthesized. *In vitro* evaluation of inhibition on this PPI was carried out by the method of co-immunoprecipitation. Fluorescently labeled peptide has been developed as well to verify the penetration into cytosol. Potential small-molecule disruptors are under investigations.

### 1.1 COPI secretary pathway

The secretary pathways in eukaryotic cells are responsible for biogenesis and intracellular distribution of a wide range of proteins, complex carbohydrates and lipids. Membrane traffic between endoplasmic reticulum (ER) and the Golgi apparatus is bidirectional, known as anterograde and retrograde transport. This transport process is implemented by vesicular carriers, which mediate a continuous flux of proteins and lipids between these compartments, reflecting the transport of newly synthesized proteins from ER toward Golgi and the retrieval of escaped ER resident proteins.

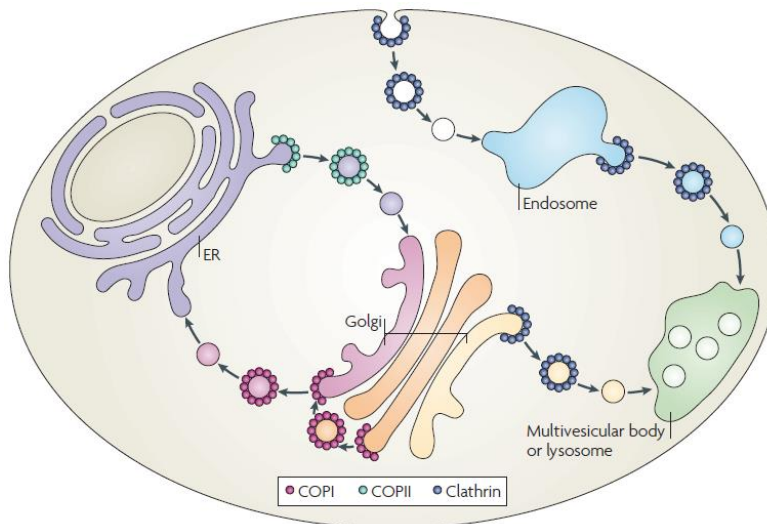


**Figure 16.** Pathways of vesicular transport by coat proteins<sup>130</sup>.

Anterograde and retrograde transport is mediated by two classes of cytosolic coat proteins, the COPII and COPI coats, respectively, which act on the membrane to capture cargo proteins into nascent vesicles<sup>131</sup>. These transport processes require a process of budding, movement, tethering, as well as uncoating and fusion of COPI and COPII carriers with their respective compartment.

COPI carriers derive from assembly of a number of protein complex, named COPI coatomer, with the major constituents being seven subunits –coat proteins:  $\alpha$ ,  $\beta$ ,  $\beta'$ ,  $\gamma$ ,  $\delta$ ,  $\epsilon$  and  $\zeta$ COP<sup>132</sup>. The assembly of coat proteins is initiated by the activation of an Arf family G protein on the membrane, thus, the formation of COPI vesicles is regulated by Arf1 and involves the stepwise recruitment to membranes of the seven coat proteins<sup>133</sup>. In detail, firstly, Arf1-GDP is activated by a Golgi-localized exchange factor to replace GDP with GTP triggering a conformational change in Arf1; next, Arf1-GTP recruits the heptameric coatomer through a direct GTP-dependent interaction<sup>134</sup>, thus, coatomer is incorporated en bloc to the Golgi membrane<sup>135</sup>; finally, membrane-associated coatomer binds to cargo molecules and self-assembles to form a polyhedral cage<sup>136</sup>. Well characterized cargo proteins of COPI vesicles include the KDEL receptors<sup>137</sup>, certain p24 family members<sup>138</sup> and SNAREs (soluble *N*-ethylmaleimide-sensitive factor attachment protein receptors)<sup>139</sup>.

As aforementioned, a coatomer complex structurally consists of seven subunits, named coat protein:  $\alpha$ ,  $\beta$ ,  $\beta'$ ,  $\gamma$ ,  $\delta$ ,  $\epsilon$  and  $\zeta$ COP<sup>140</sup>. Each coatomer has two main subcomplexes: the  $\gamma$ - $\zeta$ - $\delta$ - $\beta$ -COP tetrameric complex, which constitutes the inner layer core; and the  $\alpha$ - $\beta'$ - $\epsilon$ -COP trimeric complex, which forms the outer layer of the COPI coat.

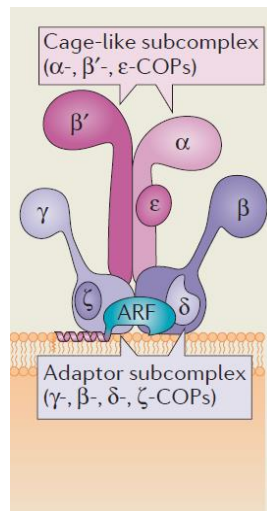


**Figure 17.** Structure of a coatamer complex.

## 1.2 Mechanism of coatamer recruitment to membranes

COPI, COPII and clathrin-coated vesicles mediate vesicular transport inside an eukaryotic cell<sup>141</sup>. The transport mediated by clathrin-coated vesicles was the first secretory pathway identified and investigated; it contributed for the later elucidation of mechanism for the remaining two pathways: COPI and COPII. Clathrin-coated vesicles are responsible for traffic pathways from the plasma membrane to the early endosome and from the Golgi to the endosome<sup>142</sup>. Assembly of clathrin proteins requires the adaptor protein (AP) complexes. In particular, AP2 is a typical component of AP complexes which is well studied. The molecular mechanism of its recruitment to membranes via phosphatidyl inositol-4,5-bisphosphate (PtdIns4,5P2a) have been explored in considerable detail, and this body of work serves as a framework for exploring coat recruitment to membranes<sup>143</sup>.

Based on the extreme structure homology between AP2 and COPI complexes, Goldberg and coworkers have pushed further on the investigation of mechanism of recruitment of coatamer *via* Arf1. According to this study<sup>144</sup>, the heptameric coatamer has a total of two binding sites for Arf1-GTP: two molecules of Arf1-ATP are bound to  $\beta$ COP and  $\gamma$ COP. In fact, using two methods (fluorometric assay and pull-down assay), the research group was able to find that Arf1-GTP has no interactions with  $\alpha\beta'\epsilon$ -COP, it rather binds to a  $\gamma\zeta$ -COP complex, in addition to interaction with  $\beta\gamma$ -COP. This result was further confirmed by the crystal structure of  $\gamma\zeta$ -COP complexed to Arf1.



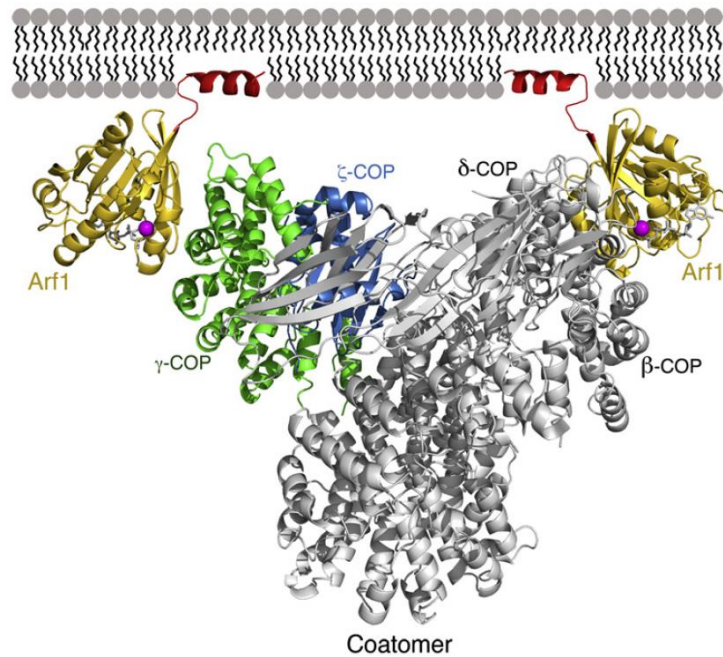


**Figure 18.** Model for membrane recruitment of coatamer<sup>144</sup>.

### 1.3 ζCOP

Zeta-COP (ζCOP), reported for the first time by Kuge et al, is a 20kD coat protein that exists in cytosol both as free monomer and bound to the coatamer complex<sup>140c</sup>. In this paper, the authors used an anti-ζCOP antibody and found that it inhibited partially the cell-free intra-Golgi transport and completely blocks the formation of COPI vesicles in a free-cell system, suggesting the importance of this subunit.

Inside the coatamer complex, ζCOP is bound to γCOP to form a dimer, which is further associated with βγ-COP giving a tetrameric structure. Later, the group of Futatsumori<sup>145</sup> discovered the existence of two homologs of ζCOP (ζCOP1 and ζCOP2) and γCOP (γCOP1 and γCOP2). The isoforms share 75% and 80% of amino acids, respectively. This study also showed that ζCOP2 and γCOP2 are expressed ubiquitously suggesting their fundamental role in cellular function. Furthermore, yeast two-hybrid analysis indicated that γCOP1 and γCOP2 could directly interact with ζCOP1 and ζCOP2. The author concluded that ζCOP2 and γCOP2 can form a COPI complex in place of the original isoform 1, thus, these isoforms are functionally redundant. This observation has been confirmed with later studies conducted by Wegmann and others<sup>146</sup>. In fact, different combinations have been identified for COPI complex and ζ1-γ1, ζ1-γ2, ζ2-γ1 represent the major coatamer population in mammals. These isotypic coatamers are likely characterized by different functions in cell. Infact, significant localization differences for COPI-isoforms do exist, with a

preference for  $\zeta 1\text{-}\gamma 1$  and  $\zeta 1\text{-}\gamma 2$ -coatamer in the early Golgi apparatus and  $\zeta 2\text{-}\gamma 1$ -coatamer in the late Golgi apparatus, suggesting distinct functions for coatamer isoforms<sup>147</sup>.

#### 1.4 $\zeta$ COP1 as a potential cancer target

A tumor cell growth-inhibition screening conducted by Shtutman et al. identified COPZ1, the gene encoding  $\zeta$ COP1, as a promising cancer target<sup>148</sup>. In this screening, a library of genetic inhibitors, including antisense cDNAs and shRNA, was employed in a growth inhibition study conducted on multiple cell lines: MDA-MB-231 (breast cancer), PC3 (prostate cancer), T24 (bladder carcinoma), and HT1080 (fibrosarcoma), as well as human telomerase reverse transcriptase (hTERT)-immortalized BJ normal foreskin fibroblasts (BJ-hTERT).

Among the genes enriched by growth-inhibition screening, gene COPZ1 which encodes the  $\zeta$ COP1 protein, emerged as an interesting target. For a deeper investigation, they used siRNAs against COPZ1 and other genes encoding  $\alpha$ ,  $\beta$ ,  $\beta'$ ,  $\gamma 1/\gamma 2$ ,  $\delta$ ,  $\varepsilon$  and  $\zeta 2$ -COPs to reduce their RNA levels by 90%. The results showed that knockdown of COPZ1 by siRNAs inhibited the growth of tumor cells, however, the growth of immortalized normal BJ-hTERT fibroblasts or normal human prostate epithelial cells was not inhibited by this knockdown, in contrast with siRNAs targeting other coatamer subunits ( $\alpha$ ,  $\beta$ ,  $\beta'$ ,  $\gamma$ ,  $\delta$ ,  $\varepsilon$ -COPs) which did not show this tumor selectivity. Importantly, no growth inhibition was observed with knockdown of COPZ2, the gene encoding the isoform  $\zeta$ COP2, but the growth of normal cells is inhibited by the simultaneous knockdown of both COPZ1 and COPZ2.

Further studies revealed that the tumor selectivity of COPZ1 knockdown was correlated with COPZ2 downregulation observed in tumor cells. In fact, the mRNA level of  $\zeta$ COP2 is drastically reduced in tumor cells as consequence of gene silencing of COPZ2, whereas the expression of COPZ1 and other COPs was relatively uniform among the normal and tumor tissues. Thus, while normal cells express two isoforms,  $\zeta$ COP1 and  $\zeta$ COP2, tumor cells have only  $\zeta$ COP1. As a consequence, normal cells are not killed by *COPZ1* knockdown, because the isoform  $\zeta$ COP2 can functionally replace  $\zeta$ COP1; whereas tumor cells cannot survive the same  $\zeta$ COP1 depletion, because of absence of  $\zeta$ COP2. As a result, normal COPZ2-expressing cells survive COPZ1 depletion, COPZ2-deficient tumor cells are killed by COPZ1 knockdown.

Surprisingly, the restoration of COPZ2 expression in tumor cells did not inhibit their growth *in vitro* or *in vivo*, indicating that COPZ2 is not a tumor suppressor. The selective silencing of COPZ2 in tumor cells was later discovered to be correlated to the silencing of a tumor suppressor, microRNA-152<sup>149</sup>. In fact, the first intron of the COPZ2 gene encodes a microRNA, miR-152, which was reported to be silenced in some cancers<sup>150</sup> and displayed certain tumor-suppressive activities<sup>151</sup>. (The

COPZ1 gene also hosts a microRNA, miR-148b, which is homologous to miR-152). When miR-152 was expressed in different tumor cell lines, their growth was inhibited. Hence, miR-152 is indeed a tumor suppressor, in agreement with the recent paradigm that microRNAs are key regulators of carcinogenesis and other phenotypic transitions. miR-152 and its host gene COPZ2 are transcribed from the same promoter. Hence, COPZ2 shutdown in tumor cells is a consequence of the silencing of tumor-suppressive miR-152, leading in its turn to tumor dependence on the COPZ1 gene.

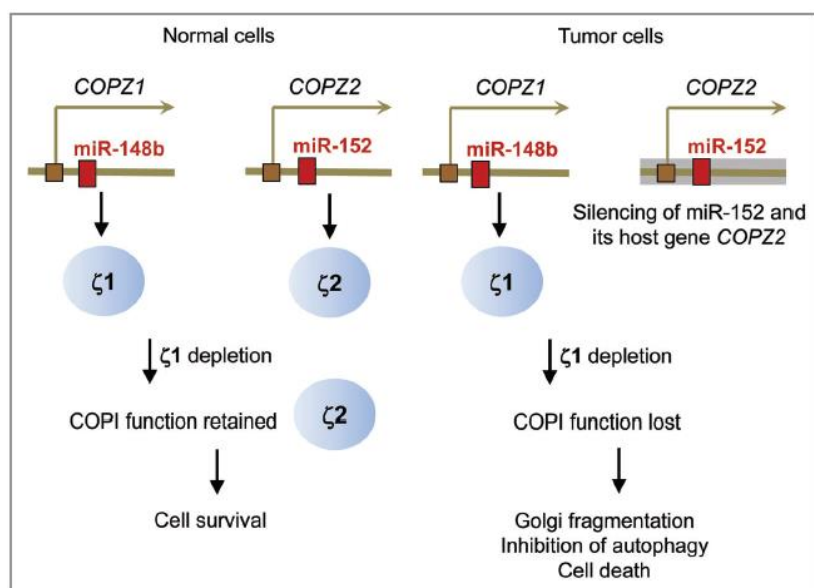


**Figure 19.** Mechanism of tumor dependence on COPZ1<sup>152</sup>.

Tumor cells treated with siRNA against COPZ1 showed fragmentation and disappearance of Golgi apparatus, the same effect was observed in normal cells upon knockdown of COPZ1 and COPZ2 together. Furthermore, tumor cells transfected with siRNA targeting COPZ1 undergo apoptosis.

Based on these observations, our hypothesis is that a correct function of ζCOP1 is crucial for the survival of tumor cells and could be a promising target for the development of anticancer drugs. Compounds capable of interfering with the function of ζCOP1, through the inhibition of the association of ζCOP1 to the coatamer complex could exert selective antitumor activity. Since the main function of ζCOP1 is to form a dimer with γCOP1 within the coatamer complex, disrupters of this ζCOP1/γCOP1 protein-protein interaction could impair the correct function of ζCOP1, thus, being potential anticancer drugs.

## 2. Drug design

Protein-protein interactions (PPIs) became recently an interesting target in the world of drug discovery. Over the past decades, much progress in our understanding of PPIs has been achieved. To date, more than 40 PPIs have been targeted<sup>153</sup> and several inhibitors, most of them small molecules, have reached clinical trials.

The drug design of disrupter for this  $\zeta$ COP1/ $\gamma$ COP1 protein-protein interaction was evolved in two directions: i) Design of a peptide-based inhibitor based on crystal structure analysis; ii) Identification of potential small-molecule inhibitors of  $\zeta$ COP1/ $\gamma$ COP1 interaction through library screening.

For the design of peptide-based PPI inhibitor, the first efforts were focused on the computational analysis of the interface between the two proteins of interest. Crystal structure of  $\zeta$ COP1/ $\gamma$ COP1 from Protein Data Bank was used for the analysis. *In silico* analysis of the interface between  $\zeta$ COP1 and the Arf1/coatomer complex revealed the presence of an alpha helix in  $\zeta$ COP1 close enough to the surface of  $\gamma$ COP1 to form a series of hydrogen bonds and hydrophobic interactions that hold the proteins together in the coatomer complex. Furthermore, a mutagenesis study conducted by Yu et al.<sup>154</sup>, identified three cluster zones on  $\zeta$ COP1 that form hydrophobic bonds and salt bridges with  $\gamma$ COP1, one of which includes the alpha helix identified in computational studies. Therefore, the purpose is to construct a peptide that mimics this alpha helix of  $\zeta$ COP1, that could function as a competitive inhibitor for the interaction with  $\gamma$ COP1, thus impairing the association of  $\zeta$ COP1.

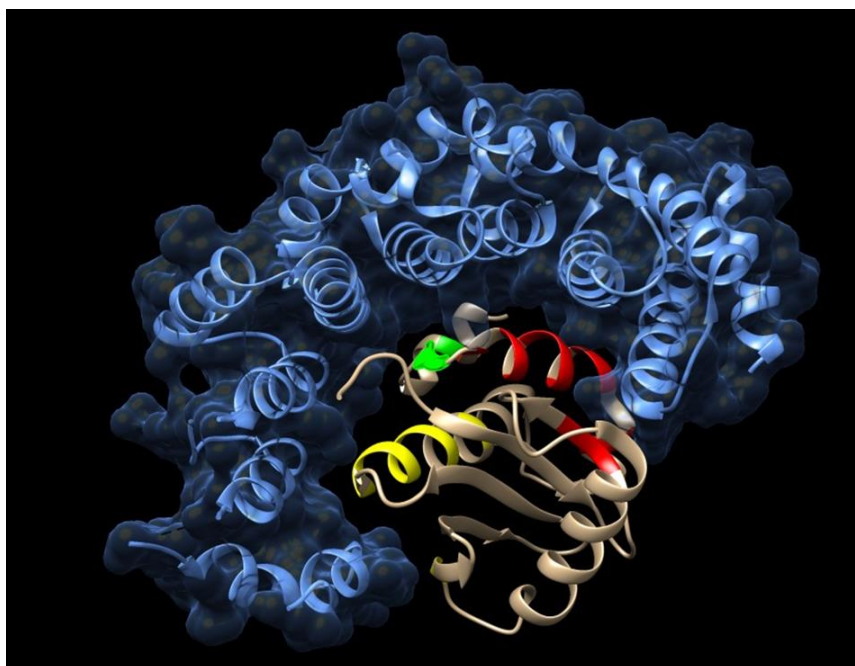


**Figure 20.** Crystal structure of dimer  $\zeta$ COP1 (golden yellow) and  $\gamma$ COP1(blue). The three cluster zones important for the protein-protein interactions are colored in red, green and yellow. -Images constructed using Chimera 1.10.2.

The primary sequence of this alpha-helix has been elucidated and the most important residues turned out to be N117 through G131(sequence NMEGLFLAVDEIVDG). In particular, E119, D126 and D130 of this sequence on  $\zeta$ COP1 seemingly can form salt bridge with R86 and R126 on  $\gamma$ COP1, whereas F122 and L123 likely form hydrophobic interactions with L52, Y53 and M87 of  $\gamma$ COP1. Considering the excessive length of the entire sequence, and also for the reason of synthetic accessibility, the peptide designed will have a reduced number of residues.

Generally, linear peptides have poor cell permeability due to the high hydrophilicity and molecular size, and also, peptides can lose their shape when taken out of context. Thus, chemical interventions to enhance cellular penetration and stabilize their bioactive structure are generally required. Moreover, chemical modification such as cyclization generally increases the proteolytic stability of a peptide. Cyclization through all-hydrocarbon bond has emerged as one such solution, conferring stable  $\alpha$ -helical structure, protease resistance and cellular penetrance<sup>155</sup>. Therefore, the designed peptide will be cyclized through formation of all-hydrocarbon bond to give a “stapled” peptide **75**, where the two residues not involved in interaction with  $\gamma$ COP1 are replaced by two unnatural amino acids that allow the all-hydrocarbon bond formation.

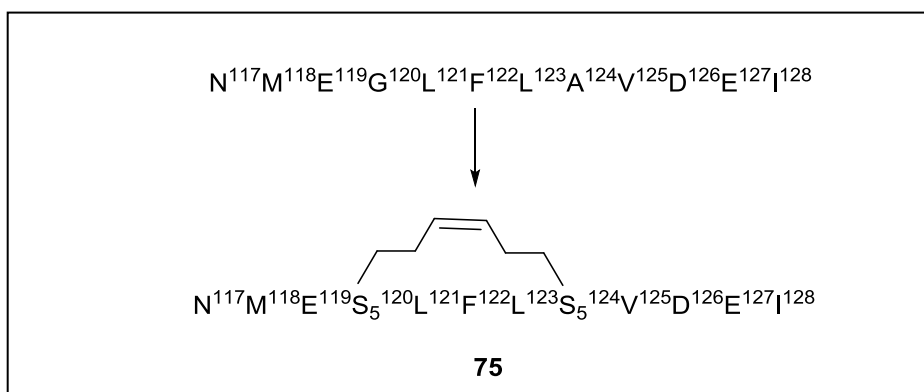
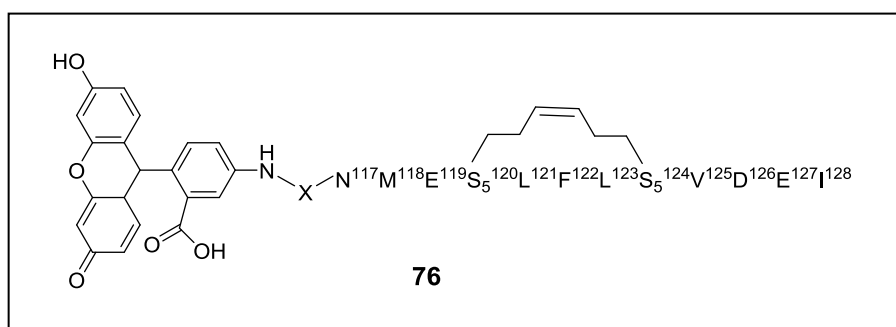


**Figure 21.** Drug design of compound **75**.

In order to investigate the actual cellular penetrance of this molecule through a cell imaging visualization, a fluorescein-labeled staple peptide has been designed. The *N*-terminal of the peptide has been coupled to the fluorophore through an aliphatic linker to give the compound **76**.



These peptide-based compounds are supposedly capable of interacting with  $\gamma$ COP1 at the specific area of interface with  $\zeta$ COP1, thus, inhibiting the protein-protein interaction of interest. Concerning the screening of potential small-molecule disrupters for the  $\zeta$ COP1/ $\gamma$ COP1 protein-protein interaction, *in silico* docking simulations have been conducted using  $\zeta$ COP1 crystallographic structure. A library of small-molecule compounds (ZINC free database of commercially available compounds for virtual screening) was docked to the protein within a box created at the interface that defines the areas of  $\zeta$ COP1 to be examined with ligand poses.

### 3. Methods

The compounds **75** and **76** were synthesized using the standard solid phase peptide synthesis procedure. Firstly, the cytotoxicity of the compounds was examined using MTS cell viability assay. Secondly, the compound **75** was subject to co-immunoprecipitation assay to examine its inhibition

activity on  $\zeta$ COP1/ $\gamma$ COP1 protein-protein interaction. Additionally, the fluorescent peptide was subject to cell fluorescence imaging studies. A number of potential small-molecule disrupters have been identified through docking studies.

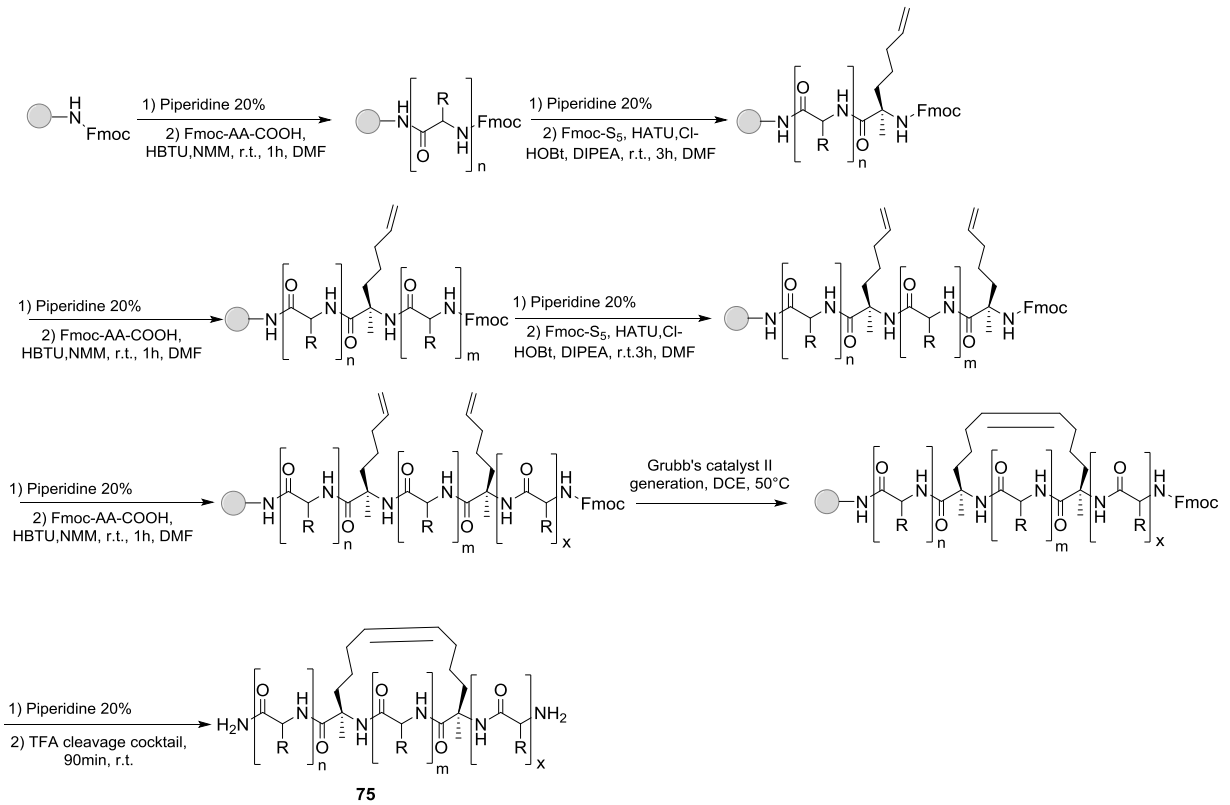
### 3.1 Chemical synthesis

The compounds **75** and **76** have been synthesized following the Scheme 5. Briefly, the peptides are synthesized using the standard Fmoc/*t*-Bu solid phase peptide synthesis procedure. The Fmoc group on aminomethylated polystyrene resin was cleaved and the Fmoc-protected amino acids were added in sequence using 2-(1*H*-benzotriazol-1-yl)-1,1,3,3-tetramethyluronium hexafluorophosphate (HBTU) as coupling agent in basic conditions. The olefin amino acid was coupled using a mixture of 1-[Bis(dimethylamino)methylene]-1*H*-1,2,3-triazolo[4,5-*b*]pyridinium 3-oxid hexafluorophosphate (HATU)/6-Chloro-1-hydroxybenzotriazole (Cl-HOBt). Each coupling reaction was monitored by colorimetric test using Kaiser reagent. All-hydrocarbon bond was formed using Grubb's catalyst in a ring-closing metathesis reaction. Once completed the sequence, the peptide was cleaved from resin using a cocktail containing trifluoroacetic acid (TFA) in the presence of scavengers. Removal of TFA and precipitation in cooled ether yielded the desired cyclic peptide **75**.

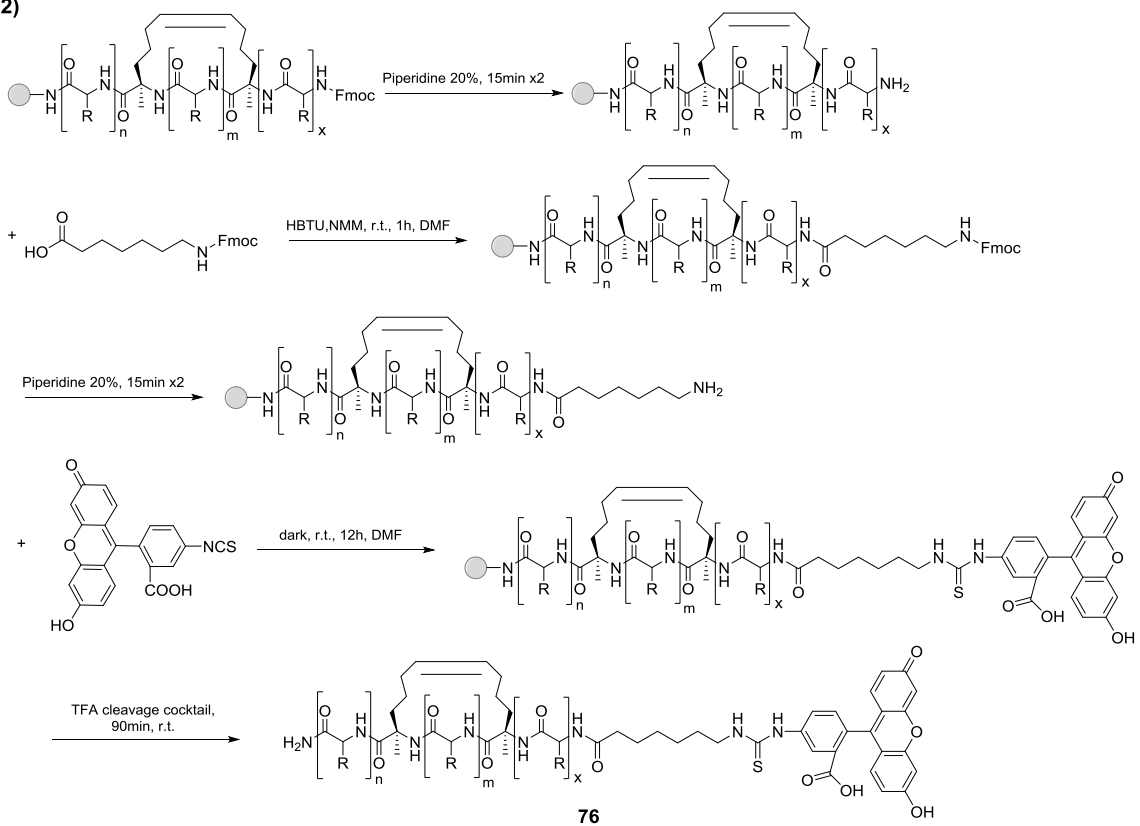
For the synthesis of **76**, additional steps were required. Once completed the peptide sequence, Fmoc group on the last amino acid was removed using piperidine followed by coupling of a non- $\alpha$ -amino acid using HBTU. Fluorescein isothiocyanate was attached and the labeled peptide was cleaved from resin and precipitated in cooled ether to give the compound **76**.

Scheme 5

1)



2)





### 3.2 Cell viability assay

The compounds **75-76** have been evaluated in cell viability assay using 3-(4,5-dimethylthiazol-2-yl)-5-(3-carboxymethoxyphenyl)-2-(4-sulfophenyl)-2H-tetrazolium (MTS) reagent and phenazine ethosulfate as electron coupling reagent. Three human tumor cell lines- Calu6 (lung adenocarcinoma), K562 (myelogenous leukemia) and PC3 (prostate cancer) were seeded in 96-well plate in triplicate and treated with drugs at concentration range of 0.1 $\mu$ M-200 $\mu$ M in incubator at 37°C for 48h and 72h for compounds **75** and **76**, respectively. A solution of MTS/phenazine ethosulfate was added to the plate and incubated for 4h. The colorimetric absorbance was measured and the data was processed.

### 3.3 Co-immunoprecipitation assay

The compound **75** has been evaluated for the ability of disruption toward the target protein-protein interaction using the co-immunoprecipitation method. Drug-treated Calu6 cells were lysed using a mild ion-strength lysis buffer; the protein fraction was collected and total protein concentration measured by bicinchoninic acid assay (BCA) assay. 1mg of protein was used for co-immunoprecipitation. Briefly, protein sample was incubated with Protein A/G agarose beads followed by addition of polyclonal antibody anti- $\gamma$ COP1 at 4°C. Centrifugation and removal of supernatant gave a pellet which was washed and suspended in SDS sample buffer for Western blot analysis. The two proteins of interest were detected in immunoblotting using monoclonal antibodies and the signal development was obtained through chemiluminescence, which was measured using an imaging device.

### 3.4 Docking studies

Small-molecule compounds available in ZINC library were docked to the crystallographic structure of  $\zeta$ COP1 using DOCK6.5 software in flexible mode.  $\zeta$ COP files were prepared for docking using Chimera software and the Computational Biology server. Spheres defining the molecular surface of  $\zeta$ COP1 were generated following determined parameters and a box was created to define the areas of  $\zeta$ COP1 to be examined with ligand poses.

### 3.5 Cell fluorescence imaging

PC3 cells were seeded in a 96-well plate in triplicate and treated with FITC-labeled drugs at 200 $\mu$ M for 6h and 12h. The imaging was executed at using fluorescence microscope. Prior to cell imaging, fixation using para-formaldehyde solution was performed.

#### 4. Results and discussions

**Cell viability assay.** As reported in Figure 22, compound **75** showed poor cytotoxic activity on the tumor cell lines examined. In fact, it inhibited only approximately 35% of tumor cell growth, at high concentration of 200 $\mu$ M on K562 cell line, while on Calu6 cells the activity was not observed. Compound **76** which bears a FITC moiety in addition to the same peptidic structure as compound **75**, exhibited an improved cytotoxicity profile on tumor cells. This fluorophore-labeled peptide was capable to cause 67% and 32% of tumor cell growth at 200 $\mu$ M and 100 $\mu$ M, respectively. Although the cytotoxic potency exhibited by compound **76** is low, in comparison with the activity profile of analog **75**, its improved potency could be due to an increased cell penetration property by addition of the lipophilic linker and fluorescein moiety.

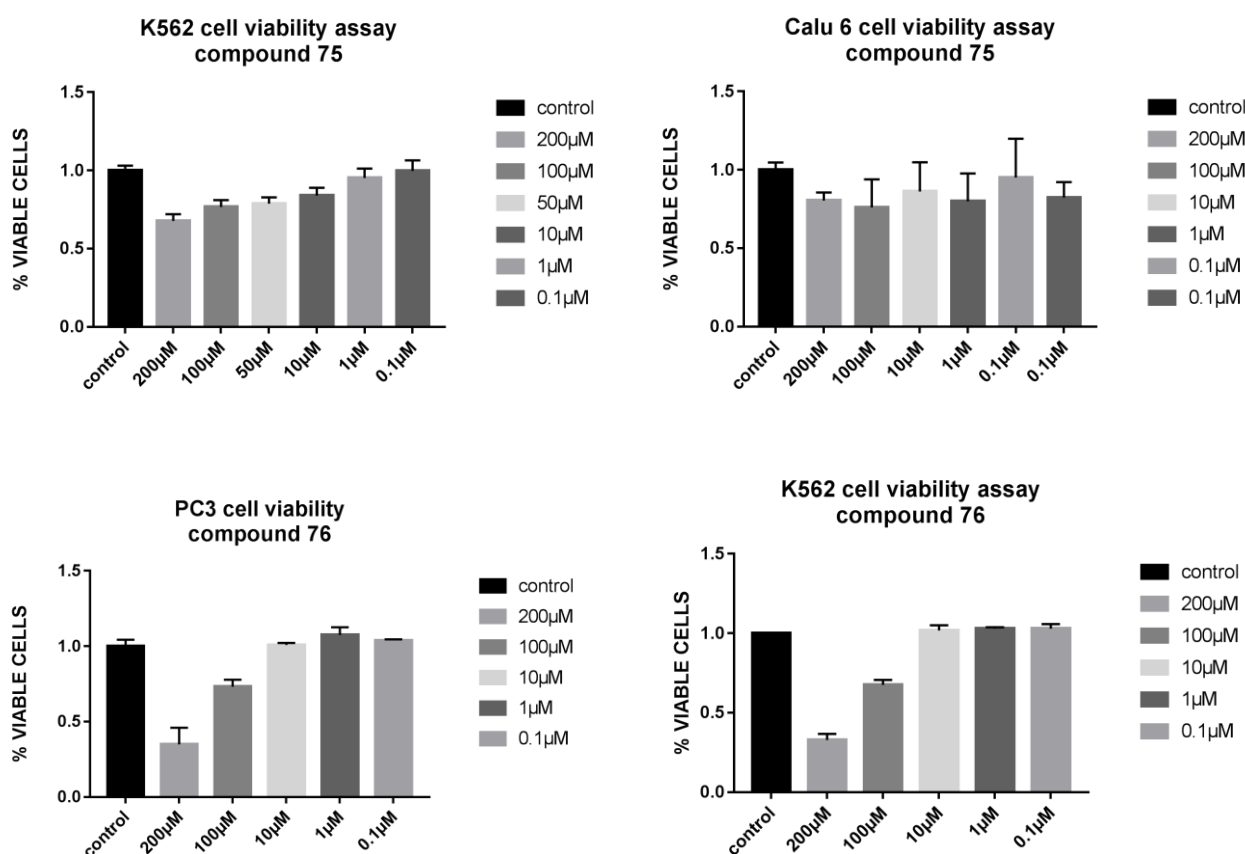


**Figure 22.** Cell viability assay results on cell lines treated with compounds **75-76**.

**Co-immunoprecipitation assay.** In literature there are very few studies on this  $\zeta$ COP/ $\gamma$ COP protein-protein interaction and no studies have been carried out on this PPI as a pathological target. Therefore, development of a method for the detection of this PPI is required. Co-immunoprecipitation

(co-IP) assay has been applied, being one of the most widely used methods of detection for protein-protein interactions. Co-IP method development requires the identification of appropriate cell lysis conditions and proper antibody to capture the bait-protein, in this case, the  $\gamma$ COP protein, and efficient antibodies for Western blot analysis. The method has been developed using a NP-400 lysis buffer of mild strength, and a goat polyclonal antibody against  $\gamma$ COP1 which was capable of capturing the target protein. Finally, using two mouse monoclonal antibodies, the two proteins of interest were efficiently detected in immunoblotting. Once the method was developed, compound **75** has been tested on its inhibition activity on the target PPI. Calu6 cells were treated with compound **75** at 50 $\mu$ M for 48h. As showed in Figure 23, unfortunately, this peptide-based compound was not able to disrupt the targeted PPI. Compound **76** is being tested using the same method.

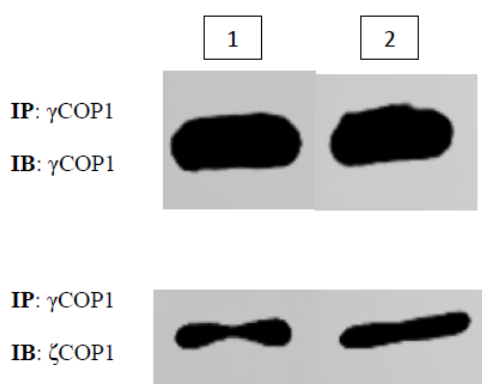


**Figure 23.** Co-IP experiments conducted on Calu6 cell line. 1) Negative control; 2) Sample treated with compound **75**.

**Docking studies.** Virtual screening using ZINC compounds library for potential small-molecule disrupters for the target PPI has been conducted and identified totally 17 compounds with grid score below -66. About 34.000.000 total compounds of the library have been firstly filtered, based on purchasability and Lipinski's definitions; afterwards, compounds were docked in flexible mode into the  $\zeta$ COP1 at the critical areas identified. Other parameters, such as Z-score representing the energy separation between the native fold and the average of misfolds, logP and formal charge, were taken into consideration for the method optimization. The identified compounds are being purchased and will be subject to co-immunoprecipitation assay as previously described.

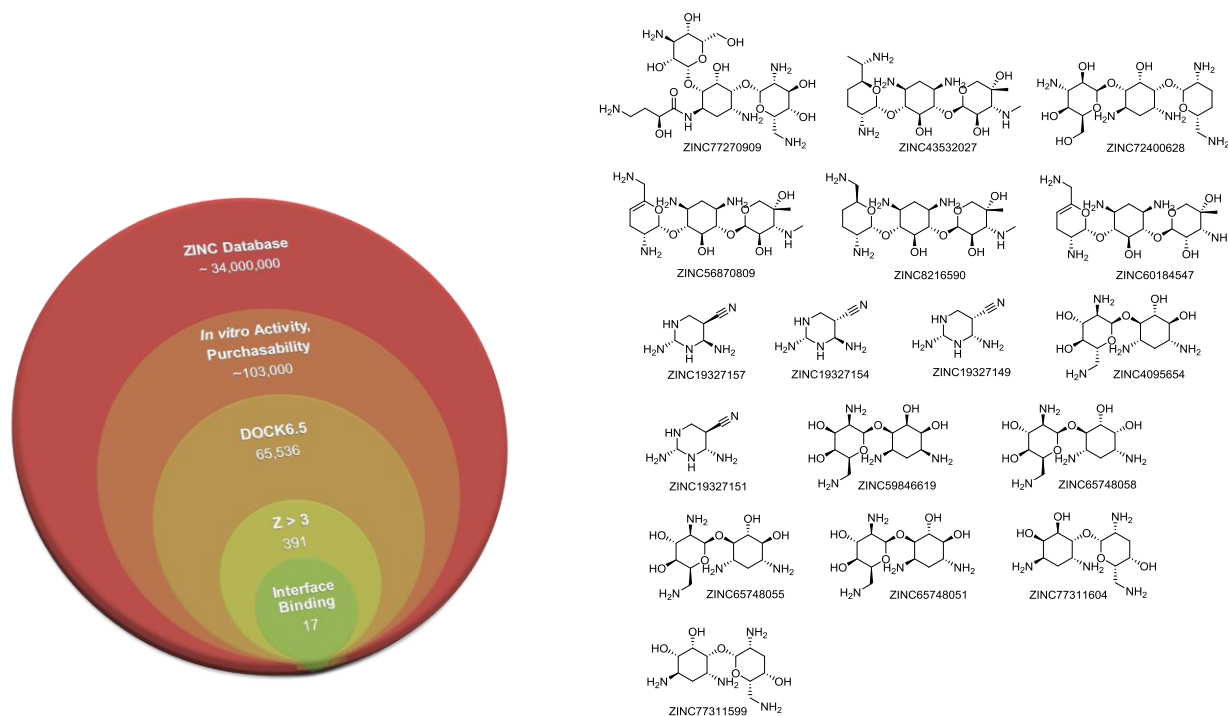


**Figure 24.** Docking process representation and results.

**Cell fluorescence imaging studies.** As shown in Figure 25, PC3 cells treated with fluorescent compound **76** emitted fluorescence signals. Fluorescent spots could be observed inside the cell indicating the actual penetrance of the compound.

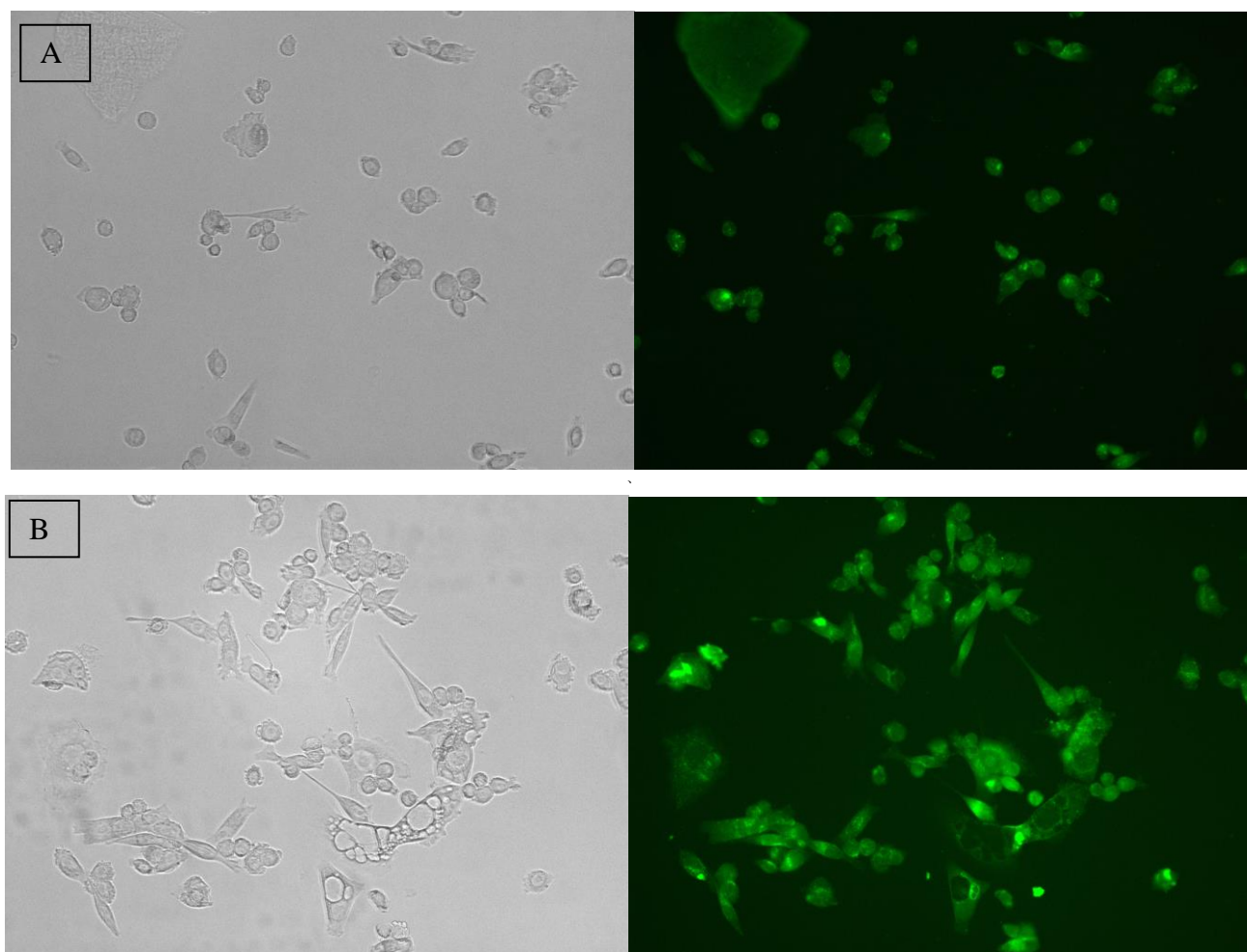


**Figure 25.** Images of PC3 cells treated with fluorophore-labeled peptide (compound **76**) at 200 $\mu$ M. A) 6h treatment. B) 12h treatment.

## 5. Conclusions

The compounds **75** and **76** showed poor cytotoxic activity in all the tumor cell lines examined, with **76** that exhibited a slightly more potent tumor cell cytotoxic effect. At the time of edition of the present manuscript, only compound **75** has been evaluated in co-immunoprecipitation assay, however, it did not show detectable inhibition activity on the  $\zeta$ COP1/ $\gamma$ COP1 protein-protein interaction which is the desired target. This inactivity could be due to poor cellular penetrance of peptide-based compounds. However, fluorophore-labeled analog **76** showed actual penetrance into the intracellular environment, as demonstrated by cell imaging studies. Further studies are underway for a better clarification. In particular, compound **76** will be subject to co-immunoprecipitation studies, as well as the small molecules identified by docking studies as potential disruptors of  $\zeta$ COP1/ $\gamma$ COP1

protein-protein interaction. Finally, 17 compounds identified through virtual screening assays are currently under investigation as small-molecules disrupters of  $\zeta$ COP1/ $\gamma$ COP1 protein-protein interaction.

## Experimental section

### 1. Chemistry

The reactions were monitored by thin layer chromatography (TLC) (Fertigplatten SIL G 25 UV<sub>254</sub> MN, 0.25mm) using silica gel-coated plates. The compounds were purified by gravity or flash column chromatography using silica gel columns (Agela Technologies, Cleanert Silica 40-60 $\mu$ m, 60 $\text{\AA}$ ). Melting points were determined in glass capillary tubes using Buchi 530. The synthesized compounds were characterized by <sup>1</sup>H and <sup>13</sup>C NMR spectroscopy (Varian Gemini 200/400) and ESI mass spectrometry (Waters ZQ 4000). All chemical shift values are reported in ppm and are relative to the Tetramethylsilane (TMS) as shift reference; the peaks multiplicity are given as s (singlet), br s (broad singlet), d (doublet), t (triplet), q (quartet) or m (multiplet). The chemicals and solvents were purchased from Sigma Aldrich and TCI. The purity of the peptid-based compounds was determined using Waters UPLC equipment and the mass spectra was produced by Waters LC-MS device. The compounds are named using ChemDraw Ultra 15.0.

**(E)-3-(4-nitrophenyl)-1-(pyridin-3-yl)prop-2-en-1-one (5):** 3-acetylpyridine was dissolved in a 1:1 H<sub>2</sub>O/MeOH mixture and this solution was treated with nitrobenzaldehyde (3 eq) and KOH (3 eq) and stirred for 30min. The mixture was filtered, and the precipitated product was washed with a minimum amount of ethanol to give the compound **5** as a yellow solid, which is used for the next step without purification. Yield: 75%; mp: 182-184 °C; <sup>1</sup>H NMR (CDCl<sub>3</sub>):  $\delta$  9.21 (s, 1H), 8.78 (d, 1H), 8.34 (m, 3H), 7.90 (m, 3H), 7.68 (d, 1H), 7.48 (m, 1H); MS (ESI) = 255 (M+H)<sup>+</sup>.

**(E)-3-(4-aminophenyl)-1-(pyridin-3-yl)prop-2-en-1-one (6):** The compound **5** was dissolved in ethanol and treated with SnCl<sub>2</sub>·5H<sub>2</sub>O (5 eq) and the reaction was stirred at 70°C for 30 min under N<sub>2</sub>. 30 ml of H<sub>2</sub>O was added and the pH was neutralized with a solution of 5% NaHCO<sub>3</sub>. The aqueous phase was extracted with ethyl acetate. The organic phase was dried over Na<sub>2</sub>SO<sub>4</sub>, filtered and evaporated to yield a residue which was purified by flash chromatographic column using ethyl acetate as eluent. Yield: 57%; mp: 167-169 °C; <sup>1</sup>H NMR (CDCl<sub>3</sub>):  $\delta$  9.28 (d, 1H), 8.76-8.25(m, 2H), 7.87(d, 1H), 7.46 (m, 3H), 7.27 (d, 1H), 6.77 (d, 2H), 4.09 (s, 2H); MS (ESI) = 225 (M+H)<sup>+</sup>.

**(M/E)-3-(4-isothiocyanatophenyl)-1-(pyridin-3-yl)prop-2-en-1-one (7):** **6** was dissolved in dichloromethane and the mixture was stirred under N<sub>2</sub>, a solution of 1,1'-Thiocarbonyldi-2(1H)-pyridone in dichloromethane was added dropwise. The mixture was stirred overnight at room temperature. The solvent was evaporated and the residue purified by flash chromatography using a

mixture of EtOAc/Petroleum ether (5:5) as eluent. Yield: 62%;  $^1\text{H}$  NMR ( $\text{CDCl}_3$ ):  $\delta$  9.25 (s, 1H), 8.71-8.33(m, 2H), 7.62(d, 1H), 7.22 (m, 3H), 7.13 (d, 1H), 6.80 (d, 2H); MS (ESI) = 267 (M+H) $^+$ .

**General procedure A: synthesis of azidoalkyl carboxylic acids (8-10).** The appropriate commercially purchased bromoalkyl carboxylic acid was dissolved in anhydrous DMF,  $\text{NaN}_3$  (4 eq) was added and the reaction was stirred at 60°C for 5h. The reaction was diluted with  $\text{H}_2\text{O}$  and the aqueous phase was acidified with HCl 2N and extracted with dichloromethane. The organic phase was washed using a saturated solution of NaCl and dried over  $\text{MgSO}_4$ . Solvent evaporation under reduced pressure gave the desired azidoalkyl carboxylic acid which is used for the next step without further purification.

**3-azidopropanoic acid (8):** Azide **8** was prepared from 3-bromopropionic acid using general procedure A and obtained as a pale yellow oil, 70% yield;  $^1\text{H}$ -NMR ( $\text{CDCl}_3$ ):  $\delta$  3.61-3.57 (t, J = 6.4 Hz, 2H), 2.66-2.62 (t, J = 6.4 Hz, 2H).

**5-azidopentanoic acid (9):** Azide **9** was prepared from 5-bromovaleric acid using general procedure A and obtained as a yellow-red oil, 85% yield;  $^1\text{H}$  NMR ( $\text{CDCl}_3$ ):  $\delta$  11.7 (brs, 1H), 3.27 (t, J= 6.45 Hz, 2H), 2.36 (t, J= 6.95 Hz, 2H), 1.75 (m, 4H)

**6-azidohexanoic acid (10):** Azide **10** was prepared from 6-bromohexanoic acid using general procedure A and obtained as a yellow-red oil, 85% yield;  $^1\text{H}$  NMR ( $\text{CDCl}_3$ ):  $\delta$  1.42 (m, 2H), 1.64 (m, 4H), 2.36 (t, 2H, J = 7 Hz), 3.27 (t, 2H, J = 7 Hz), 9.70 (brs, 1H).

**General procedure B: Synthesis of trityl-protected hydroxamic acids (11-13).** The appropriate azidoalkyl carboxylic acid (1 eq) was dissolved in anhydrous THF and N-methylmorpholine (1 eq) was added. The mixture was cooled on ice bath and stirred for 5 min. Isobutyl chloroformate (IBCF) (1eq) was added dropwise and the resulting mixture was stirred on ice bath for 10 min, followed by addition of O-tritylhydroxylamine (1 eq) and N-methylmorpholine (2 eq). The reaction was warmed to room temperature and stirred overnight. The mixture was poured into a solution of HCl 2N and extracted with EtOAc. The organic phase was dried over  $\text{Na}_2\text{SO}_4$  and removal of solvent gave a residue, which was purified by flash chromatography using mobile phase EtOAc/petroleum ether (2:8).



**3-azido-N-(trityloxy)propanamide (11):** The compound **11** was prepared from **8** using general procedure B and isolated as white solid with 35% yield.  $^1\text{H NMR}$  ( $\text{CDCl}_3$ ):  $\delta$  1.90 (t, 2H), 2.4 (t, 2H), 7.29–7.38 (m, 15H); MS (ESI) = 373 ( $\text{M}+\text{H}$ ) $^+$ .

**5-azido-N-(trityloxy)pentanamide (12):** The compound **12** was prepared from **9** using general procedure B and isolated as white solid with 42% yield.  $^1\text{H NMR}$  ( $\text{CDCl}_3$ ):  $\delta$  1.11–1.21 (m, 2H), 1.44 (m, 2H), 1.77 (t, 2H), 3.24 (t, 2H), 7.29–7.38 (m, 15H); MS (ESI) = 401 ( $\text{M}+\text{H}$ ) $^+$ .

**6-azido-N-(trityloxy)hexanamide (13):** The compound **13** was prepared from **10** using general procedure B and isolated as white solid with 40% yield.  $^1\text{H NMR}$  ( $\text{CDCl}_3$ ):  $\delta$  1.50 (m, 4H), 1.35 (m, 4H), 2.45 (t, 2H), 7.29–7.38 (m, 15H); MS (ESI) = 415 ( $\text{M}+\text{H}$ ) $^+$ .

**General procedure C: Azide reduction to amines (14-16).** The azide derivative (1 eq) was dissolved in methanol and triphenylphosphine (1.6 eq) was added followed by several drops of  $\text{H}_2\text{O}$ . The reaction was stirred overnight at room temperature. The solvent was removed and the residue was purified by flash chromatography using a mixture of DCM/MeOH/ammonia solution (9:1:0.1) as eluent.

**3-amino-N-(trityloxy)propanamide (14):** The compound **14** was obtained from **11** using general procedure C and isolated as white solid with 55% yield.  $^1\text{H NMR}$  ( $\text{CDCl}_3$ ):  $\delta$  2.85 (t, 2H), 2.13 (t, 2H), 7.25–7.45 (m, 15H); MS (ESI) = 347 ( $\text{M}+\text{H}$ ) $^+$ .

**5-amino-N-(trityloxy)pentanamide (15):** The compound **15** was obtained from **12** using general procedure C and isolated as white solid with 62% yield.  $^1\text{H NMR}$  ( $\text{CDCl}_3$ ):  $\delta$  1.08–1.25 (m, 4H), 2.53 (t, 2H), 3.34 (t, 2H), 3.47 (brs, 2H), 7.23–7.40 (m, 15H); MS (ESI) = 375 ( $\text{M}+\text{H}$ ) $^+$ .

**6-amino-N-(trityloxy)hexanamide (16):** The compound **16** was obtained from **13** using general procedure C and isolated as white solid with 65% yield.  $^1\text{H NMR}$  ( $\text{CDCl}_3$ ):  $\delta$  1.38–1.55 (m, 6H), 2.63 (t, 2H), 3.28 (t, 2H), 3.50 (brs, 2H), 7.20–7.42 (m, 15H); MS (ESI) = 389 ( $\text{M}+\text{H}$ ) $^+$ .

**General procedure D: Synthesis of thiourea bond (17-19):** Compound **7** was dissolved in DCM and the appropriate amine derivative was added. The resulting mixture was stirred overnight at room temperature. The solvent was evaporated and the residue was purified using flash chromatography using a mixture of EtOAc/petroleum ether (6:4) to afford the desired product.

**(E)-3-(3-(4-(3-oxo-3-(pyridin-3-yl)prop-1-en-1-yl)phenyl)thioureido)-N-(trityloxy)propanamide (17):** The compound **17** was prepared from **14** using general procedure D; yellow oil, yield 65%; <sup>1</sup>H NMR (CDCl<sub>3</sub>): δ 2.95 (t, 2H), 3.17 (t, 2H), 6.75 (d, 2H), 7.15-7.47 (m, 21H), 8.17-8.79 (m, 2H), 9.23 (s, 1H); MS (ESI) = 614 (M+H)<sup>+</sup>.

**(E)-5-(3-(4-(3-oxo-3-(pyridin-3-yl)prop-1-en-1-yl)phenyl)thioureido)-N-(trityloxy)pentanamide (18):** The compound **18** was prepared from **15** using general procedure D; yellow oil, yield 62%; <sup>1</sup>H NMR (CDCl<sub>3</sub>): δ 1.48-1.57 (m, 4H), 2.35 (t, 2H), 3.47 (t, 2H), 6.62 (d, 2H), 7.24-7.45 (m, 20H), 8.20-8.39 (m, 2H), 9.10 (s, 1H); MS (ESI) = 641 (M+H)<sup>+</sup>.

**(E)-6-(3-(4-(3-oxo-3-(pyridin-3-yl)prop-1-en-1-yl)phenyl)thioureido)-N-(trityloxy)hexanamide (19):** The compound **19** was prepared from **16** using general procedure D; yellow oil, 60% yield; <sup>1</sup>H NMR (CDCl<sub>3</sub>): δ 1.43-1.62 (m, 6H), 2.35 (t, 2H), 3.47 (t, 2H), 6.65 (d, 2H), 7.25-7.67 (m, 20H), 8.37-8.89 (m, 2H), 9.17 (s, 1H); MS (ESI) = 655(M+H)<sup>+</sup>.

**General procedure E: Trityl deprotection to afford hydroxamic acids (2-4):** The trityl-protected derivative was dissolved in anhydrous DCM and TFA was added, the color of the reaction turned into intense yellow. Triethylsilane was added dropwise until the reaction returned to the original color. The reaction was monitored by TLC. Once completed, the reaction mixture was concentrated under vacuum to afford a brown-red residue, which was dissolved in a minimum amount of DCM and the product was precipitated from ether. The precipitated was collected by filtration and finally washed with ether.

**(E)-N-hydroxy-3-(3-(4-(3-oxo-3-(pyridin-3-yl)prop-1-en-1-yl)phenyl)thioureido)propanamide (2):** The compound **2** was prepared from **17** using general procedure E and obtained as a yellow-red solid with 41% yield. <sup>1</sup>H NMR (CDCl<sub>3</sub>): δ 2.56 (t, 2H), 3.02 (t, 2H), 6.68 (d, 2H), 7.35-7.77 (m, 5H), 8.17-8.79 (m, 2H), 9.12 (s, 1H); 7.35 (brs, 2H); MS (ESI) = 371 (M+H)<sup>+</sup>.

**(E)-N-hydroxy-5-(3-(4-(3-oxo-3-(pyridin-3-yl)prop-1-en-1-yl)phenyl)thioureido)pentanamide (3):** The compound **3** was prepared from **18** using general procedure E and obtained as a yellow-red solid with 54% yield. <sup>1</sup>H NMR (CDCl<sub>3</sub>): δ 1.43-1.52 (m, 4H), 2.47 (t, 2H), 3.49 (t, 2H), 6.74 (d, 2H), 7.30-7.41 (m, 4H), 8.37-8.48 (m, 3H), 9.20 (s, 1H); MS (ESI) = 399 (M+H)<sup>+</sup>.

**(E)-N-hydroxy-6-(3-(4-(3-oxo-3-(pyridin-3-yl)prop-1-en-1-yl)phenyl)thioureido)hexanamide (4):**

The compound **4** was prepared from **19** using general procedure E and obtained as a brown-red solid with 59% yield. <sup>1</sup>H NMR (CDCl<sub>3</sub>): δ 1.76-2.02 (m, 6H), 2.45 (t, 2H), 3.60 (t, 2H), 7.02 (d, 2H), 7.25-7.67 (m, 5H), 8.25-8.79 (m, 2H), 9.07 (s, 1H), 7.45 (brs, 2H); MS (ESI) = 413 (M+H)<sup>+</sup>.

**Synthesis of pyridinium-*p*-toluenesulfonate:** *p*-toluenesulfonic acid monohydrate (1 eq) was added to a solution of pyridine (3 eq) and the mixture was stirred at room temperature for 20 min, pyridine in excess was removed on rotavapor to give pyridinium-*p*-toluenesulfonate as a white solid in quantitative yield. M.P.=121°C

**General procedure F: Tetrahydropyranyl ethers 25-29.** 3,4-dihydro-2H-pyran (10 eq) was added dropwise to a solution of the appropriate aldehyde (1eq) in dichloromethane. Pyridinium-*p*-toluenesulfonate (2 eq) was added and the reaction was stirred at room temperature for 12h. Upon completion of the reaction, the mixture was washed with saturated NaHCO<sub>3</sub> solution, H<sub>2</sub>O and brine. The organic phase was dried over Na<sub>2</sub>SO<sub>4</sub> and concentrated at reduced pressure to give a residue, which was purified by flash chromatography.

**3-methoxy-4-((tetrahydro-2H-pyran-2-yl)oxy)benzaldehyde (25):** The compound **25** was prepared following general procedure F and obtained as yellow oil in 62% yield. Mobile phase for flash chromatography: DCM/MeOH (9:1); <sup>1</sup>H-NMR (CDCl<sub>3</sub>, 400 MHz) δ 1.51-1.56 (m, 1H), 1.63-1.66 (m, 2H), 1.79-1.83 (m, 1H), 2.10-2.14 (m, 1H), 3.48-3.54 (m, 1H), 3.83-3.89 (m, 1H), 3.95 (s, 3H), 5.31-5.37 (m, 1H), 7.18 (d, 2H), 7.62 (s, 1H), 7.71 (d, 1H), 9.74 (s, 1H).

**3-ethoxy-4-((tetrahydro-2H-pyran-2-yl)oxy)benzaldehyde (26):** The compound **26** was prepared following general procedure F and obtained as yellow oil in 77% yield. Mobile phase for flash chromatography: DCM/MeOH (9:1); <sup>1</sup>H-NMR (CDCl<sub>3</sub>, 400 MHz) δ 1.42-1.56 (m, 3H), 1.61-1.71 (m, 2H), 1.72-1.79 (m, 1H), 2.05-2.12 (m, 1H), 3.33-3.41 (m, 1H), 3.78-3.85 (m, 1H), 3.91 (s, 3H), 5.22-5.27 (m, 1H), 7.11 (d, 2H), 7.67 (s, 1H), 7.81 (d, 1H), 9.88 (s, 1H).

**3,4-bis((tetrahydro-2H-pyran-2-yl)oxy)benzaldehyde (27):** The compound **27** was prepared following general procedure F and obtained as yellow oil in 45% yield. Mobile phase for flash chromatography: DCM/MeOH (9.5: 0.5); <sup>1</sup>H-NMR (CDCl<sub>3</sub>, 400 MHz) δ 1.59-1.94 (m, 8H), 2.01-2.14 (m, 2H), 3.59-3.72 (m, 2H), 3.82-3.96 (m, 2H), 5.39-5.41 (m, 2H), 7.13 (d, 2H), 7.44 (s, 1H), 7.77 (d, 1H), 9.63 (s, 1H).

**4-((tetrahydro-2H-pyran-2-yl)oxy)benzaldehyde (28):** The compound **28** was prepared following general procedure F and obtained as yellow oil in 80% yield. Mobile phase for flash chromatography: Petroleum ether/ EtOAc (9: 1); <sup>1</sup>H-NMR (CDCl<sub>3</sub>, 400 MHz) δ 1.55-1.61 (m, 1H), 1.60-1.68 (m, 2H), 1.80-1.88 (m, 1H), 2.04-2.10 (m, 1H), 3.55-3.61 (m, 1H), 3.94-4.01 (m, 1H), 5.33-5.37 (m, 1H), 7.17 (d, 2H), 7.98 (d, 2H), 9.87 (s, 1H).

**3-((tetrahydro-2H-pyran-2-yl)oxy)benzaldehyde (29):** The compound **29** was prepared following general procedure F and obtained as yellow oil in 85% yield. Mobile phase for flash chromatography: Petroleum ether/ EtOAc (9: 1); <sup>1</sup>H-NMR (CDCl<sub>3</sub>, 400 MHz) δ 1.55-1.61 (m, 1H), 1.65-1.72 (m, 2H), 1.83-1.88 (m, 1H), 1.95-2.05 (m, 1H), 3.60-3.66 (m, 1H), 3.80-3.86 (m, 1H), 5.50-5.54 (m, 1H), 7.15-7.18 (m, 2H), 7.79-7.84 (m, 2H), 9.97 (s, 1H).

**General procedure G: Aldol condensation to give derivatives 30-34.** The corresponding tetrahydropyranyl ether **25-29** (1 eq) was suspended in NaOH 2.5M and 3-acetylpyridine (1 eq) was added dropwise. The mixture was stirred at room temperature for 12h, the reaction color switched from yellow to red/orange. The solvent was removed and the residue was purified by flash chromatography.

**(E)-3-(3-methoxy-4-((tetrahydro-2H-pyran-2-yl)oxy)phenyl)-1-(pyridin-3-yl)prop-2-en-1-one (30):** The compound **30** was prepared from **25** using general procedure G and obtained as a yellow oil with 51% yield. Mobile phase for flash chromatography: DCM/MeOH (9:1) <sup>1</sup>H NMR (CDCl<sub>3</sub>, 400MHz): δ 1.61-1.68 (m, 2H), 1.77-1.88 (m, 2H), 1.91-2.01 (m, 2H), 3.52-3.59 (m, 1H), 3.81-3.87 (m, 1H), 3.91 (s, 3H), 5.29-5.38 (m, 1H), 6.84 (d, 1H), 7.28-7.51 (d, 4H), 7.82-7.95 (d, 1H), 8.49 (d, 1H), 8.86 (m, 1H), 9.35 (d, 1H).

**(E)-3-(3-ethoxy-4-((tetrahydro-2H-pyran-2-yl)oxy)phenyl)-1-(pyridin-3-yl)prop-2-en-1-one (31):** The compound **31** was prepared from **26** using general procedure G and obtained as a yellow oil with 60% yield. Mobile phase for flash chromatography: DCM/MeOH (9:1) <sup>1</sup>H NMR (CDCl<sub>3</sub>, 400MHz): δ 1.42-1.56 (m, 4H), 1.61-1.71 (m, 2H), 1.72-1.79 (m, 1H), 2.05-2.12 (m, 1H), 3.33-3.41 (m, 1H), 3.78-3.85 (m, 1H), 3.91 (s, 3H), 5.22-5.27 (m, 1H), 6.84 (d, 1H), 7.28-7.51 (d, 4H), 7.82-7.95 (d, 1H), 8.49 (d, 1H), 8.86 (m, 1H), 9.35 (d, 1H).

**(E)-3-(3,4-bis((tetrahydro-2H-pyran-2-yl)oxy)phenyl)-1-(pyridin-3-yl)prop-2-en-1-one (32):** The compound **32** was prepared from **27** using general procedure G and obtained as a yellow oil with 45% yield. Mobile phase for flash chromatography: DCM/MeOH (9:1) <sup>1</sup>H NMR (CDCl<sub>3</sub>, 400MHz):

$\delta$ 1.54-1.89 (m, 8H), 2.06-2.47 (m, 4H), 3.77-3.95 (m, 2H), 5.30-5.51 (m, 2H), 5.81-5.92 (m, 2H), 6.89 (d, 1H), 7.31-7.55 (d, 4H), 7.83-7.95 (d, 1H), 8.44 (d, 1H), 8.91 (m, 1H), 9.32 (d, 1H).

**(E)-1-(pyridin-3-yl)-3-(4-((tetrahydro-2H-pyran-2-yl)oxy)phenyl)prop-2-en-1-one (33):** The compound **33** was prepared from **28** using general procedure G and obtained as a yellow oil with 38% yield. Mobile phase for flash chromatography: DCM/toluene/MeOH (8:1:1).  $^1\text{H}$  NMR ( $\text{CDCl}_3$ , 400MHz):  $\delta$ 1.49-1.57 (m, 2H), 1.64-1.69 (m, 2H), 1.77-1.99 (m, 2H), 3.79-3.84 (m, 1H), 3.91-3.95 (m, 1H), 5.89-5.94 (m, 1H), 6.92 (d, 1H), 7.34-7.58 (d, 4H), 7.84-91 (d, 2H), 8.32 (d, 1H), 8.82 (m, 1H), 9.23 (d, 1H).

**(E)-1-(pyridin-3-yl)-3-(3-((tetrahydro-2H-pyran-2-yl)oxy)phenyl)prop-2-en-1-one (34):** The compound **34** was prepared from **29** using general procedure G and obtained as a yellow oil with 42% yield. Mobile phase for flash chromatography: DCM/MeOH (9.7:0.3).  $^1\text{H}$  NMR ( $\text{CDCl}_3$ , 400MHz):  $\delta$ 1.53-1.62 (m, 2H), 1.61-1.73 (m, 2H), 1.81-1.95 (m, 2H), 3.61-3.64 (m, 1H), 3.89-3.94 (m, 1H), 5.67-5.71 (m, 1H), 6.72 (d, 1H), 6.98 (d, 1H), 7.13-7.33 (m, 4H), 7.60 (d, 1H), 7.82 (m, 1H), 8.35 (d, 1H), 8.81 (d, 1H).

**General procedure H: Deprotection on hydroxyl groups to give products 20-24.** The appropriate THP-protected derivative **30-34** was dissolved in MeOH and *p*-toluenesulfonic acid in catalytic amount was added. The solution was stirred at room temperature for 12h. The solvent was removed and the residue purified by flash chromatography.

**(E)-3-(4-hydroxy-3-methoxyphenyl)-1-(pyridin-3-yl)prop-2-en-1-one (20):** The compound **20** was prepared from **30** using general procedure H and obtained as a yellow oil with 39% yield. Mobile phase for flash chromatography: DCM/MeOH (9.8:0.2).  $^1\text{H}$  NMR ( $\text{CD}_3\text{OD}$ , 400 MHz):  $\delta$ 3.98 (s, 3H), 6.97 (d, 1H), 7.15 (d, 1H), 7.23-7.27 (m, 2H), 7.34 (d, 1H), 7.48 (m, 1H), 7.80 (m, 1H), 8.30 (m, 1H), 8.81 (m, 1H), 8.23 (m, 1H);  $^{13}\text{C}$ -NMR ( $\text{CD}_3\text{OD}$ , 100 MHz):  $\delta$ 56.00, 110.80, 115.09, 118.88, 123.92, 126.89, 136.02, 146.50, 147.04, 148.99, 149.42, 152.67, 189.01; MS ( $\text{ESI}^+$ ): 256 ( $\text{M}+\text{H}$ ) $^+$ .

**(E)-3-(3-ethoxy-4-hydroxyphenyl)-1-(pyridin-3-yl)prop-2-en-1-one (21):** The compound **21** was prepared from **31** using general procedure H and obtained as a yellow oil with 30% yield. Mobile phase for flash chromatography: DCM/toluene/MeOH (9:0.9:0.1).  $^1\text{H}$  NMR ( $\text{CDCl}_3$ , 400 MHz):  $\delta$ 1.50 (t, 3H), 4.21 (q, 2H), 6.98 (d, 1H), 7.13 (d, 1H), 7.14-7.34 (m, 3H), 7.47 (d, 1H), 7.77 (d, 1H), 8.29 (m, 1H), 8.80 (m, 1H), 9.23 (m, 1H);  $^{13}\text{C}$  NMR ( $\text{CDCl}_3$ , 100 MHz):  $\delta$ 14.78, 64.71, 110.94,

114.98, 118.89, 123.75, 126.92, 136.00, 146.24, 146.56, 148.99, 149.48, 152.75, 189.04; MS (ESI<sup>+</sup>): 270 (M+H)<sup>+</sup>.

**(E)-3-(3,4-dihydroxyphenyl)-1-(pyridin-3-yl)prop-2-en-1-one (22):** The compound **22** was prepared from **32** using general procedure H and obtained as a yellow oil with 22% yield. Mobile phase for flash chromatography: DCM/MeOH (9.5:0.5). <sup>1</sup>H NMR (CD<sub>3</sub>OD, 400 MHz): δ6.95 (d, 2H), 7.34-7.44 (m, 3H), 7.87 (d, 1H), 8.32 (m, 1H), 8.91(d, 1H), 9.29 (d, 1H); MS (ESI<sup>+</sup>): 242 (M+H)<sup>+</sup>.

**(E)-3-(4-hydroxyphenyl)-1-(pyridin-3-yl)prop-2-en-1-one (23):** The compound **23** was prepared from **33** using general procedure H and obtained as a yellow oil with 38% yield. Mobile phase for flash chromatography: DCM/MeOH (9.5:0.5). <sup>1</sup>H NMR (CD<sub>3</sub>OD, 400 MHz): δ6.91 (d, 2H), 7.38-7.58 (m, 4H), 7.82 (d, 1H), 8.22 (m, 1H), 8.81 (d, 1H), 9.23 (d, 1H); MS (ESI<sup>+</sup>): 226 (M+H)<sup>+</sup>.

**(E)-3-(3-hydroxyphenyl)-1-(pyridin-3-yl)prop-2-en-1-one (24):** The compound **24** was prepared from **34** using general procedure H and obtained as a yellow oil with 21% yield. Mobile phase for flash chromatography: DCM/MeOH (9.5:0.5). <sup>1</sup>H NMR (CD<sub>3</sub>OD, 400 MHz): δ6.69 (d, 1H), 7.02 (d, 1H), 7.11-7.35 (m, 4H), 7.69 (d, 1H), 7.91 (m, 1H), 8.44 (d, 1H), 8.98 (d, 1H); MS (ESI<sup>+</sup>): 226 (M+H)<sup>+</sup>.

**General procedure for the synthesis of compound 55.** The monoprotected cadaverine **55** was obtained from reaction of 1,5-diaminopentane (cadaverine) with Boc<sub>2</sub>O in equimolar ratio. The solution of 1,5-diaminopentane in MeOH/triethylamine was cooled down to 0°C and stirred for 10min, followed by addition of Boc<sub>2</sub>O solution dropwise under nitrogen. The resulting mixture was allowed to warm to room temperature and stirred overnight. The solvent was evaporated and the residue dissolved in DCM and washed with H<sub>2</sub>O. Concentration of the organic phase gave a residue which was purified by gravity chromatography using mixture of DCM/MeOH/ammonia hydroxide (8:2:0.1) as mobile phase. Results of structure analysis were in agreement with data reported in literature.

**General procedure for the synthesis of compounds 56-59.** Ethyl trifluoroacetate (1eq) was added dropwise to a solution of polyamine **51-55** (1 eq) in MeOH at -78°C under nitrogen. The mixture was stirred for 30 min followed by addition of Boc<sub>2</sub>O solution dropwise. The reaction was allowed to warm to room temperature and stirred for 16h. Afterwards, 8 ml of H<sub>2</sub>O and 3 ml of concentrated NaOH were added and the reaction was continued at room temperature for 20h. The solvent was removed and the residue was dissolved in DCM and washed with H<sub>2</sub>O. The organic layer was dried

over Na<sub>2</sub>SO<sub>4</sub> and concentrated to give yellow oil, followed by purification with flash chromatography: mobile phase DCM/MeOH/ammonia hydroxide (9:1:0.1). Results of structure analysis were in agreement with data reported in literature.

**General procedure I: synthesis of compounds 60-64.** To a solution of fluorescein isothiocyanate (1 eq) and the appropriate Boc-protected polyamine **55-59** (1 eq) in DMF, triethylamine (1 eq) was added and the solution was stirred at room temperature for 12h. The residue obtained after the removal of solvent was purified by flash chromatography using a mixture of DCM/MeOH/formic acid (9.5:0.5:0.01).

**5-(3-(5-((tert-butoxycarbonyl)amino)pentyl)thioureido)-2-(6-hydroxy-3-oxo-3H-xanthen-9-yl)benzoic acid (60).** The compound **60** was prepared following the general procedure I and isolated as yellow oil in 65% yield.

**5-(3-(3-((tert-butoxycarbonyl)(3-((tert-butoxycarbonyl)amino)propyl)amino)propyl)thioureido)-2-(6-hydroxy-3-oxo-3H-xanthen-9-yl)benzoic acid (61).** The compound **61** was prepared following the general procedure I and isolated as yellow oil in 75% yield.

**5-(3-(9,12-bis(tert-butoxycarbonyl)-2,2-dimethyl-4-oxo-3-oxa-5,9,12-triazapentadecan-15-yl)thioureido)-2-(6-hydroxy-3-oxo-3H-xanthen-9-yl)benzoic acid (62).** The compound **62** was prepared following the general procedure I and isolated as yellow oil in 73% yield.

**5-(3-(3-((tert-butoxycarbonyl)(3-((tert-butoxycarbonyl)(3-(methylamino)propyl)amino)propyl)amino)propyl)thioureido)-2-(6-hydroxy-3-oxo-3H-xanthen-9-yl)benzoic acid (63).** The compound **63** was prepared following the general procedure I and isolated as yellow oil in 76% yield.

**5-(3-(9,14-bis(tert-butoxycarbonyl)-2,2-dimethyl-4-oxo-3-oxa-5,9,14-triazaheptadecan-17-yl)thioureido)-2-(6-hydroxy-3-oxo-3H-xanthen-9-yl)benzoic acid (64).** The compound **64** was prepared following the general procedure I and isolated as yellow oil in 80% yield.

**General procedure J: synthesis of compounds 65-69.** The solution of 4-chloro-7-nitrobenzofurazan (0.5 eq) and the respective Boc-protected polyamine **55-59** (1 eq) in 5ml of dioxane was stirred at room temperature for 12h, protected from exposure to the light. The solvent was evaporated and the resulting residue was purified by flash chromatography using a mixture of petroleum ether/ethyl acetate (6:4) as mobile phase.

**tert-butyl (5-((7-nitrobenzo[c][1,2,5]oxadiazol-4-yl)amino)pentyl)carbamate (65).** The compound **65** was prepared following the general procedure J and isolated as yellow solid in 65% yield.

**tert-butyl(3-((tert-butoxycarbonyl)amino)propyl)(3-((7-nitrobenzo[c][1,2,5]oxadiazol-4-yl)amino)propyl)carbamate (66).** The compound **66** was prepared following the general procedure J and isolated as yellow solid in 85% yield.

**tert-butyl(2-((tert-butoxycarbonyl)(3-((7-nitrobenzo[c][1,2,5]oxadiazol-4-yl)amino)propyl)amino)ethyl)(3-((tert-butoxycarbonyl)amino)propyl)carbamate (67).** The compound **67** was prepared following the general procedure J and isolated as yellow solid in 89% yield.

**tert-butyl(3-((tert-butoxycarbonyl)(3-((tert-butoxycarbonyl)amino)propyl)amino)propyl)(3-((7-nitrobenzo[c][1,2,5]oxadiazol-4-yl)amino)propyl)carbamate (68).** The compound **68** was prepared following the general procedure J and isolated as yellow solid in 88% yield.

**tert-butyl(4-((tert-butoxycarbonyl)(3-((tert-butoxycarbonyl)amino)propyl)amino)butyl)(3-((7-nitrobenzo[c][1,2,5]oxadiazol-4-yl)amino)propyl)carbamate (69).** The compound **68** was prepared following the general procedure J and isolated as yellow solid in 81% yield.

**General procedure K: synthesis of compounds 70-74.** 7-Amino-4-methyl-3-coumarinylacetic acid (1 eq) and N-hydroxysuccinimide (1.5 eq) were dissolved in DMF and the solution was cooled on ice bath. Dicyclohexylcarbodiimide (1.5 eq) was added and the reaction was allowed to warm to room temperature and stirred for 3h. Removal of solvent gave a brown solid which was used directly for the next step: the solid was dissolved in DMF at 0°C, Boc-protected polyamine (1.2 eq) and DIPEA (1.2 eq) were added in sequence and the mixture was stirred at room temperature for 16h. The solvent was evaporated to give a residue which was purified by flash chromatography using a mixture of EtOAc/Toluene/petroleum ether (8:1:1) as mobile phase.

**tert-butyl (5-(2-(7-amino-4-methyl-2-oxo-2H-chromen-3-yl)acetamido)pentyl)carbamate (70).** The compound **70** was prepared following the general procedure K and isolated as yellow oil in 55% yield.

**tert-butyl(3-(2-(7-amino-4-methyl-2-oxo-2H-chromen-3-yl)acetamido)propyl)(3-((tert-butoxycarbonyl)amino)propyl)carbamate (71).** The compound **71** was prepared following the general procedure K and isolated as yellow oil in 83% yield.



***tert*-butyl(2-((3-(2-(7-amino-4-methyl-2-oxo-2H-chromen-3-yl)acetamido)propyl)(*tert*-butoxycarbonyl)amino)ethyl)(3-((*tert*-butoxycarbonyl)amino)propyl)carbamate (72).** The compound **72** was prepared following the general procedure K and isolated as yellow oil in 89% yield.

***tert*-butyl(3-((3-(2-(6-amino-1-methyl-3-oxo-3,4-dihydronaphthalen-2-yl)acetamido)propyl)(*tert*-butoxycarbonyl)amino)propyl)(3-((*tert*-butoxycarbonyl)amino)propyl)carbamate (73).** The compound **73** was prepared following the general procedure K and isolated as yellow oil in 90% yield.

***tert*-butyl(3-(2-(7-amino-4-methyl-2-oxo-2H-chromen-3-yl)acetamido)propyl)(4-((*tert*-butoxycarbonyl)(3-((*tert*-butoxycarbonyl)amino)propyl)amino)butyl)carbamate (74).** The compound **74** was prepared following the general procedure K and isolated as yellow oil in 92% yield.

**General procedure L: Cleavage of Boc group for the synthesis of compounds 35-49.** To a solution of the appropriate conjugate fluorophore/Boc-polyamine in methanol, HCl 2N was added and the resulting mixture was stirred for 12h at room temperature. The solvent was removed and the residue was dissolved in H<sub>2</sub>O and washed with ethyl acetate. The aqueous phase was evaporated and the resulting residue was dried at vacuum pump to give the final products **35-49** as chlorohydrate salts.

**5-(3-(5-aminopentyl)thioureido)-2-(6-hydroxy-3-oxo-3H-xanthen-9-yl)benzoic acid (35):** The compound **35** was obtained from **60** using general procedure L and isolated as yellow oil with 75% yield. <sup>1</sup>H-NMR (400 MHz, CDCl<sub>3</sub>): δ1.26-1.29 (m, 2H), 1.50-1.54 (m, 4H), 2.00 (brs, 1H), 2.65 (t, 2H), 3.67 (t, 2H), 4.00 (brs, 1H), 5.06-5.11 (m, 3H), 5.82-5.84 (m, 1H), 6.44-6.47 (m, 2H), 6.64-6.68 (m, 1H), 6.97-6.98 (m, 2H), 7.20-7.34 (m, 4H), 7.81 (d,1H), 11.00 (brs, 1H).

**5-(3-(3-((3-aminopropyl)amino)propyl)thioureido)-2-(6-hydroxy-3-oxo-3H-xanthen-9-yl)benzoic acid (36).** The compound **36** was obtained from **61** using general procedure L and isolated as yellow oil with 72% yield; <sup>1</sup>H-NMR (CDCl<sub>3</sub>, 400 MHz): δ1.93-1.94 (m, 2H), 2.93-2.98 (m, 8H), 6.81 (s, 1H), 7.12 (d, 1H), 7.21-7.24 (m, 2H), 7.59-7.61 (m, 1H), 8.05 (s, 1H); MS(ESI): 522(M+H)<sup>+</sup>.

**5-(3-(3-((2-((3-aminopropyl)amino)ethyl)amino)propyl)thioureido)-2-(6-hydroxy-3-oxo-3H-xanthen-9-yl)benzoic acid (37)**. The compound **37** was obtained from **62** using general procedure L and isolated as yellow oil with 72% yield. <sup>1</sup>H-NMR (CDCl<sub>3</sub>, 400 MHz): δ 1.97-2.04 (m, 4H), 2.99 (t, 2H), 3.01-3.16 (m 4H), 3.18-3.40 (m, 4H), 3.60 (t, 2H), 6.74-6.79 (m, 4H), 7.04 (d, 1H), 7.22 (d, 1H), 7.63 (d, 1H), 8.11 (s, 1H); MS(ESI): 565 (M+H)<sup>+</sup>.

**5-(3-(3-((3-((3-aminopropyl)amino)propyl)amino)propyl)thioureido)-2-(6-hydroxy-3-oxo-3H-xanthen-9-yl)benzoic acid (38)**. The compound **38** was obtained from **63** using general procedure L and isolated as yellow oil with 71% yield. <sup>1</sup>H-NMR (CDCl<sub>3</sub>, 400 MHz): δ 1.94-2.02 (m, 6H), 2.94-3.06 (m, 10H), 3.62 (t, 2H), 6.79-6.82 (m, 4H), 7.14 (d, 1H), 7.23 (d, 1H), 7.62 (d, 1H), 8.05 (s, 1H); MS(ESI): 579 (M+H)<sup>+</sup>.

**5-(3-(3-((4-((3-aminopropyl)amino)butyl)amino)propyl)thioureido)-2-(6-hydroxy-3-oxo-3H-xanthen-9-yl)benzoic acid (39)**. The compound **39** was obtained from **64** using general procedure L and isolated as yellow oil with 71% yield. <sup>1</sup>H-NMR (CDCl<sub>3</sub>, 400 MHz): δ 1.91-2.05 (m, 6H), 2.90-3.10 (m, 12H), 3.71 (t, 2H), 6.72-6.81 (m, 4H), 7.17 (d, 1H), 7.26 (d, 1H), 7.69 (d, 1H), 8.01 (s, 1H); MS(ESI): 593 (M+H)<sup>+</sup>.

**N1-(7-nitrobenzo[c][1,2,5]oxadiazol-4-yl)pentane-1,5-diamine (40)**. The compound **40** was obtained from **65** using general procedure L and isolated as yellow solid with 75% yield. <sup>1</sup>H-NMR (400 MHz, CDCl<sub>3</sub>): δ 1.39-1.44 (m, 2H), 1.59-1.74 (m, 4H), 2.88-2.91 (t, 2H), 3.44 (brs, 2H), 6.17-6.20 (d, 1H), 8.29-8.31 (d, 1H).

**N1-(3-aminopropyl)-N3-(7-nitrobenzo[c][1,2,5]oxadiazol-4-yl)propane-1,3-diamine (41)**. The compound **41** was obtained from **66** using general procedure L and isolated as yellow solid with 83% yield. <sup>1</sup>H-NMR (CDCl<sub>3</sub>, 400 MHz): δ 1.95-2.09 (m, 4H), 2.97 (t, 2H), 3.06 (t, 2H), 3.11 (t, 2H), 3.58 (t, 2H), 6.24 (d, 1H), 8.36 (d, 1H).; MS(ESI): 295 (M+H)<sup>+</sup>.

**N1-(2-((3-aminopropyl)amino)ethyl)-N3-(7-nitrobenzo[c][1,2,5]oxadiazol-4-yl)propane-1,3-diamine (42)**. The compound **42** was obtained from **67** using general procedure L and isolated as yellow solid with 88% yield. <sup>1</sup>H-NMR (CDCl<sub>3</sub>, 400 MHz): δ 1.97-2.13 (m, 4H), 2.99 (t, 2H), 3.10 (t, 2H), 3.19 (t, 2H), 3.36-3.40 (m, 4H), 3.59 (t, 2H), 6.23 (d, 1H), 8.33 (d, 1H).; MS(ESI): 339 (M+H)<sup>+</sup>.

**N1-(3-aminopropyl)-N3-(3-((7-nitrobenzo[c][1,2,5]oxadiazol-4-yl)amino)propyl)propane-1,3-diamine (43)**. The compound **43** was obtained from **68** using general procedure L and isolated as

yellow solid with 86% yield. <sup>1</sup>H-NMR (CDCl<sub>3</sub>, 400 MHz): δ1.99-2.10 (m, 8H), 2.97-3.14 (m, 8H), 3.10 (t, 2H), 6.29 (d, 1H), 8.40 (d, 1H); MS(ESI): 352 (M+H)<sup>+</sup>.

**N1-(3-aminopropyl)-N4-(3-((7-nitrobenzo[c][1,2,5]oxadiazol-4-yl)amino)propyl)butane-1,4-diamine (44)**. The compound **44** was obtained from **69** using general procedure L and isolated as yellow solid with 88% yield. <sup>1</sup>H-NMR (CDCl<sub>3</sub>, 400 MHz): δ1.95-2.07 (m, 10H), 2.96-3.19 (m, 8H), 3.15 (t, 2H), 6.33(d,1H), 8.49(d,1H); MS(ESI): 366 (M+H)<sup>+</sup>.

**2-(7-amino-4-methyl-2-oxo-2H-chromen-3-yl)-N-(5-aminopentyl)acetamide (45)**. The compound **45** was obtained from **70** using general procedure L and isolated as red solid with 80% yield. <sup>1</sup>H-NMR (400 MHz, CDCl<sub>3</sub>): δ1.15-1.21 (m, 2H), 1.31-1.35 (t, 2H), 1.45-1.50 (m, 2H), 2.15 (s, 3H), 2.77-2.81(t,2H), 2.97-3.00(t,2H), 3.36(s,2H), 7.10-7.15 (t, 2H), 7.59-7.61 (d, 1H).

**2-(7-amino-4-methyl-2-oxo-2H-chromen-3-yl)-N-(3-((3-aminopropyl)amino)propyl)acetamide (46)**. The compound **46** was obtained from **71** using general procedure L and isolated as red solid with 78% yield. <sup>1</sup>H-NMR (CDCl<sub>3</sub>, 400 MHz): δ1.82-1.85 (m, 2H), 1.92-1.97 (m, 2H), 2.37 (s, 3H), 2.99-3.07 (m, 4H), 3.32-3.36 (m, 4H), 3.57 (s, 2H), 7.16 (m, 2H), 7.78 (d, 1H); MS(ESI): 347 (M+H)<sup>+</sup>.

**2-(7-amino-4-methyl-2-oxo-2H-chromen-3-yl)-N-(3-((2-((3-aminopropyl) amino)ethyl)amino)propyl)acetamide (47)**. The compound **47** was obtained from **72** using general procedure L and isolated as red solid with 86% yield. <sup>1</sup>H-NMR (CDCl<sub>3</sub>, 400 MHz): δ1.80-1.83 (m, 2H), 1.98-2.01 (m, 2H), 2.31 (s, 3H), 2.97-3.05 (m, 4H), 3.12 (t, 2H), 3.22 (t,2 H), 3.32-3.35 (m, 4H), 3.53 (s, 2H), 7.11 (m, 2H), 7.72 (d, 1H); MS(ESI): 390 (M+H)<sup>+</sup>.

**2-(7-amino-4-methyl-2-oxo-2H-chromen-3-yl)-N-(3-((3-((3-aminopropyl)amino)propyl)amino)propyl)acetamide (48)**. The compound **48** was obtained from **73** using general procedure L and isolated as red solid with 87% yield. <sup>1</sup>H-NMR (CDCl<sub>3</sub>, 400 MHz): δ1.78-1.81 (m, 4H), 1.94-2.01 (m, 2H), 2.35 (s, 3H), 2.91-3.00 (m, 4H), 3.15 (t, 2H), 3.19 (t,2 H), 3.31-3.36 (m, 4H), 3.57 (s, 2H), 7.21 (m, 2H), 7.82 (d, 1H); MS(ESI): 404 (M+H)<sup>+</sup>.

**2-(7-amino-4-methyl-2-oxo-2H-chromen-3-yl)-N-(3-((4-((3-aminopropyl)amino)butyl)amino)propyl)acetamide (49)**. The compound **49** was obtained from **74** using general procedure L and isolated as red solid with 91% yield. <sup>1</sup>H-NMR (CDCl<sub>3</sub>, 400 MHz): δ1.73-1.80 (m, 6H), 1.92-1.99 (m,

2H), 2.31 (s, 3H), 2.94-3.02 (m, 4H), 3.19 (t, 2H), 3.21 (t, 2H), 3.32-3.37 (m, 4H), 3.61 (s, 2H), 7.16 (m, 2H), 7.77 (d, 1H); MS(ESI): 418 (M+H)<sup>+</sup>.

**General procedure for the synthesis of all-hydrocarbon stapled peptide (75).** Aminomethylated polystyrene resin-Rink amide resin LL (0.25mmol, substitution 0.35mmol/g)- was placed in a polypropylene reaction vessel and allowed to swell in 10ml of DMF/DCM for 30 minutes followed by washing using DMF. The Fmoc group that protects the amine group, both on the resin linker and each amino acid, was removed with 8ml of piperidine 20% in DMF. For the coupling of non-olefinic amino acids, freshly prepared amino acid solution in DMF activated by coupling reagent- HBTU (4 eq), N-methylmorpholine (8 eq)- was added to the reaction vessel, and the coupling reaction was conducted at room temperature for 1h. Each coupling reaction outcome was verified using Kaiser reagents. For the coupling of olefinic amino acids, unnatural amino acid (2eq), HATU (2eq), Cl-HOBt (2eq) and DIPEA (4eq) were dissolved in DMF and the solution was added to the reaction vessel. The reaction was continued for 3h at room temperature. For the reaction of ring closing metathesis, the resin-bound peptide with completed sequence was washed by DCM and 1,2-DCE. The resin was placed in a two-neck round-bottom flask and treated with a 10mM solution of Grubb's catalyst II generation (0.2eq) in 1,2-dichloroethane. The mixture is stirred under a continuous N<sub>2</sub> flow for 12h at 50°C. At the completion, the resin is washed and dried under vacuum. After the removal of Fmoc group from the last residue, the resin-bound peptide washed and dried under vacuum overnight. The peptide was cleaved using a TFA cleavage cocktail containing TFA, triisopropylsilane, 1,2-ethanedithiol and H<sub>2</sub>O for 90min at room temperature. Afterwards, the TFA solution was concentrated with a gentle stream of N<sub>2</sub> and the peptide was precipitated with cold diethyl ether. The residue was dried under vacuum to give a brown-black solid, which was purified in C-18 reverse phase (20-40µm, 100 Å) using gradient system H<sub>2</sub>O/acetonitrile. The fractions were collected and dried using lyophilizer to give a white solid.

**General procedure for the synthesis of fluorophore-labeled stapled peptide (76).** Once the peptide sequence was completed, Fmoc group on the last residue was removed. A mixture of Fmoc-protected non- $\alpha$ -amino acid, HOBt and NMM in DMF was added, the reaction was kept on rotator for 1h at room temperature. The Fmoc-group was removed and fluorescein isothiocyanate in DMF was added and the reaction, protected from light, was allowed to continue for 12h at room temperature. The resin was cleaved and the residue was purified following the same procedure as for compound **75**. The final compound was isolated as a yellow solid.

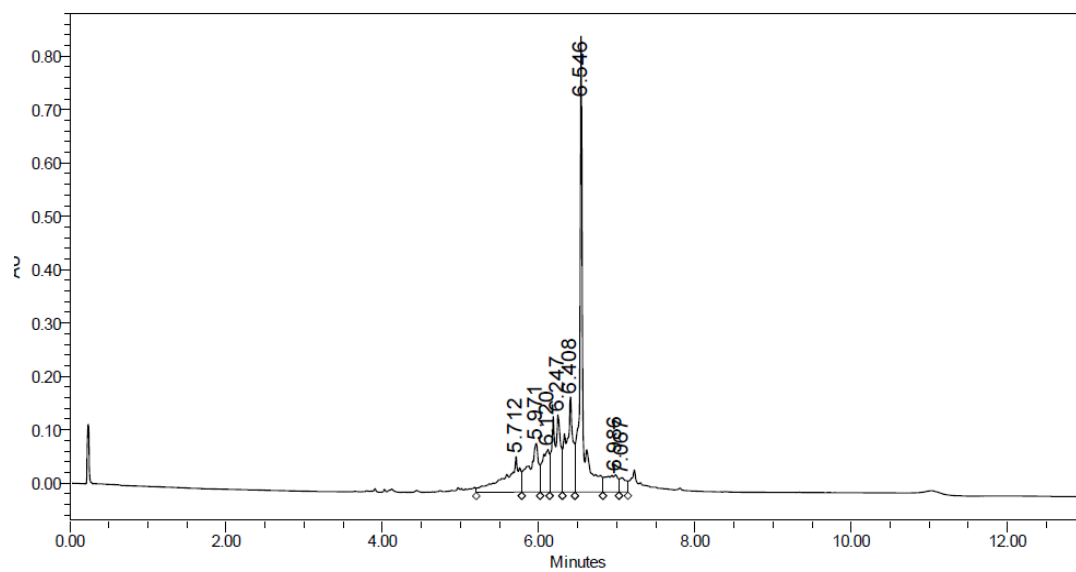
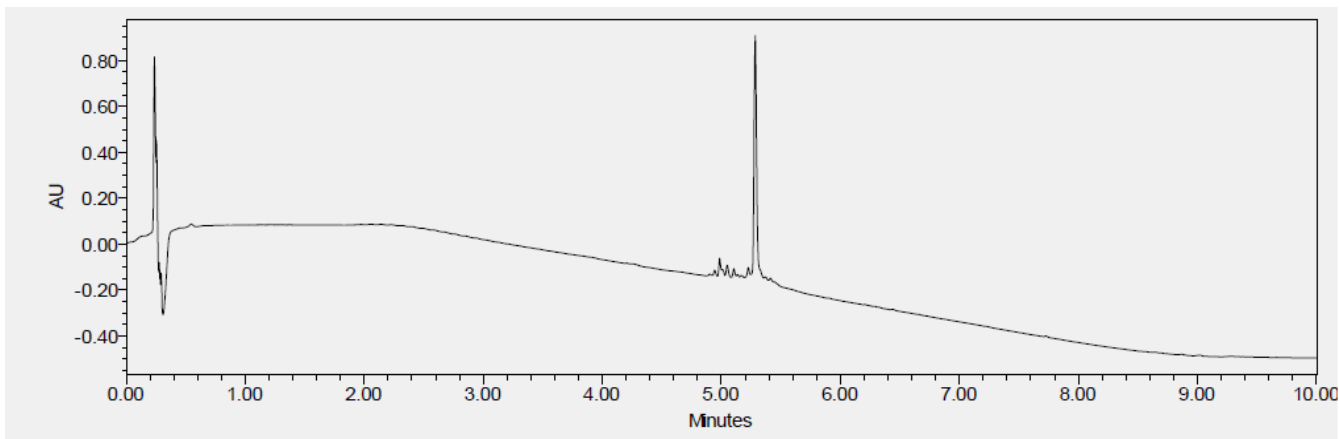


**Figure 26.** Chromatogram showing the purity results for compounds **75** (above) and **76** (below).

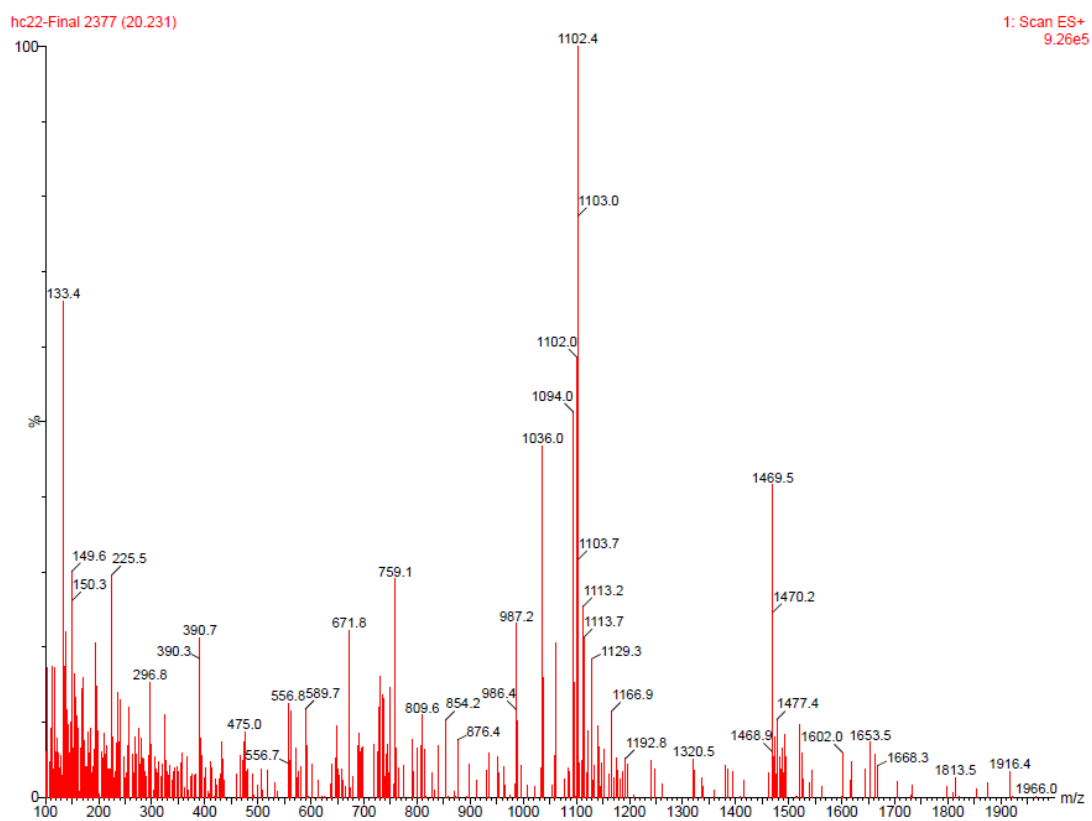
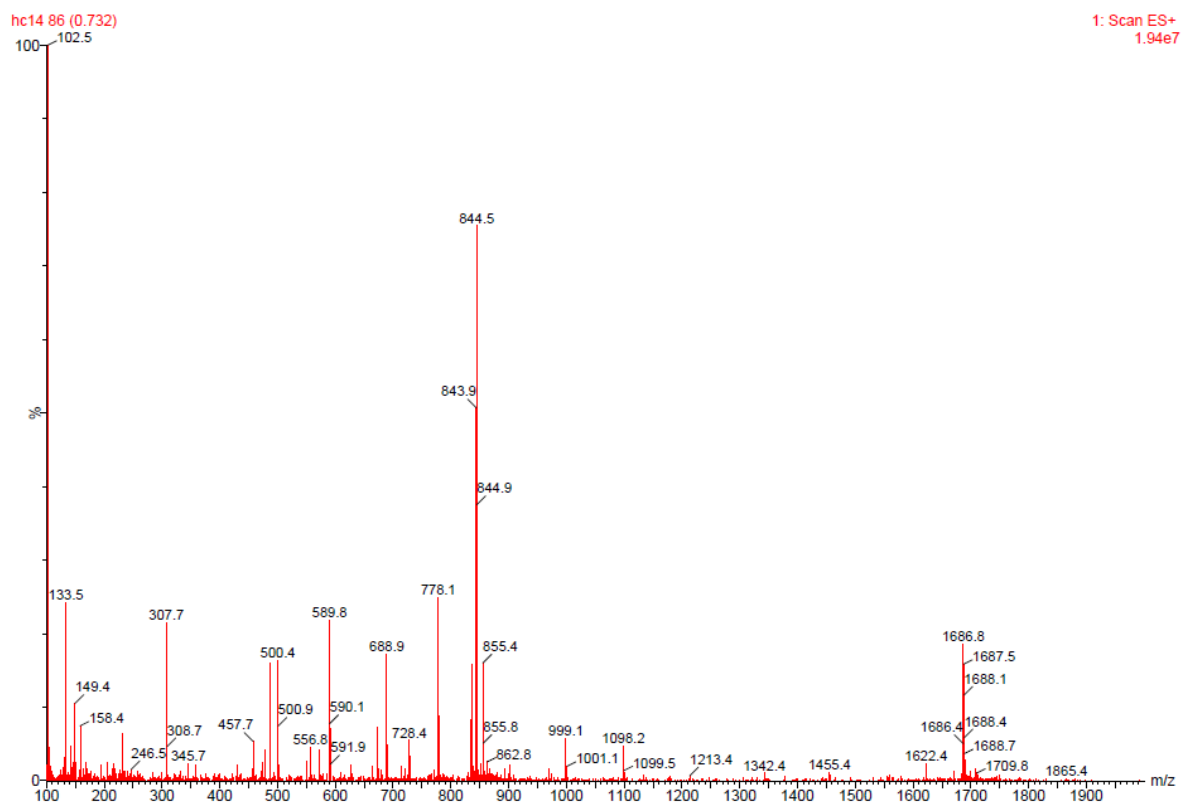


**Figure 27.** Mass spectra for compounds **75** (above) and **76** (below).

## 2. Biology

### 1) *In vitro* TG2 inhibition assay

Kinetic runs were recorded on a UV-visible spectrophotometer at 405nm and 25°C, in a buffer composed of 3.33mM CaCl<sub>2</sub>, 50µM EDTA and 0.1M MOPS (pH 7.0). All aqueous solutions were prepared using deionized water. Each kinetic assay was performed using 180µL of buffer, 5µL of a DMSO stock solution of substrate N-Cbz-Glu(γ-p-nitrophenylester)Gly (2.2mM), 10µL of a solution of hTG2 at 0.05 U/mL (final concentration of 2.5mU/mL), in the presence of 0-5µL (contingent on solubility) of a DMSO stock solution of the test inhibitor. The volume of DMSO was then adjusted so that it represented 5% of the final volume. IC<sub>50</sub> values were obtained as the negative x-intercept of a Dixon plot.

### 2) *In vitro* measurement of antioxidant activity

Solvents of the highest purity grade were used as received. Cumene was twice percolated on an alumina column before use. AIBN was recrystallized from methanol. Autoxidation experiments were performed in a two-channel oxygen uptake apparatus, based on a Validyne DP 15 differential pressure transducer. In a typical experiment, an air-saturated solution of cumene containing AIBN was equilibrated with an identical reference solution. After equilibration, and when a constant O<sub>2</sub> consumption was reached, a concentrated solution of test compound (final concentration = 5-15µM) was injected in the sample flask. The oxygen consumption in the sample was measured after calibration of the apparatus from the differential pressure recorded with time between the two channels.

### 3) *In vitro* evaluation of inhibition on Aβ<sub>42</sub> self-aggregation by Thioflavin T (ThT) assay

1,1,1,3,3,3-Hexafluoro-2-propanol (HFIP)-pretreated Aβ<sub>42</sub> samples (Bachem AG, Switzerland) were resolubilized with a CH<sub>3</sub>CN/0.3 mM Na<sub>2</sub>CO<sub>3</sub>/250mM NaOH (48.4:48.4:3.2) mixture to have a stable stock solution ([Aβ<sub>42</sub>]=500µM). Tested inhibitors were dissolved in MeOH and diluted in the assay buffer. Experiments were performed by incubating the peptide diluted in 10mM phosphate buffer (pH 8.0) containing 10mM NaCl at 30°C (Thermomixer Comfort, Eppendorf, Italy) for 24h (final Aβ concentration=50µM) with and without inhibitor.

Inhibition studies were performed by incubating Aβ<sub>42</sub> samples under the assay conditions reported above, with and without tested inhibitors. Inhibitors were screened at 10µM in a 0.2:1 ratio with Aβ<sub>42</sub>. After incubation, samples were diluted to a final volume of 2.0mL with 50mM glycine-NaOH buffer (pH 8.5) containing 1.5µM ThT. A 300s time scan of fluorescence intensity was performed (λ<sub>exc</sub>=446

nm;  $\lambda_{em}=490$  nm), and values at plateau were averaged after subtracting the background fluorescence of 1.5 $\mu$ M ThT solution. Blanks containing inhibitor and ThT were also prepared and taken into account for quenching and fluorescence properties. The fluorescence intensities were compared and the percentage inhibition was calculated.

#### 4) *In vitro* GSK3 $\beta$ inhibition assay by UHPLC/UV analysis

Stock standard solutions of ATP and ADP (1mM) were prepared in buffer A composed of 6mM ammonium acetate and 1.6 mM magnesium acetate (pH7.4). Stock standard solutions of 1 mM GSM and 100 ng/ $\mu$ L GSK3 $\beta$  were prepared in the buffer A, divided in aliquots and stored at -80°C. The test inhibitors were dissolved in DMSO in order to obtain 1 mg/mL stock solutions stored at -20°C.

The UHPLC/UV analysis was carried out by using a JascoX-LC (Jasco Europe, Cremella, Italy). Instrument control, data acquisition and processing were performed using software CromNAVControl Center. A reversed phase column (Kinetex 1.7  $\mu$ m, C8, 50x2.1 mm) was equilibrated with a mobile phase consisting of buffer containing 20 mM sodium phosphate and 5 mM tetra-n-butylammonium/methanol. Optimized chromatographic separation of ATP and ADP was carried out under isocratic conditions with a flow rate of 0.4 mL/min. The eluent was monitored at 260 nm for nucleotide detection.

The inhibition studies were performed by setting the assay solutions, composed of GSK3 $\beta$  (2.5ng/ $\mu$ L), ATP (250 $\mu$ M), GSM (250 $\mu$ M), in presence of increased concentrations of test inhibitors. The solutions were incubated at 30°C for 30 min. After incubation, assay reactions were stopped adding 40  $\mu$ L of methanol. An additional 40 $\mu$ L volume of mobile phase buffer for chromatographic analysis was further added to the assay reaction. An aliquot of 1 $\mu$ L of the reaction mixture was injected into the chromatograph under the chromatographic conditions previously described. The peak areas were compared with those obtained in absence of inhibitor. Inhibition curves were obtained for each compound by plotting the inhibition percentage versus the logarithm of inhibitor concentration in the assay solution. The linear regression parameters were determined for each curve and IC<sub>50</sub> value was extrapolated.

#### 5) Cell viability assay using MTS method

The human tumor cells were cultured in complete growth media at 37°C in CO<sub>2</sub>/air (5%+95%) humidified atmosphere. The assay was performed in triplicate for each test compound. A 50 $\mu$ l of cell solution with appropriate concentration were dispensed in 96-well plates and were incubated for 24h. Cells were treated with the test compounds at a range of concentration 0.1 $\mu$ M-200 $\mu$ M, prepared as 50 $\mu$ l solution in culture media. Treated cells were incubated for 72h at 37°C in CO<sub>2</sub>/air (5%+95%)



humidified atmosphere. Afterwards, 20µl of a solution containing MTS reagent/phenazine ethosulfate (19:1) were added. After 4h incubation, the absorbance at wavelength 490nm was measured using SpectraMax M5 instrument (Molecular Devices). Blank control without cells were taken into account as reference for fluorescence-quenching effect.

#### 6) Co-immunoprecipitation assay

Cells grown in complete culture media were cultured in 100mm dish cells incubated for 24h at 37°C. Cell lysis was performed using 300µl lysis Buffer (0.025M Tris, 0.15M NaCl, 0.001M EDTA, 1% NP-400, 5% glycerol, pH 7.4) containing 5% of Protease/Phosphatase inhibitor cocktail at 4°C for 20 minutes. The lysate was centrifuged at 13000xg for 10min at 4°C to afford the pellet which was discarded. The supernatant was transferred to a pre-cooled 1.5ml centrifuge tube and the protein concentration was measured using BCA assay. 1mg of cell protein was used for co-immunoprecipitation. 5µg of affinity purified polyclonal antibody was used to capture the bait protein  $\gamma$ COP1. In a 1.5ml microcentrifuge tube the antibody was added to the cell lysate and the mixture was incubated overnight at 4°C. Afterwards, Protein A/G agarose beads was added and the mixture was allowed to incubate overnight at 4°C. At the completion of incubation, the mixture was subject to centrifugation at 1000xg for 5 minute at 4°C to yield a pellet. The supernatant was removed carefully, followed by 4 times washing using 1ml of cooled PBS buffer.

The pellet obtained after co-immunoprecipitation was suspended in 30µl of 2X SDS sample buffer containing  $\beta$ -mercaptoethanol, in order to elute the proteins of interest. The sample was heated at 75°C for 20min and 20µl of sample was loaded on 12% SDS-PAGE gel (Mini-Protean TGX gels). Protein separation and blotting on PVDF membrane were performed. The blot was blocked with non-fat milk for 4h at 4°C, followed by primary antibody incubation overnight at 4°C. As primary antibodies, mouse monoclonal antibody anti- $\zeta$ COP1 and antibody anti- $\gamma$ COP1 have been used for immunodetection. Incubation with secondary antibody -goat anti-mouse IgG HPR- was performed at room temperature for 1 hour. The signal development was obtained through chemiluminescence. After adding the enzyme substrate (Clarity Western ECL substrate), the chemiluminescent signal was measured using LICOR Odyssey FC Imaging system.

#### 7) Fluorescence cell imaging

PC3 cells were cultured in complete growth media at 37°C in CO<sub>2</sub>/air (5%+95%) were seeded in triplicate in 96-well plate at concentration of 5000cells/50µl culture media. 50µl drug solution in culture media was added to a final concentration of 200µM and the incubation was performed for 72h at 37°C. Culture media was removed and the cells were rinsed with 100µl PBS (x3) and fixed

with 4% para-formaldehyde in PBS for 10min at 37°C. Fixation solution was removed and the cells were washed with 100µl PBS (x2). Cell suspension was viewed for fluorescence signal using Hermes WiScan (Idea Biomedical). The imaging system is able to generate 10x images.

#### 8) Docking studies

Docking simulations were performed using Dock6.5 and Chimera1.10.2 (UCSF Chimera software) based on the crystal structure of the  $\zeta$ COP1/ $\gamma$ COP1 complex bound to Arf1 (PDB code: 3TJZ). The PDB file was acquired and edited using GEdit to contain only the  $\zeta$ COP1 subunit. The coordinate file was then read into Chimera, where all hydrogen atoms were erased. Next, the DockPrep command was executed, and the resulting structure was saved in mol2 format. The cleaned PDB and prepped mol2 files were transferred to the Computational Biology server to generate a molecular surface file. Spheres defining the molecular surface of  $\zeta$ COP1 were generated from an input file and were used to create a box that defines the areas of  $\zeta$ COP1 to be examined with ligand poses. Finally, using the charged  $\zeta$ COP file – and constrained by the parameters of the box – an energy grid was computed. Ligands were docked against the energy grid using the determine parameters. The assay was run for each of the three ZINC databases (acidic, basic, and neutral) contained in the Computational Biology cluster. Each ligand was docked in flexible mode using 500 orientations.

## List of Figures/Tables

<b>Figure 1.</b> TG2 transamidation and deamidation catalytic mechanism.....	6
<b>Figure 2.</b> X-ray crystal structures of two conformations (open and closed) of human TG2 in complex with GDP in $\beta$ 1-barrel (A) and with peptidic inhibitor in the active site (B) .....	7
<b>Figure 3.</b> General structure of cinnamoyl derivatives and their SAR tendencies.....	14
<b>Figure 4.</b> Dual-target ligand design strategy.....	16
<b>Figure 5.</b> Effect of HDAC inhibitors on chromatin remodelling and transcription.....	21
<b>Figure 6.</b> Representation of TSA in the active-site of HDLP.....	23
<b>Figure 7.</b> TSA and general structural illustration of HDAC inhibitors.....	23
<b>Figure 8.</b> FDA approved HDACs inhibitors.....	24
<b>Table 1.</b> Isoform-specific HDAC inhibitors.....	25
<b>Figure 9.</b> Drug design of compounds <b>2-4</b> .....	26
<b>Table 2.</b> IC <sub>50</sub> values of the TG2 inhibitors <b>2-4</b> .....	29
<b>Figure10.</b> Chemical structure of different classes of polyphenols.....	35
<b>Figure11.</b> General structure-activity relationships for hydroxycinnamic acids.....	37
<b>Figure12.</b> Drug design of compounds <b>20-24</b> .....	38
<b>Table 3.</b> Results of antioxidant activity, inhibition activity on TG2, A $\beta$ self-aggregation and GSK3 $\beta$ for compounds <b>20-24</b> and Ethyl ferulate as reference compound.....	43
<b>Figure 13.</b> Jabłonski diagram.....	45
<b>Figure14.</b> Generic absorption and emission spectra.....	46
<b>Figure 15.</b> Equilibrium between the open and closed forms of fluorescein.....	49
<b>Table 4.</b> Six classes of small-molecule fluorephores.....	52
<b>Table 5.</b> Drug design of compounds <b>35-49</b> .....	54
<b>Figure 16.</b> Pathways of vesicular transport by coat proteins <sup>130</sup> .....	59
<b>Figure 17.</b> Structure of coatomer.....	60
<b>Figure 18.</b> Model for membrane recruitment of coatomer <sup>144</sup> .....	61
<b>Figure 19.</b> Mechanism of tumor dependence on COPZ1 <sup>152</sup> .....	63
<b>Figure 20.</b> Crystal structure of dimer $\zeta$ COP1 (golden yellow) and $\gamma$ COP1(blue).....	65
<b>Figure 21.</b> Drug design of compound <b>75</b> .....	66
<b>Figure 22.</b> Cell viability assay results on cell lines treated with compounds <b>75-76</b> .....	70
<b>Figure 23.</b> Co-IP experiments conducted on Calu6 cell line. 1) Control; 2) Sample treated with compound <b>75</b> .....	71
<b>Figure 24.</b> Docking process representation and results.....	72
<b>Figure 25.</b> Images of PC3 cells treated with fluorophore-labeled peptide (compound <b>76</b> ) at 200 $\mu$ M. A) 6h treatment. B) 12h treatment.....	73
<b>Figure 26.</b> Chromatogram showing the purity results for compounds <b>75</b> (above) and <b>76</b> (below).....	89
<b>Figure 27.</b> Mass spectra for compounds <b>75</b> (above) and <b>76</b> (below).....	90

## Acknowledgements

The present manuscript is a summary of my three-year doctoral study/research, carried out for the first two years in the Department for Life Quality Sciences at the University of Bologna, with the research topics discussed in the Section I of the present thesis, and for the third year in the Department of Drug Discovery and Biomedical Sciences at the Medical University of South Carolina, with the research project presented in Section II.

First and foremost, I would like to thank my PhD supervisor, Professor Tumiatti Vincenzo, for the guidance through the entire three years, and Dr. Milelli Andrea for mentoring me during the my first two-year PhD research at the Department for Life Quality Sciences in Rimini. I also would like to thank Professor Patrick M. Woster, who mentored me for the third year of my PhD in his laboratory at the Department of Drug Discovery and Biomedical Sciences in Charleston.

In addition, I would like to thank the research groups involved in the present investigation:

- Professor Andrisano Vincenza, Dr. De Simone Angela, Department for Life Quality Sciences, University of Bologna;
- Professor Valgimigli Luca, Dr. Andrea Baschieri, Department of Chemistry "Giacomo Ciamician", University of Bologna;
- Dr. Bartolini Manuela, Department of Pharmacy and Biotechnology, University of Bologna;
- Dr. Basso Manuela, Centro per la Biologia Integrata, University of Trento;
- Professor Jeffrey W. Keillor, Department of Chemistry and Biomolecular Sciences, University of Ottawa;
- Professor Patrick M. Woster, Dr. Isuru R. Kumarasinghe, Jonathan Turner, Department of Drug Discovery and Biomedical Sciences, Medical University of South Carolina.

I would like to thank A.R.O.P. onlus association and the Faculty of Fashion Culture and Technology of University of Bologna- Rimini campus, for offering me the part-time jobs which represented an important financial support during my first two years of PhD; In addition, I would like to thank the Department of Life Quality Sciences (University of Bologna) and the Department of Drug Discovery and Biomedical Sciences (Medical University of South Carolina) for providing me with scholarships and stipends, so that I could carry out the exchange program as visiting scholar in the United States.

At the end, I acknowledge the understanding and patience from my family –my parents, my sisters Xiaojie and Tingting, my partner Mohamed- that helped me to overcome difficult times and to eventually complete the three-year doctoral course.

## References

1. Griffin, M.; Casadio, R.; Bergamini, C. M., Transglutaminases: nature's biological glues. *Biochem. J.* **2002**, *368* (2), 377-396.
2. Case, A.; Stein, R. L., Kinetic analysis of the action of tissue transglutaminase on peptide and protein substrates. *Biochemistry* **2003**, *42* (31), 9466-9481.
3. Esposito C, C. I., Mammalian transglutaminases. Identification of substrates as a key to physiological function and physiopathological relevance. *FEBS J* **2005**, *272* (3), 615-631.
4. Lai, T.-S.; Slaughter, T. F.; Peoples, K. A.; Hettasch, J. M.; Greenberg, C. S., Regulation of human tissue transglutaminase function by magnesium-nucleotide complexes Identification of distinct binding sites for Mg-GTP and Mg-ATP. *J. Biol. Chem.* **1998**, *273* (3), 1776-1781.
5. Zhang, J.; Lesort, M.; Guttman, R. P.; Johnson, G. V., Modulation of the in situ activity of tissue transglutaminase by calcium and GTP. *J. Biol. Chem.* **1998**, *273* (4), 2288-2295.
6. Lai, T.; Hausladen, A.; Slaughter, T.; Eu, J.; Stamler, J.; Greenberg, C., Calcium regulates S-nitrosylation, denitrosylation, and activity of tissue transglutaminase. *Biochemistry* **2001**, *40* (16), 4904-4910.
7. Siegel, M.; Khosla, C., Transglutaminase 2 inhibitors and their therapeutic role in disease states. *Pharmacol. Ther.* **2007**, *115* (2), 232-245.
8. Fesus, L.; Thomazy, V.; Falus, A., Induction and activation of tissue transglutaminase during programmed cell death. *FEBS Lett.* **1987**, *224* (1), 104-108.
9. Janiak, A.; Zemskov, E. A.; Belkin, A. M., Cell surface transglutaminase promotes RhoA activation via integrin clustering and suppression of the Src-p190RhoGAP signaling pathway. *Mol. Biol. Cell* **2006**, *17* (4), 1606-1619.
10. Liu, S.; Cerione, R. A.; Clardy, J., Structural basis for the guanine nucleotide-binding activity of tissue transglutaminase and its regulation of transamidation activity. *Proceedings of the National Academy of Sciences* **2002**, *99* (5), 2743-2747.
11. Pinkas, D. M.; Strop, P.; Brunger, A. T.; Khosla, C., Transglutaminase 2 Undergoes a Large Conformational Change upon Activation. *PLoS Biol.* **2007**, *5* (12).
12. Quarsten, H.; Molberg, O.; Fugger, L.; McAdam, S.; Sollid, L., HLA binding and T cell recognition of a tissue transglutaminase-modified gliadin epitope. *Eur. J. Immunol.* **1999**, *29* (8), 2506.
13. Dieterich, W.; Ehnis, T.; Bauer, M.; Donner, P.; Volta, U.; Riecken, E.; Schuppan, D., Identification of tissue transglutaminase as the autoantigen of celiac disease. *Nat. Med.* **1997**, *3* (7), 797.
14. Shridas, P.; Sharma, Y.; Balasubramanian, D., Transglutaminase-mediated cross-linking of alpha-crystallin: structural and functional consequences. *FEBS Lett.* **2001**, *499* (3), 245.
15. Verma, A.; Wang, H.; Manavathi, B.; Fok, J. Y.; Mann, A. P.; Kumar, R.; Mehta, K., Increased expression of tissue transglutaminase in pancreatic ductal adenocarcinoma and its implications in drug resistance and metastasis. *Cancer Res.* **2006**, *66* (21), 10525-10533.
16. Mehta, K.; Fok, J.; Miller, F. R.; Koul, D.; Sahin, A. A., Prognostic significance of tissue transglutaminase in drug resistant and metastatic breast cancer. *Clin. Cancer Res.* **2004**, *10* (23), 8068-8076.
17. Fok, J. Y.; Ekmekcioglu, S.; Mehta, K., Implications of tissue transglutaminase expression in malignant melanoma. *Mol. Cancer Ther.* **2006**, *5* (6), 1493-1503.
18. Antonyak, M. A.; Li, B.; Boroughs, L. K.; Johnson, J. L.; Druso, J. E.; Bryant, K. L.; Holowka, D. A.; Cerione, R. A., Cancer cell-derived microvesicles induce transformation by transferring tissue transglutaminase and fibronectin to recipient cells. *Proceedings of the National Academy of Sciences* **2011**, *108* (12), 4852-4857.

19. (a) de Cristofaro, T.; Affaitati, A.; Cariello, L.; Avvedimento, E. V.; Varrone, S., The length of polyglutamine tract, its level of expression, the rate of degradation, and the transglutaminase activity influence the formation of intracellular aggregates. *Biochem. Biophys. Res. Commun.* **1999**, *260* (1), 150-158; (b) Junn, E.; Ronchetti, R. D.; Quezado, M. M.; Kim, S.-Y.; Mouradian, M. M., Tissue transglutaminase-induced aggregation of  $\alpha$ -synuclein: Implications for Lewy body formation in Parkinson's disease and dementia with Lewy bodies. *Proceedings of the National Academy of Sciences* **2003**, *100* (4), 2047-2052.
20. Ruan, Q.; Johnson, G., Transglutaminase 2 in neurodegenerative disorders. *Frontiers in bioscience: a journal and virtual library* **2006**, *12*, 891-904.
21. (a) Selkoe, D. J.; Ihara, Y.; Salazar, F. J., Alzheimer's disease: insolubility of partially purified paired helical filaments in sodium dodecyl sulfate and urea. *Science* **1982**, *215* (4537), 1243-1245; (b) Selkoe, D. J., Amyloid protein and Alzheimer's disease. *Sci. Am.* **1991**, *265* (5), 68-78.
22. Ikura, K.; Takahata, K.; Sasaki, R., Cross - linking of a synthetic partial - length (1 - 28) peptide of the Alzheimer  $\beta$  /A4 amyloid protein by transglutaminase. *FEBS Lett.* **1993**, *326* (1-3), 109-111.
23. Miller, M. L.; Johnson, G. V., Transglutaminase Cross - Linking of the  $\tau$  Protein. *J. Neurochem.* **1995**, *65* (4), 1760-1770.
24. Tucholski, J.; Kuret, J.; Johnson, G. V., Tau is modified by tissue transglutaminase in situ: possible functional and metabolic effects of polyamination. *J. Neurochem.* **1999**, *73*, 1871-1880.
25. Bonelli, R. M.; Aschoff, A.; Jirikowski, G., Cerebrospinal fluid tissue transglutaminase in vascular dementia. *J. Neurol. Sci.* **2002**, *203*, 207-209.
26. Zhang, W.; Johnson, B. R.; Suri, D. E.; Martinez, J.; Bjornsson, T. D., Immunohistochemical demonstration of tissue transglutaminase in amyloid plaques. *Acta Neuropathol.* **1998**, *96* (4), 395-400.
27. Johnson, G. V.; Cox, T. M.; Lockhart, J. P.; Zinnerman, M. D.; Miller, M. L.; Powers, R. E., Transglutaminase activity is increased in Alzheimer's disease brain. *Brain Res.* **1997**, *751* (2), 323-329.
28. Wilhelmus, M.; de Jager, M.; Smit, A.; van der Loo, R.; Drukarch, B., Catalytically active tissue transglutaminase colocalises with A $\beta$  pathology in Alzheimer's disease mouse models. *Sci. Rep.* **2016**, *6*, 20569.
29. Folk, J.; Cole, P., Identification of a functional cysteine essential for the activity of guinea pig liver transglutaminase. *J. Biol. Chem.* **1966**, *241* (13), 3238-3240.
30. Chica, R. A.; Gagnon, P.; Keillor, J. W.; Pelletier, J. N., Tissue transglutaminase acylation: Proposed role of conserved active site Tyr and Trp residues revealed by molecular modeling of peptide substrate binding. *Protein Sci.* **2004**, *13* (4), 979-991.
31. Pardin, C.; Gillet, S. M.; Keillor, J. W., Synthesis and evaluation of peptidic irreversible inhibitors of tissue transglutaminase. *Bioorg. Med. Chem.* **2006**, *14* (24), 8379-8385.
32. Tso, J. Y.; Bower, S. G.; Zalkin, H., Mechanism of inactivation of glutamine amidotransferases by the antitumor drug L-( $\alpha$  S, 5S)- $\alpha$ -amino-3-chloro-4, 5-dihydro-5-isoxazoleacetic acid (AT-125). *J. Biol. Chem.* **1980**, *255* (14), 6734-6738.
33. Choi, K.; Siegel, M.; Piper, J.; Yuan, L.; Cho, E.; Strnad, P.; Omary, B.; Rich, K.; Khosla, C., Chemistry and biology of dihydroisoxazole derivatives: selective inhibitors of human transglutaminase 2. *Chem. Biol.* **2005**, *12* (4), 469-475.
34. Yuan, L.; Siegel, M.; Choi, K.; Khosla, C.; Miller, C. R.; Jackson, E.; Piwnica-Worms, D.; Rich, K., Transglutaminase 2 inhibitor, KCC009, disrupts fibronectin assembly in the extracellular matrix and sensitizes orthotopic glioblastomas to chemotherapy. *Oncogene* **2007**, *26* (18), 2563-2573.
35. Powers, J. C.; Asgian, J. L.; Ekici, Ö. D.; James, K. E., Irreversible inhibitors of serine, cysteine, and threonine proteases. *Chem. Rev.* **2002**, *102* (12), 4639-4750.

36. Wityak, J.; Prime, M. E.; Brookfield, F. A.; Courtney, S. M.; Erfan, S.; Johnsen, S.; Johnson, P. D.; Li, M.; Marston, R. W.; Reed, L., SAR development of lysine-based irreversible inhibitors of transglutaminase 2 for Huntington's disease. *ACS Med. Chem. Lett.* **2012**, *3* (12), 1024-1028.
37. Lorand, L.; Conrad, S. M., Transglutaminases. In *Transglutaminase*, Springer: 1984; pp 9-35.
38. Jeitner, T. M.; Delikatny, E. J.; Ahlqvist, J.; Capper, H.; Cooper, A. J., Mechanism for the inhibition of transglutaminase 2 by cystamine. *Biochem. Pharmacol.* **2005**, *69* (6), 961-970.
39. Lesort, M.; Lee, M.; Tucholski, J.; Johnson, G. V., Cystamine inhibits caspase activity Implications for the treatment of polyglutamine disorders. *J. Biol. Chem.* **2003**, *278* (6), 3825-3830.
40. Badarau, E.; Collighan, R. J.; Griffin, M., Recent advances in the development of tissue transglutaminase (TG2) inhibitors. *Amino Acids* **2013**, *44* (1), 119-127.
41. Klöck, C.; Jin, X.; Choi, K.; Khosla, C.; Madrid, P. B.; Spencer, A.; Raimundo, B. C.; Boardman, P.; Lanza, G.; Griffin, J. H., Acylideneoxindoles: a new class of reversible inhibitors of human transglutaminase 2. *Bioorg. Med. Chem. Lett.* **2011**, *21* (9), 2692-2696.
42. Kim, N.; Kwak, S. H.; Lee, S.-H.; Juvekar, V.; Lee, B.-I.; Ahn, H.-C.; Kim, S.-Y.; Gong, Y.-D., Novel 3-arylethynyl-substituted thieno [3, 4-b] pyrazine derivatives as human transglutaminase 2 inhibitors. *Organic & biomolecular chemistry* **2014**, *12* (27), 4932-4940.
43. Duval, E.; Case, A.; Stein, R. L.; Cuny, G. D., Structure–activity relationship study of novel tissue transglutaminase inhibitors. *Bioorg. Med. Chem. Lett.* **2005**, *15* (7), 1885-1889.
44. Case, A.; Stein, R. L., Kinetic analysis of the interaction of tissue transglutaminase with a nonpeptidic slow-binding inhibitor. *Biochemistry* **2007**, *46* (4), 1106-1115.
45. Pardin, C.; Pelletier, J. N.; Lubell, W. D.; Keillor, J. W., Cinnamoyl Inhibitors of Tissue Transglutaminase†. *The Journal of organic chemistry* **2008**, *73* (15), 5766-5775.
46. Pardin, C.; Roy, I.; Chica, R. A.; Bonneil, E.; Thibault, P.; Lubell, W. D.; Pelletier, J. N.; Keillor, J. W., Photolabeling of Tissue Transglutaminase Reveals the Binding Mode of Potent Cinnamoyl Inhibitors†. *Biochemistry* **2009**, *48* (15), 3346-3353.
47. Pardin, C.; Roy, I.; Lubell, W. D.; Keillor, J. W., Reversible and competitive cinnamoyl triazole inhibitors of tissue transglutaminase. *Chem. Biol. Drug Des.* **2008**, *72* (3), 189-196.
48. Morphy, R.; Kay, C.; Rankovic, Z., From magic bullets to designed multiple ligands. *Drug discovery today* **2004**, *9* (15), 641-651.
49. Bottegoni, G.; Favia, A. D.; Recanatini, M.; Cavalli, A., The role of fragment-based and computational methods in polypharmacology. *Drug discovery today* **2012**, *17* (1), 23-34.
50. Morphy, R.; Rankovic, Z., The physicochemical challenges of designing multiple ligands. *J. Med. Chem.* **2006**, *49* (16), 4961-4970.
51. Hopkins, A. L.; Mason, J. S.; Overington, J. P., Can we rationally design promiscuous drugs? *Curr. Opin. Struct. Biol.* **2006**, *16* (1), 127-136.
52. Tumiatti, V.; Minarini, A.; Bolognesi, M.; Milelli, A.; Rosini, M.; Melchiorre, C., Tacrine derivatives and Alzheimer's disease. *Curr. Med. Chem.* **2010**, *17* (17), 1825-1838.
53. Wood, P. L.; Khan, M. A.; Moskal, J. R., Cellular thiol pools are responsible for sequestration of cytotoxic reactive aldehydes: central role of free cysteine and cysteamine. *Brain Res.* **2007**, *1158*, 158-163.
54. Minarini, A.; Milelli, A.; Tumiatti, V.; Rosini, M.; Simoni, E.; Bolognesi, M.; Andrisano, V.; Bartolini, M.; Motori, E.; Angeloni, C., Cystamine-tacrine dimer: a new multi-target-directed ligand as potential therapeutic agent for Alzheimer's disease treatment. *Neuropharmacology* **2012**, *62* (2), 997-1003.
55. Patel, L.; Grossberg, G. T., Combination therapy for Alzheimer's disease. *Drugs Aging* **2011**, *28* (7), 539-546.
56. Simoni, E.; Daniele, S.; Bottegoni, G.; Pizzirani, D.; Trincavelli, M. L.; Goldoni, L.; Tarozzo, G.; Reggiani, A.; Martini, C.; Piomelli, D., Combining galantamine and memantine in multitargeted, new chemical entities potentially useful in Alzheimer's disease. *J. Med. Chem.* **2012**, *55* (22), 9708-9721.

57. Lu, C.; Guo, Y.; Yan, J.; Luo, Z.; Luo, H.-B.; Yan, M.; Huang, L.; Li, X., Design, synthesis, and evaluation of multitarget-directed resveratrol derivatives for the treatment of Alzheimer's disease. *J. Med. Chem.* **2013**, *56* (14), 5843-5859.
58. ONO, K.; YOSHIIKE, Y.; TAKASHIMA, A.; HASEGAWA, K.; NAIKI, H.; YAMADA, M., Potent anti-amyloidogenic and fibril-destabilizing effects of polyphenols in vitro: implications for the prevention and therapeutics of Alzheimer's disease. *J. Neurochem.* **2003**, *87* (1), 172-181.
59. Ritchie, C.; Bush, A.; Mackinnon, A.; Macfarlane, S.; Mastwyk, M.; MacGregor, L.; Kiers, L.; Cherny, R.; Li, Q.; Tammer, A., Metal-protein attenuation with iodochlorhydroxyquin (clioquinol) targeting Abeta amyloid deposition and toxicity in Alzheimer disease: a pilot phase 2 clinical trial. *Arch. Neurol.* **2003**, *60* (12), 1685.
60. Kazantsev, A. G.; Thompson, L. M., Therapeutic application of histone deacetylase inhibitors for central nervous system disorders. *Nature Reviews Drug Discovery* **2008**, *7* (10), 854-868.
61. Gräff, J.; Rei, D.; Guan, J.-S.; Wang, W.-Y.; Seo, J.; Hennig, K. M.; Nieland, T. J.; Fass, D. M.; Kao, P. F.; Kahn, M., An epigenetic blockade of cognitive functions in the neurodegenerating brain. *Nature* **2012**, *483* (7388), 222-226.
62. Ding, H.; Dolan, P. J.; Johnson, G. V., Histone deacetylase 6 interacts with the microtubule - associated protein tau. *J. Neurochem.* **2008**, *106* (5), 2119-2130.
63. Govindarajan, N.; Rao, P.; Burkhardt, S.; Sananbenesi, F.; Schlüter, O.; Bradke, F.; Lu, J.; Fischer, A., Reducing HDAC6 ameliorates cognitive deficits in a mouse model for Alzheimer's disease. *EMBO Mol. Med.* **2013**, *5* (1), 52-63.
64. Pandey, U. B.; Nie, Z.; Batlevi, Y.; McCray, B. A.; Ritson, G. P.; Nedelsky, N. B.; Schwartz, S. L.; DiProspero, N. A.; Knight, M. A.; Schuldiner, O., HDAC6 rescues neurodegeneration and provides an essential link between autophagy and the UPS. *Nature* **2007**, *447* (7146), 860-864.
65. Sung, Y. M.; Lee, T.; Yoon, H.; DiBattista, A. M.; Song, J. M.; Sohn, Y.; Moffat, E. I.; Turner, R. S.; Jung, M.; Kim, J., Mercaptoacetamide-based class II HDAC inhibitor lowers A $\beta$  levels and improves learning and memory in a mouse model of Alzheimer's disease. *Exp. Neurol.* **2013**, *239*, 192-201.
66. Ricobaraza, A.; Cuadrado-Tejedor, M.; Pérez-Mediavilla, A.; Frechilla, D.; Del Río, J.; García-Osta, A., Phenylbutyrate ameliorates cognitive deficit and reduces tau pathology in an Alzheimer's disease mouse model. *Neuropsychopharmacology* **2009**, *34* (7), 1721-1732.
67. Finnin, M. S.; Donigian, J. R.; Cohen, A.; Richon, V. M.; Rifkind, R. A.; Marks, P. A.; Breslow, R.; Pavletich, N. P., Structures of a histone deacetylase homologue bound to the TSA and SAHA inhibitors. *Nature* **1999**, *401* (6749), 188-193.
68. Vannini, A.; Volpari, C.; Filocamo, G.; Casavola, E. C.; Brunetti, M.; Renzoni, D.; Chakravarty, P.; Paolini, C.; De Francesco, R.; Gallinari, P., Crystal structure of a eukaryotic zinc-dependent histone deacetylase, human HDAC8, complexed with a hydroxamic acid inhibitor. *Proc. Natl. Acad. Sci. U. S. A.* **2004**, *101* (42), 15064-15069.
69. Agrawal, N.; Pallos, J.; Slepko, N.; Apostol, B. L.; Bodai, L.; Chang, L.-W.; Chiang, A.-S.; Thompson, L. M.; Marsh, J. L., Identification of combinatorial drug regimens for treatment of Huntington's disease using *Drosophila*. *Proc. Natl. Acad. Sci. U. S. A.* **2005**, *102* (10), 3777-3781.
70. (a) Selley, M.; Close, D.; Stern, S., The effect of increased concentrations of homocysteine on the concentration of (E)-4-hydroxy-2-nonenal in the plasma and cerebrospinal fluid of patients with Alzheimer's disease. *Neurobiol. Aging* **2002**, *23* (3), 383-388; (b) Dexter, D.; Carter, C.; Wells, F.; Javoy - Agid, F.; Agid, Y.; Lees, A.; Jenner, P.; Marsden, C. D., Basal lipid peroxidation in substantia nigra is increased in Parkinson's disease. *J. Neurochem.* **1989**, *52* (2), 381-389; (c) Arlt, S.; Beisiegel, U.; Kontush, A., Lipid peroxidation in neurodegeneration: new insights into Alzheimer's disease. *Curr. Opin. Lipidol.* **2002**, *13* (3), 289-294.
71. Ermak, G.; Davies, K. J., Calcium and oxidative stress: from cell signaling to cell death. *Mol. Immunol.* **2002**, *38* (10), 713-721.



72. Yamamoto, K.; Ishikawa, T.; Sakabe, T.; Taguchi, T.; Kawai, S.; Marsala, M., The hydroxyl radical scavenger Nicaraven inhibits glutamate release after spinal injury in rats. *Neuroreport* **1998**, *9* (7), 1655-1659.
73. Mattson, M., Excitotoxic and excitoprotective mechanisms: abundant targets for the prevention and treatment of neurodegenerative disorders. *Neuromolecular Med.* **2003**, *3* (2), 65.
74. (a) Lovell, M.; Robertson, J.; Teesdale, W.; Campbell, J.; Markesbery, W., Copper, iron and zinc in Alzheimer's disease senile plaques. *J. Neurol. Sci.* **1998**, *158* (1), 47-52; (b) Smith, M. A.; Harris, P. L.; Sayre, L. M.; Perry, G., Iron accumulation in Alzheimer disease is a source of redox-generated free radicals. *Proceedings of the National Academy of Sciences* **1997**, *94* (18), 9866-9868.
75. Sayre, L.; Perry, G.; Harris, P.; Liu, Y.; Schubert, K.; Smith, M., In situ oxidative catalysis by neurofibrillary tangles and senile plaques in Alzheimer's disease: a central role for bound transition metals. *J. Neurochem.* **2000**, *74* (1), 270-279.
76. (a) Opazo, C.; Huang, X.; Cherny, R. A.; Moir, R. D.; Roher, A. E.; White, A. R.; Cappai, R.; Masters, C. L.; Tanzi, R. E.; Inestrosa, N. C., Metalloenzyme-like Activity of Alzheimer's Disease  $\beta$ -Amyloid Cu-dependent catalytic conversion of dopamine, cholesterol, and biological reducing agents to neurotoxic H<sub>2</sub>O<sub>2</sub>. *J. Biol. Chem.* **2002**, *277* (43), 40302-40308; (b) Huang, X.; Cuajungco, M. P.; Atwood, C. S.; Hartshorn, M. A.; Tyndall, J. D.; Hanson, G. R.; Stokes, K. C.; Leopold, M.; Multhaup, G.; Goldstein, L. E., Cu (II) potentiation of Alzheimer A $\beta$  neurotoxicity correlation with cell-free hydrogen peroxide production and metal reduction. *J. Biol. Chem.* **1999**, *274* (52), 37111-37116.
77. Dong, J.; Atwood, C. S.; Anderson, V. E.; Siedlak, S. L.; Smith, M. A.; Perry, G.; Carey, P. R., Metal binding and oxidation of amyloid- $\beta$  within isolated senile plaque cores: Raman microscopic evidence. *Biochemistry* **2003**, *42* (10), 2768-2773.
78. Stamer, K.; Vogel, R.; Thies, E.; Mandelkow, E.; Mandelkow, E.-M., Tau blocks traffic of organelles, neurofilaments, and APP vesicles in neurons and enhances oxidative stress. *The Journal of cell biology* **2002**, *156* (6), 1051-1063.
79. David, D. C.; Hauptmann, S.; Scherping, I.; Schuessel, K.; Keil, U.; Rizzu, P.; Ravid, R.; Dröse, S.; Brandt, U.; Müller, W. E., Proteomic and functional analyses reveal a mitochondrial dysfunction in P301L tau transgenic mice. *J. Biol. Chem.* **2005**, *280* (25), 23802-23814.
80. Dumont, M.; Stack, C.; Elipenahli, C.; Jainuddin, S.; Gerges, M.; Starkova, N. N.; Yang, L.; Starkov, A. A.; Beal, F., Behavioral deficit, oxidative stress, and mitochondrial dysfunction precede tau pathology in P301S transgenic mice. *The FASEB Journal* **2011**, *25* (11), 4063-4072.
81. Pérez, M.; Cuadros, R.; Smith, M.; Perry, G.; Avila, J., Phosphorylated, but not native, tau protein assembles following reaction with the lipid peroxidation product, 4-hydroxy-2-nonenal. *FEBS Lett.* **2000**, *486* (3), 270-274.
82. Liu, Q.; Smith, M. A.; Avilá, J.; DeBernardis, J.; Kansal, M.; Takeda, A.; Zhu, X.; Nunomura, A.; Honda, K.; Moreira, P. I., Alzheimer-specific epitopes of tau represent lipid peroxidation-induced conformations. *Free Radic. Biol. Med.* **2005**, *38* (6), 746-754.
83. Gamblin, T. C.; King, M. E.; Kuret, J.; Berry, R. W.; Binder, L. I., Oxidative regulation of fatty acid-induced tau polymerization. *Biochemistry* **2000**, *39* (46), 14203-14210.
84. Lovell, M. A.; Xiong, S.; Xie, C.; Davies, P.; Markesbery, W. R., Induction of hyperphosphorylated tau in primary rat cortical neuron cultures mediated by oxidative stress and glycogen synthase kinase-3. *J. Alzheimers Dis.* **2004**, *6* (6), 659-671.
85. Lee, K.-Y.; Koh, S.-H.; Noh, M. Y.; Park, K.-W.; Lee, Y. J.; Kim, S. H., Glycogen synthase kinase-3 $\beta$  activity plays very important roles in determining the fate of oxidative stress-inflicted neuronal cells. *Brain Res.* **2007**, *1129*, 89-99.
86. Stocker, R., Dietary and pharmacological antioxidants in atherosclerosis. *Curr. Opin. Lipidol.* **1999**, *10* (6), 589-598.
87. Pandey, K. B.; Rizvi, S. I., Plant polyphenols as dietary antioxidants in human health and disease. *Oxid. Med. Cell. Longev.* **2009**, *2* (5), 270-278.

88. Serafini, M., The role of antioxidants in disease prevention. *Medicine* **2006**, *34* (12), 533-535.
89. Bravo, L., Polyphenols: chemistry, dietary sources, metabolism, and nutritional significance. *Nutr. Rev.* **1998**, *56* (11), 317-333.
90. Leopoldini, M.; Russo, N.; Chiodo, S.; Toscano, M., Iron chelation by the powerful antioxidant flavonoid quercetin. *J. Agric. Food Chem.* **2006**, *54* (17), 6343-6351.
91. Groot, H. d.; Rauen, U., Tissue injury by reactive oxygen species and the protective effects of flavonoids. *Fundam. Clin. Pharmacol.* **1998**, *12* (3), 249-255.
92. (a) Fukumoto, L.; Mazza, G., Assessing antioxidant and prooxidant activities of phenolic compounds. *J. Agric. Food Chem.* **2000**, *48* (8), 3597-3604; (b) Maurya, D. K.; Devasagayam, T. P. A., Antioxidant and prooxidant nature of hydroxycinnamic acid derivatives ferulic and caffeic acids. *Food Chem. Toxicol.* **2010**, *48* (12), 3369-3373.
93. Lambert, J. D.; Elias, R. J., The antioxidant and pro-oxidant activities of green tea polyphenols: a role in cancer prevention. *Arch. Biochem. Biophys.* **2010**, *501* (1), 65-72.
94. Kumar, S.; Pandey, A. K., Chemistry and biological activities of flavonoids: an overview. *The Scientific World Journal* **2013**, 2013.
95. Gülçin, İ., Antioxidant properties of resveratrol: a structure–activity insight. *Innovative Food Science & Emerging Technologies* **2010**, *11* (1), 210-218.
96. Shahidi, F.; Naczk, M.; Griffiths, W., Food Phenolics: Sources, Chemistry, Effects, Applications. *Trends in Food Science and Technology* **1996**, *7* (7), 243.
97. Chen, J. H.; Ho, C.-T., Antioxidant activities of caffeic acid and its related hydroxycinnamic acid compounds. *J. Agric. Food Chem.* **1997**, *45* (7), 2374-2378.
98. Stadler, R. H.; Welti, D. H.; Stämpfli, A. A.; Fay, L. B., Thermal decomposition of caffeic acid in model systems: identification of novel tetraoxygenated phenylindan isomers and their stability in aqueous solution. *J. Agric. Food Chem.* **1996**, *44* (3), 898-905.
99. Sato, Y.; Itagaki, S.; Kurokawa, T.; Ogura, J.; Kobayashi, M.; Hirano, T.; Sugawara, M.; Iseki, K., In vitro and in vivo antioxidant properties of chlorogenic acid and caffeic acid. *Int. J. Pharm.* **2011**, *403* (1), 136-138.
100. Kikuzaki, H.; Hisamoto, M.; Hirose, K.; Akiyama, K.; Taniguchi, H., Antioxidant properties of ferulic acid and its related compounds. *J. Agric. Food Chem.* **2002**, *50* (7), 2161-2168.
101. Zang, L.-Y.; Cosma, G.; Gardner, H.; Shi, X.; Castranova, V.; Vallyathan, V., Effect of antioxidant protection by p-coumaric acid on low-density lipoprotein cholesterol oxidation. *American Journal of Physiology-Cell Physiology* **2000**, *279* (4), C954-C960.
102. Baum, B.; Perun, A., Antioxidant efficiency versus structure. *Polymer Engineering & Science* **1962**, *2* (3), 250-259.
103. Natella, F.; Nardini, M.; Di Felice, M.; Scaccini, C., Benzoic and cinnamic acid derivatives as antioxidants: structure-activity relation. *J. Agric. Food Chem.* **1999**, *47* (4), 1453-1459.
104. Cheng, C.-Y.; Su, S.-Y.; Tang, N.-Y.; Ho, T.-Y.; Chiang, S.-Y.; Hsieh, C.-L., Ferulic acid provides neuroprotection against oxidative stress-related apoptosis after cerebral ischemia/reperfusion injury by inhibiting ICAM-1 mRNA expression in rats. *Brain Res.* **2008**, *1209*, 136-150.
105. Gim, S.-A.; Koh, P.-O., Ferulic acid prevents the injury-induced decrease of  $\gamma$ -enolase expression in brain tissue and HT22 cells.
106. Pereira, P.; de Oliveira, P.; Ardenghi, P.; Rotta, L.; Henriques, J.; Picada, J., Neuropharmacological analysis of caffeic acid in rats. *Basic Clin. Pharmacol. Toxicol.* **2006**, *99* (5), 374-378.
107. Shah, K.; Weissleder, R., Molecular optical imaging: applications leading to the development of present day therapeutics. *NeuroRx* **2005**, *2* (2), 215-225.
108. Lavis, L. D.; Chao, T.-Y.; Raines, R. T., Fluorogenic label for biomolecular imaging. *ACS Chem. Biol.* **2006**, *1* (4), 252-260.

109. Zimmerman, M.; Ashe, B.; Yurewicz, E.; Patel, G., Sensitive assays for trypsin, elastase, and chymotrypsin using new fluorogenic substrates. *Anal. Biochem.* **1977**, *78* (1), 47-51.
110. Wegener, D.; Wirsching, F.; Riester, D.; Schwienhorst, A., A fluorogenic histone deacetylase assay well suited for high-throughput activity screening. *Chem. Biol.* **2003**, *10* (1), 61-68.
111. Lavis, L. D.; Chao, T. Y.; Raines, R. T., Latent blue and red fluorophores based on the trimethyl lock. *Chembiochem* **2006**, *7* (8), 1151-1154.
112. Lavis, L. D.; Rutkoski, T. J.; Raines, R. T., Tuning the pK<sub>a</sub> of fluorescein to optimize binding assays. *Anal. Chem.* **2007**, *79* (17), 6775-6782.
113. (a) Sun, W.-C.; Gee, K. R.; Klaubert, D. H.; Haugland, R. P., Synthesis of fluorinated fluoresceins. *The Journal of Organic Chemistry* **1997**, *62* (19), 6469-6475; (b) Mchedlov-Petrosyan, N. O.; Rubtsov, M. I.; Lukatskaya, L. L., Ionization and tautomerism of chloro-derivatives of fluorescein in water and aqueous acetone. *Dyes and pigments* **1992**, *18* (3), 179-198.
114. Brinkley, M., A brief survey of methods for preparing protein conjugates with dyes, haptens and crosslinking reagents. *Bioconjug. Chem.* **1992**, *3* (1), 2-13.
115. Graber, M. L.; DiLillo, D. C.; Friedman, B. L.; Pastoriza-Munoz, E., Characteristics of fluoroprobes for measuring intracellular pH. *Anal. Biochem.* **1986**, *156* (1), 202-212.
116. (a) Inglese, J.; Johnson, R. L.; Simeonov, A.; Xia, M.; Zheng, W.; Austin, C. P.; Auld, D. S., High-throughput screening assays for the identification of chemical probes. *Nat. Chem. Biol.* **2007**, *3* (8), 466-479; (b) Martin, V. V.; Rothe, A.; Gee, K. R., Fluorescent metal ion indicators based on benzoannelated crown systems: a green fluorescent indicator for intracellular sodium ions. *Bioorg. Med. Chem. Lett.* **2005**, *15* (7), 1851-1855; (c) Song, F.; Garner, A. L.; Koide, K., A highly sensitive fluorescent sensor for palladium based on the allylic oxidative insertion mechanism. *J. Am. Chem. Soc.* **2007**, *129* (41), 12354-12355; (d) Yoon, S.; Miller, E. W.; He, Q.; Do, P. H.; Chang, C. J., A bright and specific fluorescent sensor for mercury in water, cells, and tissue. *Angewandte Chemie International Edition* **2007**, *46* (35), 6658-6661.
117. Urano, Y.; Kamiya, M.; Kanda, K.; Ueno, T.; Hirose, K.; Nagano, T., Evolution of fluorescein as a platform for finely tunable fluorescence probes. *J. Am. Chem. Soc.* **2005**, *127* (13), 4888-4894.
118. Kamiya, M.; Kobayashi, H.; Hama, Y.; Koyama, Y.; Bernardo, M.; Nagano, T.; Choyke, P. L.; Urano, Y., An enzymatically activated fluorescence probe for targeted tumor imaging. *J. Am. Chem. Soc.* **2007**, *129* (13), 3918-3929.
119. Karolin, J.; Johansson, L. B.-A.; Strandberg, L.; Ny, T., Fluorescence and absorption spectroscopic properties of dipyrrometheneboron difluoride (BODIPY) derivatives in liquids, lipid membranes, and proteins. *J. Am. Chem. Soc.* **1994**, *116* (17), 7801-7806.
120. Thompson, V.; Saldaña, S.; Cong, J.; Goll, D., A BODIPY fluorescent microplate assay for measuring activity of calpains and other proteases. *Anal. Biochem.* **2000**, *279* (2), 170.
121. Lee, L.; Spurgeon, S.; Heiner, C.; Benson, S.; Rosenblum, B.; Menchen, S.; Graham, R.; Constantinescu, A.; Upadhy, K.; Cassel, J., New energy transfer dyes for DNA sequencing. *Nucleic Acids Res.* **1997**, *25* (14), 2816-2822.
122. Liu, J.; Bhalgat, M.; Zhang, C.; Diwu, Z.; Hoyland, B.; Klaubert, D. H., Fluorescent molecular probes V: a sensitive caspase-3 substrate for fluorometric assays. *Bioorg. Med. Chem. Lett.* **1999**, *9* (22), 3231-3236.
123. Kupcho, K.; Somberg, R.; Bulleit, B.; Goueli, S. A., A homogeneous, nonradioactive high-throughput fluorogenic protein kinase assay. *Anal. Biochem.* **2003**, *317* (2), 210-217.
124. Streu, C.; Meggers, E., Ruthenium - Induced Allylcarbamate Cleavage in Living Cells. *Angewandte Chemie* **2006**, *118* (34), 5773-5776.
125. Waggoner, A., Fluorescent labels for proteomics and genomics. *Curr. Opin. Chem. Biol.* **2006**, *10* (1), 62-66.
126. Schobel, U.; Egelhaaf, H.-J.; Brecht, A.; Oelkrug, D.; Gauglitz, G., New donor-acceptor pair for fluorescent immunoassays by energy transfer. *Bioconjug. Chem.* **1999**, *10* (6), 1107-1114.

127. Bates, M.; Huang, B.; Dempsey, G. T.; Zhuang, X., Multicolor super-resolution imaging with photo-switchable fluorescent probes. *Science* **2007**, *317* (5845), 1749-1753.
128. Ghosh, P.; Whitehouse, M. W., 7-chloro-4-nitrobenzo-2-oxa-1, 3-diazole: a new fluorogenic reagent for amino acids and other amines. *Biochem. J.* **1968**, *108* (1), 155.
129. Levi, J.; Cheng, Z.; Gheysens, O.; Patel, M.; Chan, C. T.; Wang, Y.; Namavari, M.; Gambhir, S. S., Fluorescent fructose derivatives for imaging breast cancer cells. *Bioconjug. Chem.* **2007**, *18* (3), 628-634.
130. Hsu, V. W.; Lee, S. Y.; Yang, J.-S., The evolving understanding of COPI vesicle formation. *Nature Reviews Molecular Cell Biology* **2009**, *10* (5), 360-364.
131. Lee, M. C.; Miller, E. A.; Goldberg, J.; Orci, L.; Schekman, R., Bi-directional protein transport between the ER and Golgi. *Annu. Rev. Cell Dev. Biol.* **2004**, *20*, 87-123.
132. (a) Malhotra, V.; Serafini, T.; Orci, L.; Shepherd, J. C.; Rothman, J. E., Purification of a novel class of coated vesicles mediating biosynthetic protein transport through the Golgi stack. *Cell* **1989**, *58* (2), 329-336; (b) Waters, M. G.; Serafini, T.; Rothman, J. E., 'Coatomer': a cytosolic protein complex containing subunits of non-clathrin-coated Golgi transport vesicles. **1991**.
133. Orci, L.; Palmer, D. J.; Amherdt, M.; Rothman, J. E., Coated vesicle assembly in the Golgi requires only coatomer and ARF proteins from the cytosol. **1993**.
134. Serafini, T.; Orci, L.; Amherdt, M.; Brunner, M.; Kahn, R. A.; Rothman, J. E., ADP-ribosylation factor is a subunit of the coat of Golgi-derived COP-coated vesicles: a novel role for a GTP-binding protein. *Cell* **1991**, *67* (2), 239-253.
135. Hara-Kuge, S.; Kuge, O.; Orci, L.; Amherdt, M.; Ravazzola, M.; Wieland, F. T.; Rothman, J. E., En bloc incorporation of coatomer subunits during the assembly of COP-coated vesicles. *The Journal of Cell Biology* **1994**, *124* (6), 883-892.
136. Bremser, M.; Nickel, W.; Schweikert, M.; Ravazzola, M.; Amherdt, M.; Hughes, C. A.; Söllner, T. H.; Rothman, J. E.; Wieland, F. T., Coupling of Coat Assembly and Vesicle Budding to Packaging of Putative Cargo Receptors. *Cell* **1999**, *4* (96), 495-506.
137. Orci, L.; Starnes, M.; Ravazzola, M.; Amherdt, M.; Perrelet, A.; Söllner, T.; Rothman, J., Bidirectional transport by distinct populations of COPI-coated vesicles. *Cell* **1997**, *90* (2), 335.
138. Fiedler, K.; Veit, M.; Starnes, M. A.; Rothman, J. E., Bimodal interaction of coatomer with the p24 family of putative cargo receptors. *Science* **1996**, *273* (5280), 1396.
139. Lee, S. Y.; Yang, J.-S.; Hong, W.; Premont, R. T.; Hsu, V. W., ARFGAP1 plays a central role in coupling COPI cargo sorting with vesicle formation. *The Journal of cell biology* **2005**, *168* (2), 281-290.
140. (a) Waters, M.; Serafini, T.; Rothman, J., 'Coatomer': a cytosolic protein complex containing subunits of non-clathrin-coated Golgi transport vesicles. *Nature* **1991**, *349* (6306), 248; (b) Stenbeck, G.; Harter, C.; Brecht, A.; Herrmann, D.; Lottspeich, F.; Orci, L.; Wieland, F., beta'-COP, a novel subunit of coatomer. *The EMBO journal* **1993**, *12* (7), 2841; (c) Kuge, O.; Hara-Kuge, S.; Orci, L.; Ravazzola, M.; Amherdt, M.; Tanigawa, G.; Wieland, F. T.; Rothman, J. E., zeta-COP, a subunit of coatomer, is required for COP-coated vesicle assembly. *The Journal of cell biology* **1993**, *123* (6), 1727-1734.
141. Kirchhausen, T., Three ways to make a vesicle. *Nature Reviews Molecular Cell Biology* **2000**, *1* (3), 187-198.
142. Edeling, M. A.; Smith, C.; Owen, D., Life of a clathrin coat: insights from clathrin and AP structures. *Nature Reviews Molecular Cell Biology* **2006**, *7* (1), 32-44.
143. Collins, B.; McCoy, A.; Kent, H.; Evans, P.; Owen, D., Molecular architecture and functional model of the endocytic AP2 complex. *Cell* **2002**, *109* (4), 523-535.
144. Yu, X.; Breitman, M.; Goldberg, J., A Structure-Based Mechanism for Arf1-Dependent Recruitment of Coatomer to Membranes. *Cell* **2012**, *3* (148), 530-542.
145. Futatsumori, M.; Kasai, K.; Takatsu, H.; Shin, H.-W.; Nakayama, K., Identification and characterization of novel isoforms of COP I subunits. *J. Biochem.* **2000**, *128* (5), 793-801.

146. Wegmann, D.; Hess, P.; Baier, C.; Wieland, F. T.; Reinhard, C., Novel isotypic  $\gamma/\zeta$  subunits reveal three coatomer complexes in mammals. *Mol. Cell. Biol.* **2004**, *24* (3), 1070-1080.
147. Moelleken, J.; Malsam, J.; Betts, M. J.; Movafeghi, A.; Reckmann, I.; Meissner, I.; Hellwig, A.; Russell, R. B.; Söllner, T.; Brügger, B., Differential localization of coatomer complex isoforms within the Golgi apparatus. *Proceedings of the National Academy of Sciences* **2007**, *104* (11), 4425-4430.
148. Shtutman, M.; Baig, M.; Levina, E.; Hurteau, G.; Lim, C.-u.; Broude, E.; Nikiforov, M.; Harkins, T. T.; Carmack, C. S.; Ding, Y., Tumor-specific silencing of COPZ2 gene encoding coatomer protein complex subunit  $\zeta 2$  renders tumor cells dependent on its paralogous gene COPZ1. *Proceedings of the National Academy of Sciences* **2011**, *108* (30), 12449-12454.
149. Rodriguez, A.; Griffiths-Jones, S.; Ashurst, J. L.; Bradley, A., Identification of mammalian microRNA host genes and transcription units. *Genome Res.* **2004**, *14* (10a), 1902-1910.
150. (a) Hiroki, E.; Akahira, J. i.; Suzuki, F.; Nagase, S.; Ito, K.; Suzuki, T.; Sasano, H.; Yaegashi, N., Changes in microRNA expression levels correlate with clinicopathological features and prognoses in endometrial serous adenocarcinomas. *Cancer Sci.* **2009**, *1* (101), 241-249; (b) Braconi, C.; Huang, N.; Patel, T. C., MicroRNA-dependent regulation of DNA methyltransferase-1 and tumor suppressor gene expression by interleukin-6 in human malignant cholangiocytes. *Hepatology* **2010**, *51* (3), 881-890.
151. Zhu, X.-m.; Han, T.; Wang, X.-h.; Li, Y.-h.; Yang, H.-g.; Luo, Y.-n.; Yin, G.-w.; Yao, Y.-q., Overexpression of miR-152 leads to reduced expression of human leukocyte antigen-G and increased natural killer cell mediated cytotoxicity in JEG-3 cells. *Am. J. Obstet. Gynecol.* **2010**, *202* (6), 592. e1-592. e7.
152. Shtutman, M.; Roninson, I. B., A subunit of coatomer protein complex offers a novel tumor-specific target through a surprising mechanism. *Autophagy* **2011**, *7* (12), 1551-1552.
153. Basse, M. J.; Betzi, S.; Bourgeas, R.; Bouzidi, S.; Chetrit, B.; Hamon, V.; Morelli, X.; Roche, P., 2P2Idb: a structural database dedicated to orthosteric modulation of protein-protein interactions. *Nucleic Acids Res.* **2013**, *41* (D1), D824-D827.
154. Yu, W.; Lin, J.; Jin, C.; Xia, B., Solution structure of human  $\zeta$ -COP: direct evidences for structural similarity between COP I and clathrin-adaptor coats. *J. Mol. Biol.* **2009**, *386* (4), 903-912.
155. Walensky, L. D.; Bird, G. H., Hydrocarbon-Stapled Peptides: Principles, Practice, and Progress: Miniperspective. *J. Med. Chem.* **2014**, *57* (15), 6275-6288.